Hydrothermal evolution of volcanogenic Zn-Cu-Pb deposits, Taylors Brook Showing, Stirling Belt, southeastern Cape Breton Island, Nova Scotia

by

Haley D. LeBlanc

A thesis presented to the Department of Geology of

Saint Mary's University

In partial fulfillment of the requirements for the degree of

BACHELOR OF SCIENCE

IN GEOLOGY (HONOURS)

Examining committee:

Dr. Jacob Hanley, Department of Geology, Saint Mary's University

Department of Geology

Saint Mary's University

Halifax, Nova Scotia

August 17, 2016

Abstract: Hydrothermal evolution of volcanogenic Zn-Cu-Pb deposits, Taylors Brook showing, Stirling Belt, southeastern Cape Breton Island, Nova Scotia

Haley LeBlanc

The Taylors Brook showing is a suspected volcanogenic massive sulfide (VMS) occurrence (Zn-Pb-Cu-Au-Ag) that occurs within the ~680 Ma Stirling volcanosedimentary-plutonic belt, southeastern Cape Breton Island, Nova Scotia, Canada. In addition to mineralized mudstones, there are 7 associated hydrothermal vein types, characterized using three criteria: vein-filling mineral composition and alteration style, cross cutting relationships and mineralization. Mineralized (Zn-Cu-Pb-Sc-Y-Ag-Te) veins show propylitic and potassic alteration assemblages. Compositional zoning in epidote and a pyrrhotite-smythite replacement reaction indicate that the hydrothermal fluid was experiencing fluctuations in fO_2 and cooling, respectively, rendering the metals less soluble causing their precipitation.

Bulk rock geochemistry indicates mineralization anomalies are associated with host rock Zn-Pb anomalies in pyritic mudstone units and Cu anomalies in type IA (epidote-actinolite-calcite-K-feldspar-quartz-pyrite) veins. Fluid inclusion data from two generations of calcite in later type V veins suggest a $CaCl_2$-rich hydrothermal brine responsible for metal transport and deposition with bulk salinities ranging between 43-54 wt% total salt (absolute: 33-50 wt% $CaCl_2$ and up to 20 wt % NaCl). The homogenization temperatures for calcite A-hosted inclusions range from 106-306^oC (n=21) and in calcite B-hosted inclusions from 212-331^oC (n=91). Isochore ranges were plotted using microthermometric data, paired with a po-py equilibrium boundary constraint limits trapping conditions to a maximum of 400^oC and 5kbar.

The distinct Ca-Cl-rich brine composition can only be formed naturally under specific conditions. There are four conceivable explanations for this Ca rich fluid: boiling, cation exchange between Na and Ca, evaporation of Ca-rich paleoseawater and dissolution of Ca-evaporites. However, the combination of high salinity and high Ca is only possible via the latter two processes. The Taylors Brook showing has comparable mineralization to the Stirling deposit, and the Duck Pond-Lemarchant deposits of Newfoundland but has an inconsistent fluid chemistry with VMS deposits.

Date of submission: August 17, 2016

Acknowledgements

I would like to acknowledge the Nova Scotia Department of Natural Resources Geoscience and Mines Branch for giving me the opportunity to train, assist and learn from local geoscientist and GIS specialists. I would like to thank Geoff Baldwin, Trevor MacHattie and Chris White for their invaluable field knowledge. Robert Naylor and Diane Webber, for their continued consideration and support. Also I would like to thank NSDNR for funding and the opportunity to complete this Honors Thesis.

I would like to thank my amazing professors at Saint Mary's University, Andrew MacRae, Victor Owen, Pierre Jutras, Georgia Pe-Piper, Fergus Tweedale and Randy Corney. Thank you for all of your help and guidance throughout my undergraduate degree.

I would be no where without the support of my family (Stephanie, Howard, Michael and Mitchell). I would like to thank my cousin the late Nicholas Frenette for teaching me 'you have to fight through the bad days to earn the best days of your life'. My grandmother, Delphine Pancura who is a combination of warmth and kindness, laughter and love. She was a person who overlooked all my faults, praised my every success and encouraged my dreams.

Most importantly I would like to thank Dr. Jacob Hanley (Saint Mary's University), a role model, mentor and friend. He saw potential in me and helped me to reach my educational goals. Thank you for the countless hours of discussion, mentorship and for always being a positive influence that made all this possible.

Table of Contents

List of Figures and Appendices

List of Tables

1.0 Introduction

The Taylors Brook showing is a suspected volcanogenic massive sulfide (VMS) occurrence (Zn-Pb-Cu-Au-Ag) that occurs within the ~680 Ma Stirling volcanosedimentary-plutonic belt, southeastern Cape Breton Island, Nova Scotia, Canada. Previous exploration in the region recognized the showing as part of a larger mineralized district containing the polymetallic Stirling VMS deposit (Mindamar Mine, Stirling Mines Ltd.; 1.2 Mt @ 6.4% Zn, 1.5% Pb, 0.74% Cu, 2.2 oz/ton Ag, and 0.03 oz/ton Au) (O'Reilly, 2008).

The genetic relationship between the Stirling deposit and Taylors Brook occurrence is poorly understood. If a VMS the general model for these systems shows that such deposits occur in districts (i.e., multiple sites of mineralization related to hydrothermal systems around a common submarine volcanic spreading center; eg. Noranda: Hannington *et al.,* 2003, Kuroko: Ishihara, 1974, Matagami: Carr *et al*., 2008, Snow Lake: Bailes *et al.,* 1999 and Flin Flon: Koo *et al.,* 1975). Within such districts, similarities in alteration styles, metal tenor and ore mineralogy, fluid chemistry and associated hydrothermal conditions, and host rock types are expected between deposits. Determining the relationship between the Stirling deposit and the Taylors Brook occurrence first requires a systematic study of such features.

The Stirling deposit was most recently been interpreted by Macdonald and Barr (1993) to have been deposited within, and around, a trough flanked by volcanic centers in an intra-arc setting. A report compiled by Hunter and Gibson (2006; Wallbridge Mining Company Limited exploration project 1998-2005) interpreted the rocks of the Taylors Brook area to be the equivalents of those hosting the Stirling deposit, and represent a

typical submarine volcanogenic setting for massive sulphide deposition hosted within mafic flows, breccias, quartz-feldspar porphyry and mudstone/siltstone (Reid, 2014). The occurrences of VMS mineralization within the Stirling belt have similarities (ie. the association of abundant quartz-carbonate alteration with massive sulphide mineralization) to Proterozoic deposits of the Sudbury area (eg. Errington and Vermillion Zn-Cu-Pb) and the Bergslagen district of Sweden (eg. Garpenberg deposit) (Kontak, 1998).

The main objective of this thesis is to conduct a systematic study of alteration mineralogy and fluid inclusions at the Taylors Brook showing in order to determine conditions of hydrothermal activity, and the relationship of alteration to mineralization. Specifically, optical petrography, scanning electron microscopy (SEM), XRF, and fluid inclusion microscopy and microthermometry are used to characterize the alteration styles, and fluid salinity-temperature pressure characteristics associated with sulfide mineralization and associated hydrothermal events. This will contribute to a genetic and exploration model for suspected VMS mineralization occurrences in the district.

2.0 Geological Setting

The Taylors Brook showing is located in southeastern Cape Breton Island, Saint Esprit. The regional geology in the area of the showing was studied extensively by Barr et al. (1996) and the descriptions here are based on that work. Cape Breton Island is composed of four adjoining terranes: the Blair River inlier, Aspy, Bras d'Or and Avalon (Mira) terranes (Figure 1.1). The site of study lies within the Avalon terrane which docked to Laurentia approximately at 435 Ma. The Avalon Terrane is comprised of five

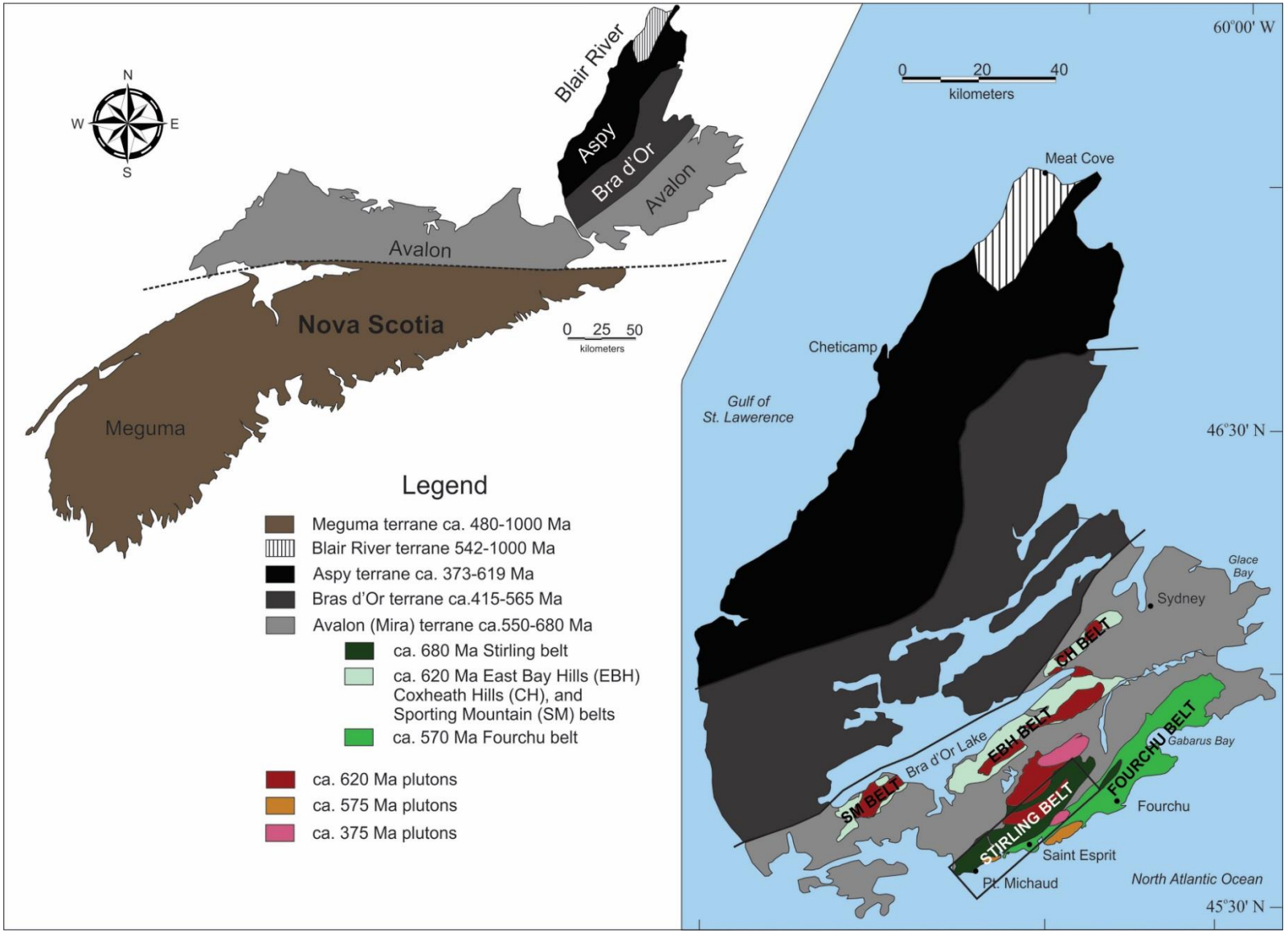
N
W
E
S
Blair River
Aspy
Bra d'Or
Avalon
Avalon
Nova Scotia
0 25 50
kilometers
Meguma
Legend
Meguma terrane ca. 480-1000 Ma
Blair River terrane 542-1000 Ma
Aspy terrane ca. 373-619 Ma
Bras d'Or terrane ca.415-565 Ma
Avalon (Mira) terrane ca.550-680 Ma
ca. 680 Ma Stirling belt
ca. 620 Ma East Bay Hills (EBH) Coxheath Hills (CH), and Sporting Mountain (SM) belts
ca. 570 Ma Fourchu belt
ca. 620 Ma plutons
ca. 575 Ma plutons
ca. 375 Ma plutons
60°00' W
0 20 40
kilometers
Meat Cove
Cheticamp
Gulf of St. Lawerence
46°30' N
Glace Bay
Sydney
CH BELT
EBH BELT
Bra d'Or Lake
SM BELT
STIRLING BELT
FOURCHU BELT
Gabarus Bay
Fourchu
Saint Esprit
Pt. Michaud
North Atlantic Ocean
45°30' N

Figure 2.1: previous page. **Regional geological map showing the alochthonous terranes of mainland Nova Scotia and Cape Breton Island.** A) Regional geological map showing the allochthonous terranes of Nova Scotia, specifically those of Cape Breton Island. B) Enlarged view of Cape Breton Island showing the detailed geology of the Avalon terrane. The five north-east trending volcanic-plutonic belts are labelled (compilation of DNR, 2010 & Petts, *et al.,* 2012). The area showing Figure 2.2 is indicated by the black box.

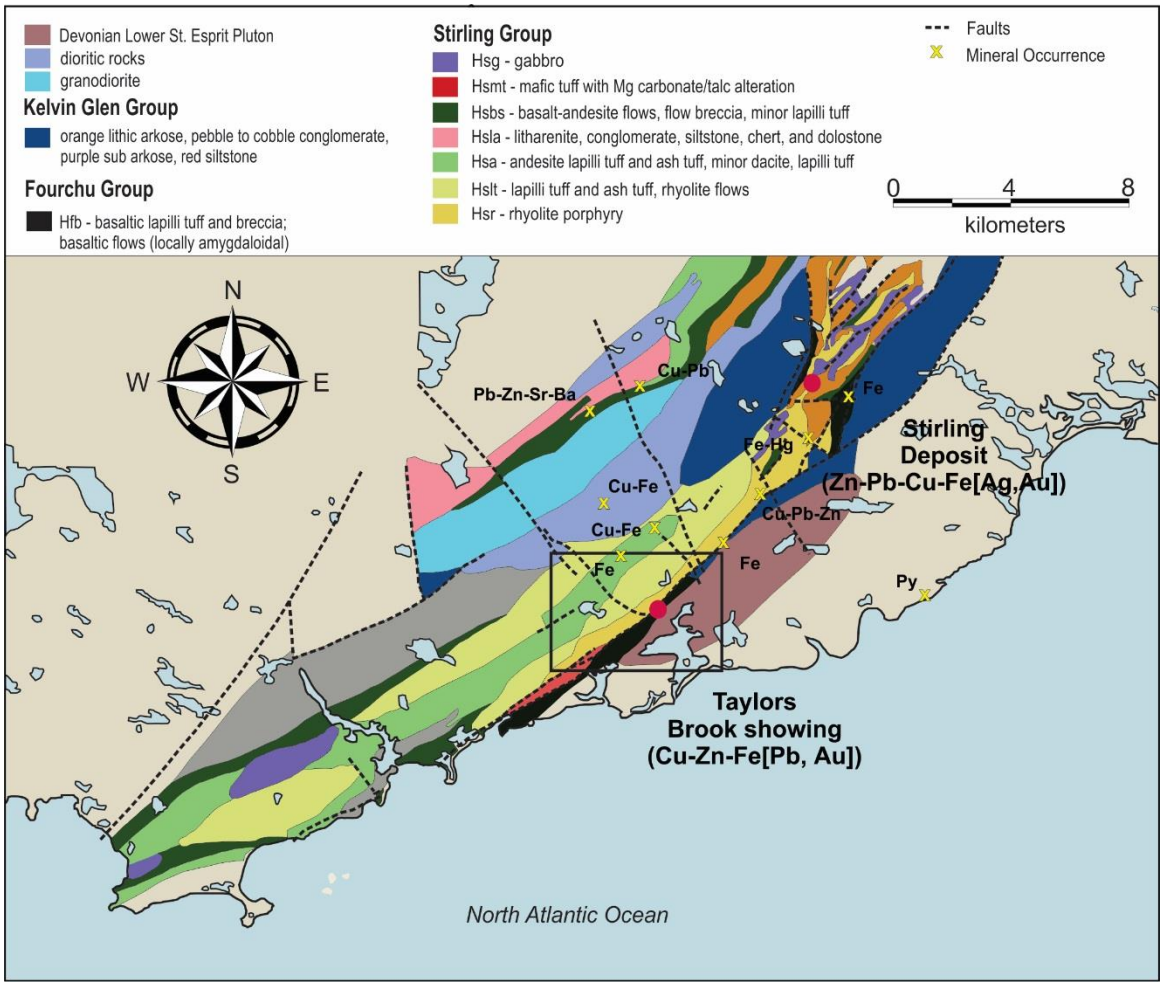

Figure 2.2: **Geological map of southeastern Cape Breton and the Stirling belt.** Map showing the Stirling belt, Stirling deposit and the Taylors Brook showing (Thundermin Resources Inc., 2012). Mineral occurrences are from the NSDNR mineral occurrence data base. The area of Figure 2.3 is indicated by the black box.

north-east trending, volcanic-plutonic belts. These include the Fourchu or Coastal Belt (575 Ma), Stirling Belt (680 Ma), East Bay Hills Belt (620 Ma), Coxheath Belt (620 Ma) and Sporting Mountain Belt (620 Ma)(Kontak, 1997). The belts were intruded by the Caplin Cove (574 Ma), St. Esprit (375 Ma), Salmon River (375 Ma), Chisholm Brook (620 Ma) and Huntington Mountain (620 Ma) plutons (Figure 2.1).

The Stirling deposit and the Taylors Brook showing are located within the Stirling Belt (Figure 2.1 and Figure 2.2). This belt consists of rocks ranging from felsic to mafic volcanic and volcaniclastics hosting lenses of fine- to coarse-grained clastic sedimentary rocks (Kontak, 1997); (Figure 2.3). The rocks are interpreted to have been deposited within and around a trough-flanked volcanic center in an intra-arc setting (Macdonald *et al.*, 1993). Locally, the Taylors Brook showing is hosted within a variety of lithologies including the Lower St. Esprit granite, basalt/andesite flows, quartz feldspar porphyry, andesitic lapilli tuff and ash. Drill hole STR 12-02, studied here, is surficially located east of the L'Archeveque Fault within the Lower Esprit Granite (Figure 2.3).

3.0 Methods

Extensive re-logging and sampling of core from hole STR-12-02 (Thundermin Resources, 2012) was done in the summer of 2015 in order to characterize and obtain samples for study. During that time, 390 bulk geochemical analyses of drill core sections were made using a X-5000 portable X-ray fluorescence spectrometer (XRF) manufactured by Innov-X Canada, with analyses taken at one meter intervals to obtain major and trace element data.

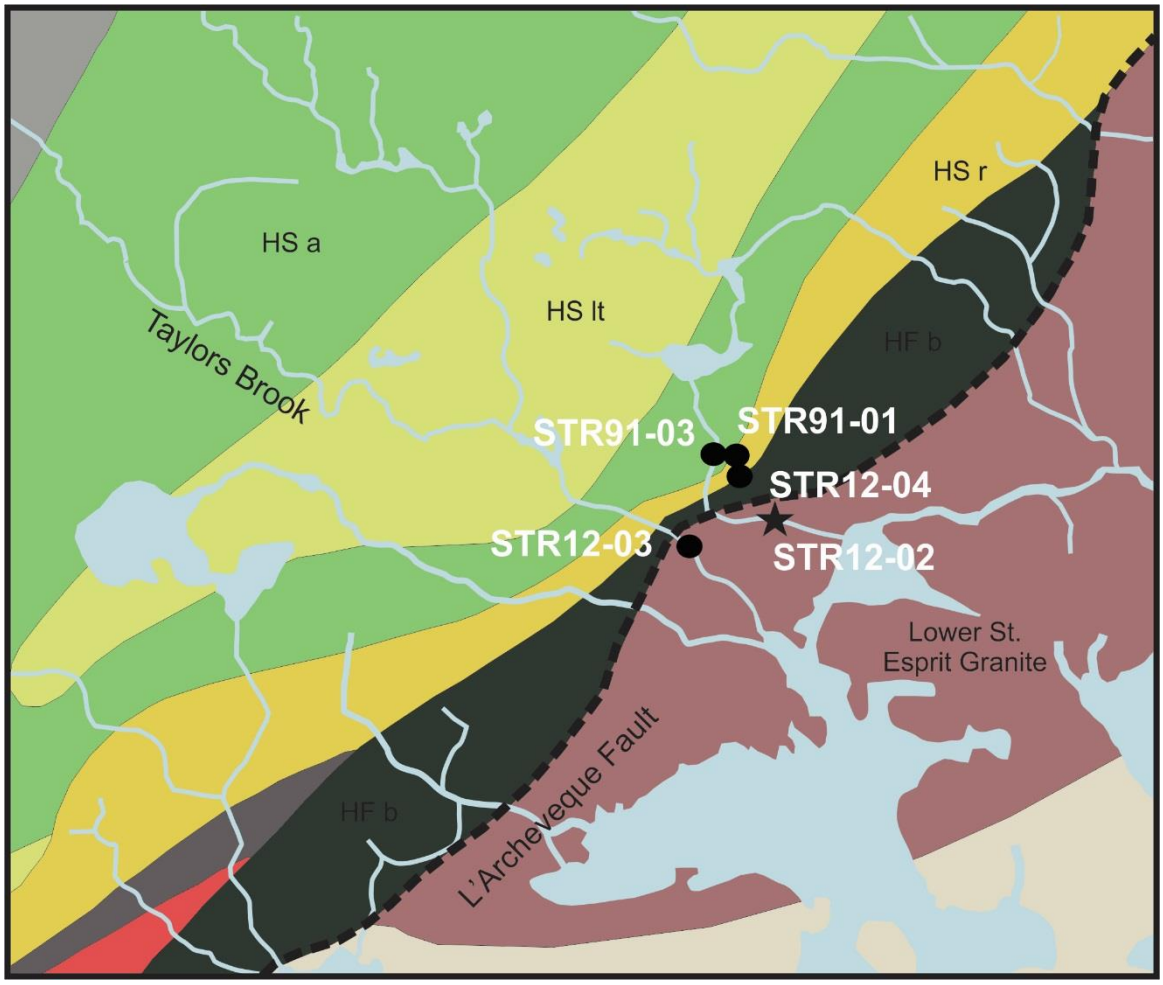

Figure 2.3: **Local geological map of the Taylors Brook showing**. Map of the Taylors Brook showing after Barr et al. (1996) and Reid (2014). All Taylors Brook showing drill hole collar locations are indicated; Holes STR-91-01 and STR-91-03 drilled by Falconbridge Ltd. in 1991 and STR-12-02, STR-12-03 and STR-12-04 drilled by Thundermin Resources Inc. in 2012. The drill hole sampled and logged for this study is denoted by the black star. Refer to legend in Figure 2.2 for lithological abbreviations.

From the drill hole 40 samples were collected that were representative of cross-cutting vein relationships and alteration and mineralization styles. The samples were cut into blocks and sent to Vancouver Petrographics for thin section preparation (19 polished thin sections for petrographic study and 28 double polished thin sections for fluid inclusion study).

Representative thin sections were chosen for SEM-BSE imaging, SEM-EDS mineral analysis and X-ray mapping. Imaging, analysis and X-ray mapping was done using a TESCAN MIRA-3 LMU Variable Pressure Schottky Field Emission Scanning Electron Microscope (FE-SEM) at Saint Mary's University. An energy dispersive X-ray Oxford INCA X-max 80 mm^2 EDS system (attached to the SEM) was operated at a working distance of 15-20 mm, a beam current of 40 μA, and an accelerating voltage of 20 kV. The FE-SEM provided quantitative EDS analyses of minerals as well as a means to identify mineral species, and solids in fluid inclusions.

Microthermometric measurements of fluid inclusions were obtained at Saint Mary's University using a Linkam FTIR 600 heating-freezing stage mounted on an Olympus BX51 microscope. The stage was calibrated using synthetic fluid inclusion standards containing pure CO_2 (melting at –56.6°C) and pure, critical density H_2O (melting at 0°C and homogenizing at 374.1°C). Total uncertainties associated with the microthermometric measurements, based on the reproducibility of measurements conducted on the standards and the measurement (read-out) precision of the controller instrumentation, range from ±2° to 3°C for temperatures recorded near the extremes of working conditions for the heating-freezing stages (–190° and 560°C), to less than ±0.2°C for temperatures recorded near 0°C. Measurements of eutectic (first) ice-melting temperatures (T_e) were obtained to

give insight into the major cation composition of the fluids within the inclusions. Final ice melting temperatures ($T_m$ice), antarcticite melting temperatures ($T_m$ant), and rarely, halite dissolution temperatures ($T_m$halite) were used variably to calculate inclusion salinities (wt% NaCl and $CaCl_2$), using the model of Steele-MacInnis et al. (2011). When both hydrohalite and antarcticite melting temperatures were measured in inclusions, $CaCl_2$ wt% equivalents were estimated graphically using the UNIQUAC model for binary $CaCl_2$-H_2O systems (Sander *et al.*, 1986). The programs BULK and ISOC (Bakker, 2003) were used to model bulk fluid densities and isochores for fluids in the $CaCl_2$-NaCl-H_2O and $CaCl_2$-H_2O systems.

4.0 Results

4.1 Mineralization and alteration

Samples were characterized using three criteria: vein-filling mineral composition and alteration style (ie. vein and wall rock assemblages), cross cutting relationships (ie. relative timing of veining styles) and mineralization (ie. presence/absence of Zn-Cu-Pb-Fe sulphides). Petrographic studies of the veins allowed for a division into 7 vein types (Figure 4.1). The relative order of formation of type IA, IB, II, III, IV, V and VI veins was determined by examination of cross cutting relationships in hand sample and thin section (oldest to youngest).

4.1.1 Type IA veins

Type IA veins show a continuous potassic alteration rind (~1 cm wide) and are rimmed with epidote. Vein minerals are epidote, quartz, carbonate, actinolite, K-feldspar and trace sulphides (Figure 4.2 B, D and I). Type 1A veins range from 0.5-

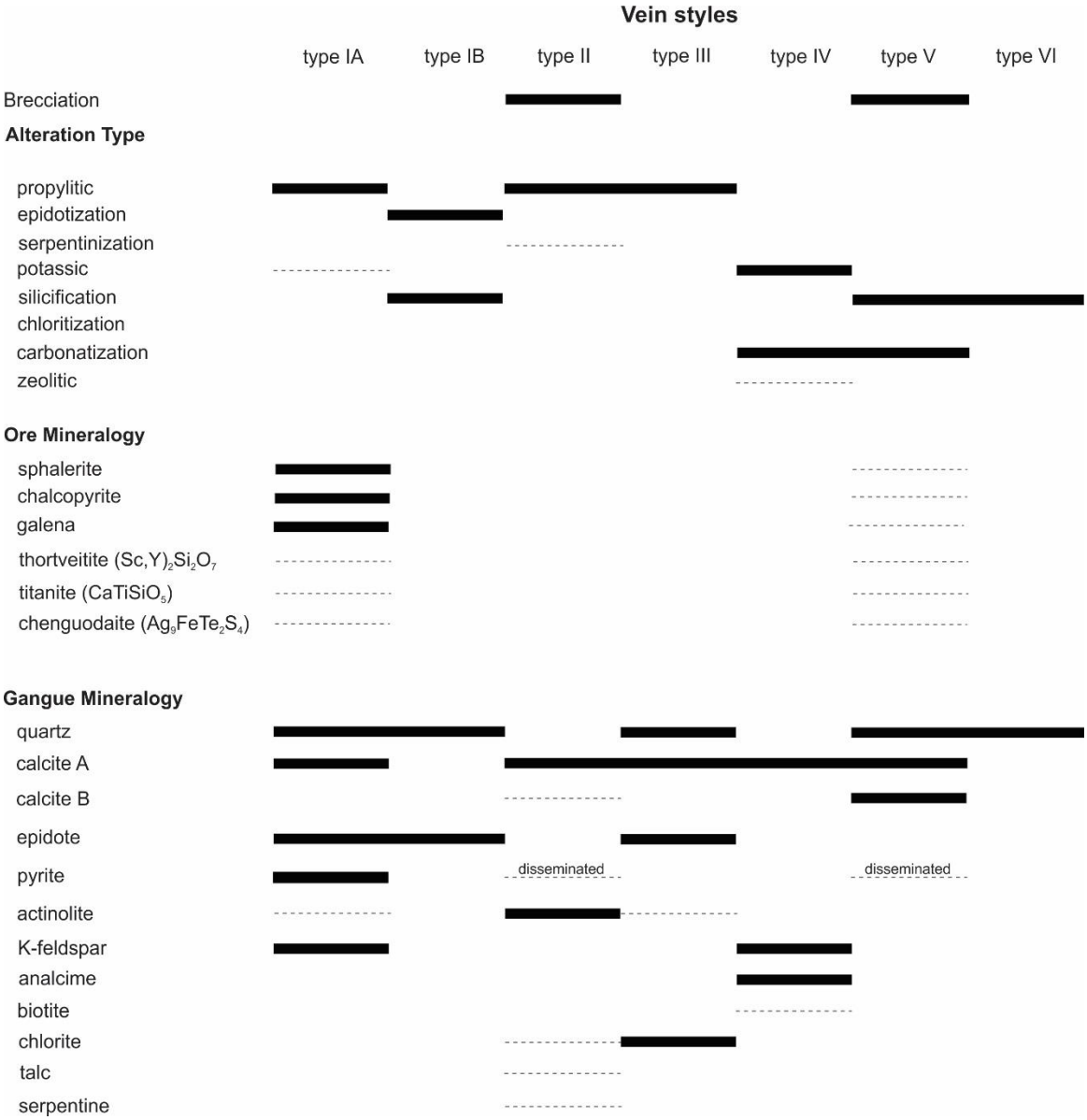

Figure 4.1: **Paragenetic summary of all vein styles, alteration types and associated ore and gangue mineralogical assemblages.**

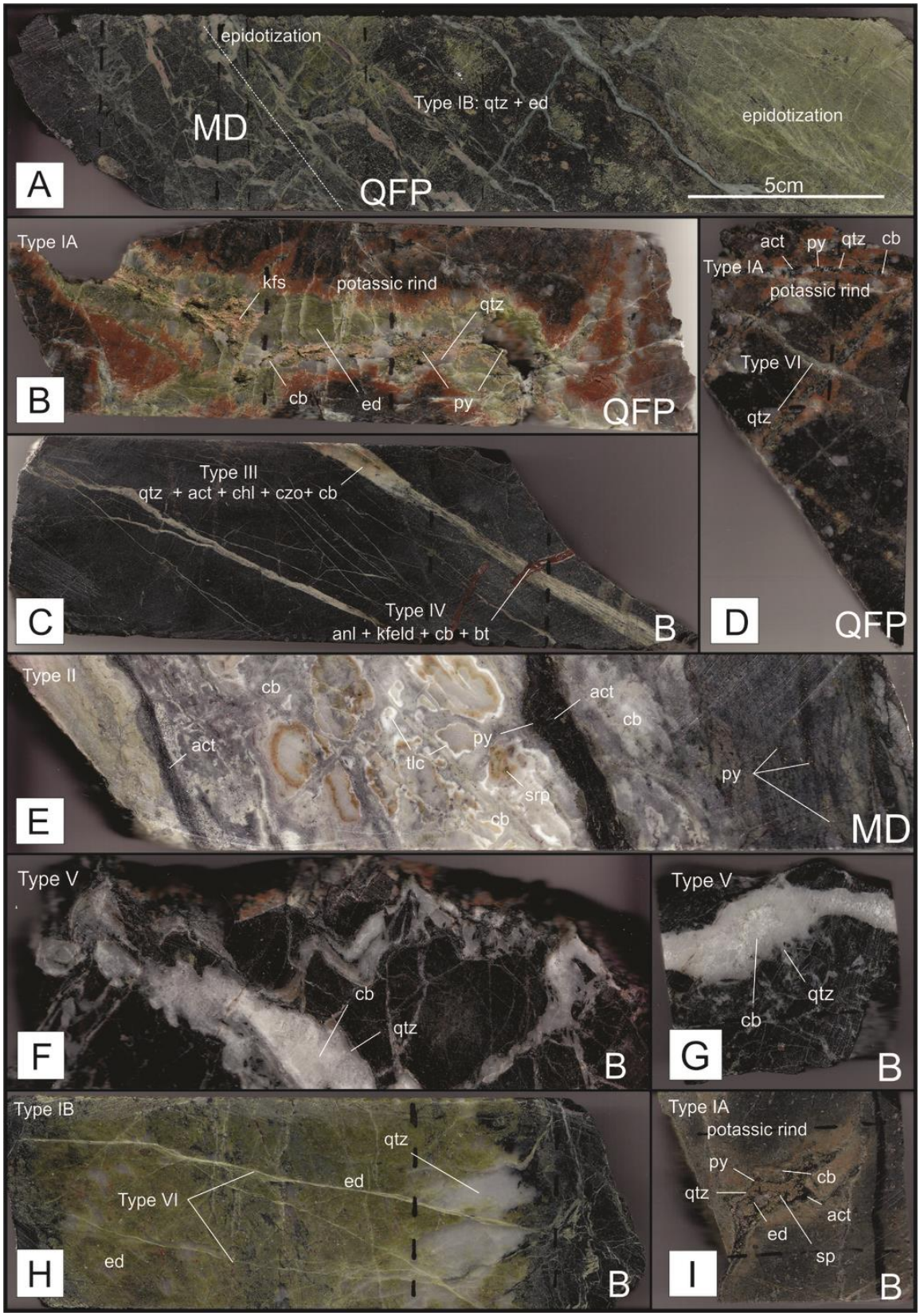
epidotization
MD
Type IB: qtz + ed
epidotization
A
QFP
5cm
Type IA
kfs
potassic rind
qtz
cb
ed
py
B
QFP
act
py
qtz
cb
Type IA
potassic rind
Type VI
qtz
Type III
qtz + act + chl + czo+ cb
C
Type IV
anl + kfeld + cb + bt
B
D
QFP
Type II
cb
act
cb
act
py
tlc
srp
cb
py
E
MD
Type V
cb
qtz
F
B
Type V
qtz
cb
G
B
Type IB
qtz
ed
Type VI
ed
H
B
Type IA
potassic rind
py
cb
qtz
act
ed
sp
I
B

Figure 4.2: previous page. **Photographs of core segments sampled from drill hole STR-12-02.** A) Sample 412.32; an image of the Quartz-Feldspar Porphyry (QFP) cut by a mafic dyke (left hand corner). Both lithologies were highly epidotized, followed by an overprinting of fractured controlled quartz-carbonate veining. Epidotization and veining postdate emplacement of the mafic dyke indicating sulphide mineralization must be younger than the mafic dyke. B) Sample 220.18; an image of the QFP containing a large (1-3cm), type IA (ed-qtz-cb-kfs) vein. This type IA vein contains minor sulphides (py), most likely indicting a higher temperature. It also displays a thick potassic rind characteristic of the type IA fluids. C) Sample 108.9; an image if basalt demonstrating exceptional cross cutting relationships between type III (qtz-act-chl-czo-cb) and type IV (anl-kfs-cb-bt) veins. The image shows that type III veins must have been in place before type IV. The type IV vein is further separated along a mini fault plane. D) Sample 284.15; an image of the QFP showing the cross cutting relationship between type IA (ed-qtz-cb-kfs-act) and type VI (qtz) veins. The image clearly displays sulphide rich type IA veins being crosscut by a later type IV vein. E) Sample 155.65; Example of a large type II (act-cb-tlc-srp-py) vein. F) Sample 106.17; an image of brecciated basalt containing a barren type II (qtz-cb) vein. G) Sample 95.1; Very similar to F) an image of brecciated basalt containing a type II (qtz-cb) vein. H) Sample 406.0; an image if basalt containing a large (10cm) type IB (ed-qtz) vein crosscut by a fracture controlled type VI. I) Sample 113.30; an image of pyritic mudstone featuring a type IA vein sulphide rich (qtz-ed-act-sp-py) vein.

Mineral abbreviations: act=actinolite, anl=analcime, bt=biotite, cb=carbonate, chl=chlorite, czo=clinozoisite, ed=epidote, kfs=k-feldspar, py=pyrite, qtz=quartz, srp=serpentine, sp=sphalerite, tlc=talc. Scale applies to all frames.

3 cm in width and have comb textured margins with a vuggy infilling. Epidote (70 vol. %) is massive, with characteristic second order interference colors in CPL and a green-yellow color in PPL, suggesting high Fe content. Two types of carbonate (A and B) are present within some veins but only carbonate A (12 vol. %) is found within type IA veins. It occurs as subhedral grains between 0.3 and 2 mm in diameter. Carbonate A has a crystalline structure with distinctive twinning planes and shows a milky appearance. The grains display fifth order interference color in CPL and are colourless-light grey in PPL. Quartz (10 vol. %) occurs as subhedral grains between 0.1 and 2 mm in diameter. The grains display a grey first order interference color in CPL and are transparent in PPL. Actinolite (2 vol. %) is commonly present as small (0.5 mm), radiating acicular grains. The actinolite displays characteristic yellow-blue second order interference colors in cross-nicols and a pale yellowish color in plane polarized light (PPL). Chalcopyrite (1 vol. %) and sphalerite (1 vol. %) are found most commonly where massive pyrite (3 vol. %) occurs. Trace minerals found within type IA veins are thortveitite ($[Sc,Y]_2Si_2O_7$), titanite ($CaTiSiO_5$) and chenguodaite ($Ag_9FeTe_2S_4$).

Figure 4.3 shows a type IA vein (SEM-BSE) with quartz as subhedral grains displaying an open-space filling texture intergrown with epidote. Massive epidote is commonly compositionally zoned surrounding sulphide mineralization. A line scan through an epidote grain showing zoning in BSE images confirmed variations of epidote-clinozoisite solid solution composition represented by an increase in Fe and a decrease in Al with dark to light BSE grayscale variations (Figure 4.4).

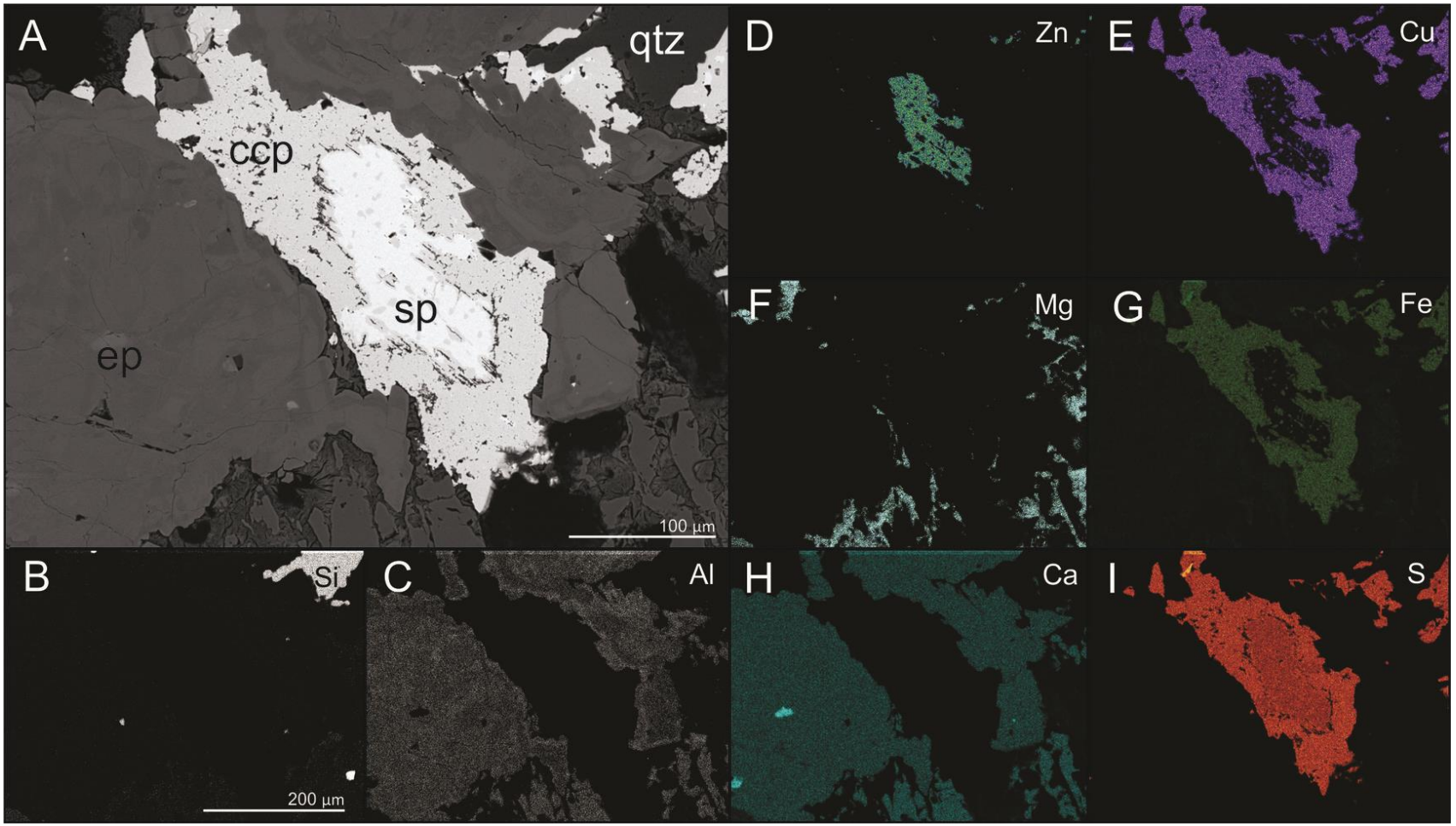

Figure 4.3: **BSE and X-ray maps of mineralized type IA vein**. A) SEM-BSE of mineralized type IA vein showing a sphalerite (sp) grain enclosed by chalcopyrite (ccp) surrounded by epidote (ep). SEM-EDS X-ray maps (B-I) are highlighting specific element distributions (higher concentration = brighter). B) Showing the distribution of Si. C) Showing the distribution of Al. D) Showing the distribution of Zn E) Showing the distribution of Cu. F) Showing the distribution of Mg. G) Showing the distribution of Fe. H) Showing the distribution of Ca and I) showing the distribution of S.

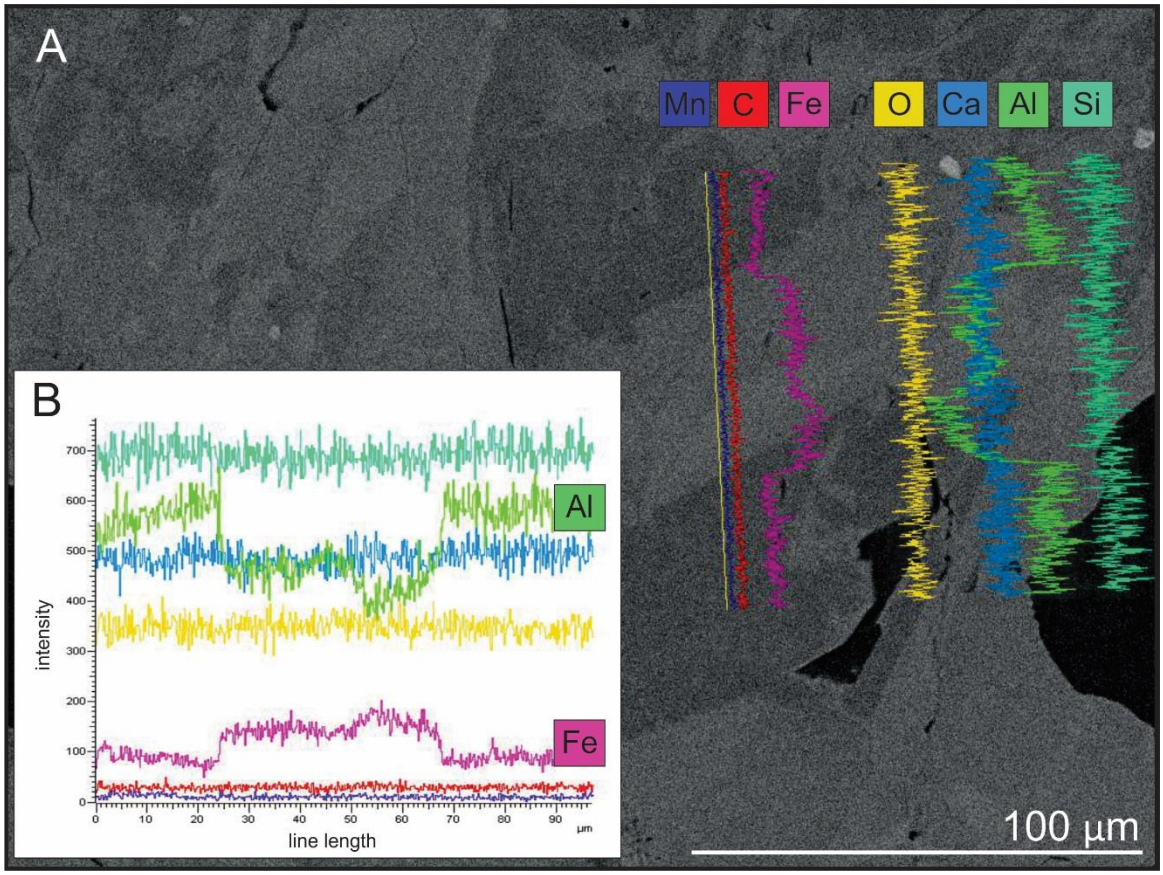

Figure 4.4: **Element SEM line scan though a section of zoned epidote** shows the variation in solid-solution from iron-rich (magenta) to aluminum-rich (green). A) SEM-BSE image showing the direct placement of the analysis line (line on left) and intensity of elements (left to right) Mg, C, Fe, O, Ca, Al and Si along that line. B) The analysis line transposed on a graph (line length vs. intensity).

Chalcopyrite displays an open-space filling texture with epidote. Sphalerite shows selective replacement texture with chalcopyrite and also chalcopyrite "disease". Galena although not present in figure 4.3 is most commonly found as traces rimming chalcopyrite, pyrite or sphalerite. Titanite and chenguodaite are both found throughout type IA veins and pyritic mudstones as microscopic (~5 μm) inclusions enclosed by most commonly pyrite but also chalcopyrite and sphalerite. These textures are representative of all type IA veins samples within this sample set.

Type IA veins have irregular vein margins and show alteration haloes of alkali feldspar and epidote. Type IA veins display propylitic-potassic alteration assemblage (epidote-actinolite-calcite-K-feldspar-quartz-pyrite) and are commonly mineralized. Figure 4.5B shows an example of this vein type, illustrating that it postdates IB veins.

4.1.2 Type IB veins

These veins contain massive epidote and quartz, and range from 2 mm to 10 cm in width (Figure 4.2H). The massive epidote (90 vol. %) is similar in its optical and textural characteristics to the epidote in type IA veins. The massive quartz (10 vol. %) displays a grey first order interference color in CPL and is transparent in PPL. Type IB veins have irregular vein margins and alteration halos of epidote. They show an epidotization-silicification alteration assemblages (epidote-quartz).

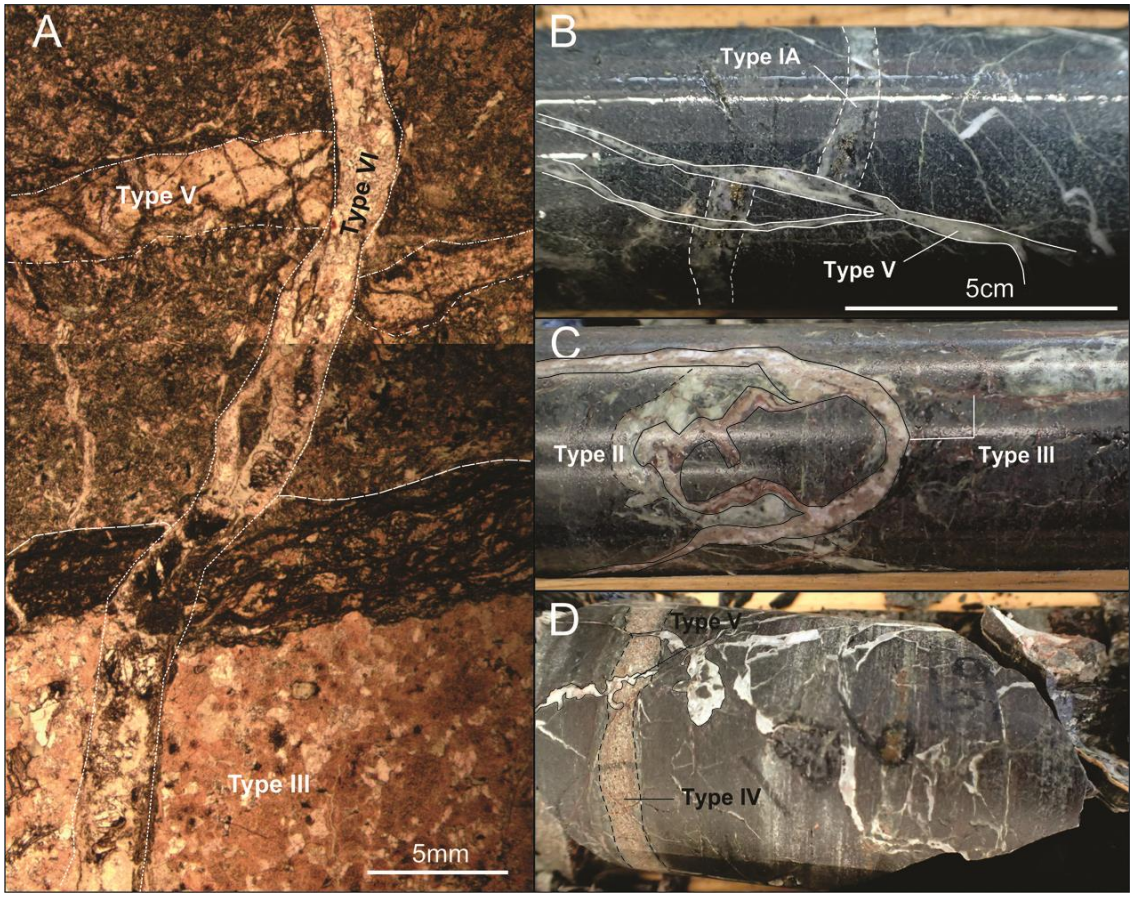

Figure 4.5: **Cross-cutting vein relationships.** Hatched lines are added to all images to help illustrate cross cutting relationships. Scale applies to all frames A) A cross-polarized transmitted light photomicrograph, of a type V vein cross-cut by a later type VI vein. A type III cross-cut by the type VI is also visible. B) A photograph of a type IA vein (note no potassic rind due to mafic host lithology) cross-cut by a later type IB. C) Photograph of a type II cross-cut by a later type III. D) Photograph of a type IV being cross cut by a type V.

4.1.3 Type II veins

Type II veins are rimmed with actinolite and are infilled with two types of carbonate (A and B), disseminated sulphides, and centrally-occurring, zoned, globular masses of serpentine and talc related to the hydrothermal alteration of orthopyroxene and olivine (Figure 4.2E). Type II veins range from 1 to 15cm in width and have a massive appearance. The majority of the veins are comprised of the two generations of massive carbonate. Carbonate A (80 vol. %) has a massive habit and a milky appearance. Carbonate B (5 vol. %) has a very crystalline appearance with distinct grain boundaries, is transparent and has very distinctive twinning planes. The grains display fifth order interference colors in CPL and are colourless-light grey in PPL. Actinolite (10 vol. %) appears to be massive around the vein boundaries. However, there are some small (0.3 mm) acicular radiating grains. The actinolite displays similar optical characteristics to that in type IA veins. Chlorite (2 vol. %) occurs as radiating grains approximately 0.2-0.5 mm in diameter. The grains show characteristic Berlin blue in CPL and are yellowish-grey in PPL. Talc (1 vol. %), serpentine (1 vol. %) and disseminated pyrite (1 vol. %) are minor phases. Type II veins have irregular vein margins and brecciated host rock clasts are commonly located within the vein. Type II veins display serpentinization-propylitic alteration assemblages (serpentine-talc-chlorite-actinolite-calcite) and are rarely mineralized. Figure 4.5C shows an example of this vein type, illustrating that it predates type III veins.

4.1.4 Type III veins

These veins contain quartz, carbonate, chlorite, actinolite and epidote (Figure 4.2C). Quartz (30 vol. %) occurs as subhedral grains 0.1-0.8 mm in diameter. The grains have the same optical characteristics as seen in type II veins. Carbonate A (40 vol. %) has the same optical and textural characteristics as in type IA veins. Epidote (26 vol. %) occurs as subhedral grains 0.2-1 mm in diameter. The grains show characteristic second order interference colors in CPL and a yellowish-green color in PPL indicating a high Al content. Chlorite (2 vol. %) occurs as radiating grains approximately 0.5mm in diameter. The grains show similar optical characteristics as type IB vein chlorite. Actinolite (2 vol. %) occurs as small (0.2-5mm) radiating grains. The actinolite displays similar optical characteristics to actinolite in type IA veins. Type III veins have defined vein margins and they contain a propylitic alteration assemblage (chlorite-epidote-actinolite-calcite). Figure 4.5C shows an example of this vein type, illustrating that they postdate type II veins.

4.1.5 Type IV veins

Type IV veins are composed of carbonate, K-feldspar, analcime and biotite (Figure 4.2C and 4.5D). Type IV veins range from 0.5-3cm in width and appear as linear veins. Carbonate A (10 vol. %) occurs as subhedral grains between 0.1-0.5 mm in diameter. The grains have the same optical characteristics as in type IA veins. K-feldspar (60 vol. %) occurs as euhedral grains 0.1-0.3 mm in length. All grains of K-feldspar show good calrsbad twinning, display a grey first-order interference color in CPL and are transparent in PPL. Analcime (15 vol. %) occurs as subhedral-euhedral grains 0.3-0.8 mm in diameter. The grains are nearly isotropic in CPL and

are transparent in PPL, showing characteristic twinning. Biotite (15 vol. %) occurs as euhedral grains 0.1-0.3 mm in length. The grains display pinkish-green fourth order interference colors in CPL and are brown and extremely pleochroic in PPL. Type IV veins have defined vein margins and show a potassic-carbonatization-zeolitic assemblage (biotite-K-feldspar-calcite-analcime).

4.1.6 Type V veins

These veins were the focus of *fluid inclusion analysis*. The veins contain bladed, comb textured, clear quartz crystals that radiate out from vein walls creating vugs infilled with carbonate A and B (former open spaces) (Figure 4.2 F and G). Type V veins range from 1 to 5cm in width and form irregular networks surrounding brecciate host fragments. Quartz (40 vol. %) occurs as large euhedral grains between 2-6 mm in length. Carbonate A (30 vol. %) occurs with the same optical and textural characteristics as in type IA veins. Carbonate B (10 vol. %) occurs as euhedral grains between 1-3mm in width. The grains have the same optical and textural characteristics as in type II veins. Type V veins comprise breccias containing host fragments but show well defined vein margins. They show a silicification-carbonatization assemblage (quartz-calcite) and are rarely mineralized. Figure 4.5D shows an example of this vein type, illustrating that they postdate of type IV veins.

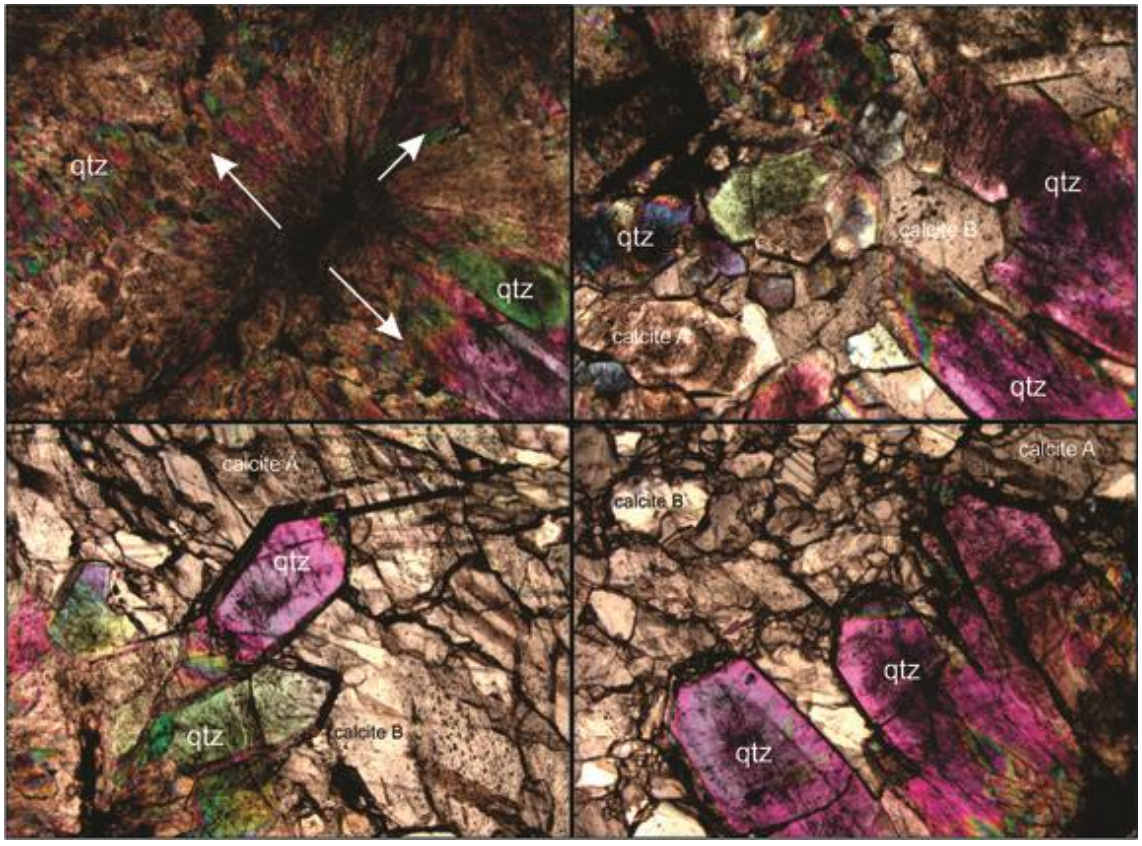

Figure 4.6: **Example of type V veins (comb texture quartz and infilling calcite).** Calcite A and B in type V veins were the focus of *fluid inclusion analysis*. Arrows are showing growth patterns in quartz away from a nucleation point. Note that the interference colors are anomalous due to thickness (100µm) of the fluid inclusion sections giving the quartz the appearance of epidote.

4.1.7 Type VI veins

The youngest vein styles contain quartz only. Type VI veins are 3 to 5mm in width. Quartz occurs as subhedral grains 0.1-0.8 mm in diameter. The grains have the same optical characteristics of type II but show a more polycrystalline texture. Type VI veins represent a silicification assemblage and have sharp vein margins. Figures 4.2A-C and Figure 4.5A show an examples of this vein type and its cross cutting relationships with other vein styles.

4.1.8 Pyritic mudstones

In the mudstones, a distinct compositional and textural boundary was seen between Fe-S phases (Figure 4.8). SEM-EDS analyses along edges of pyrite grains in contact with the other Fe-sulphide (Figure 4.8) were obtained to determine which occurrences were pyrrhotite rather than smythite. Smythite ($[Fe, Ni]_9S_{11}$) is a more Fe-rich variation of pyrite. Smythite occurs as anhedral grains that are extensively fragmented and skeletal; these enclose pyrite which occurs as cubic grains (Figure 4.8). Sphalerite, galena and chalcopyrite are found either infilling smythite fragments or rimming pyrite, pyrrhotite or smythite (Figure 4.7). This suggests Zn-Cu-Pb mineralization postdates this pyrrhotite-smythite replacement reaction. There were many examples of this replacement reaction wherever pyrite was found and one example with pyrrhotite enclosing pyrite (Figure 4.9). The compositional variation between the smythite, pyrite and pyrrhotite was confirmed with SEM-BSE and EDS X-ray mapping (Table 4.1).

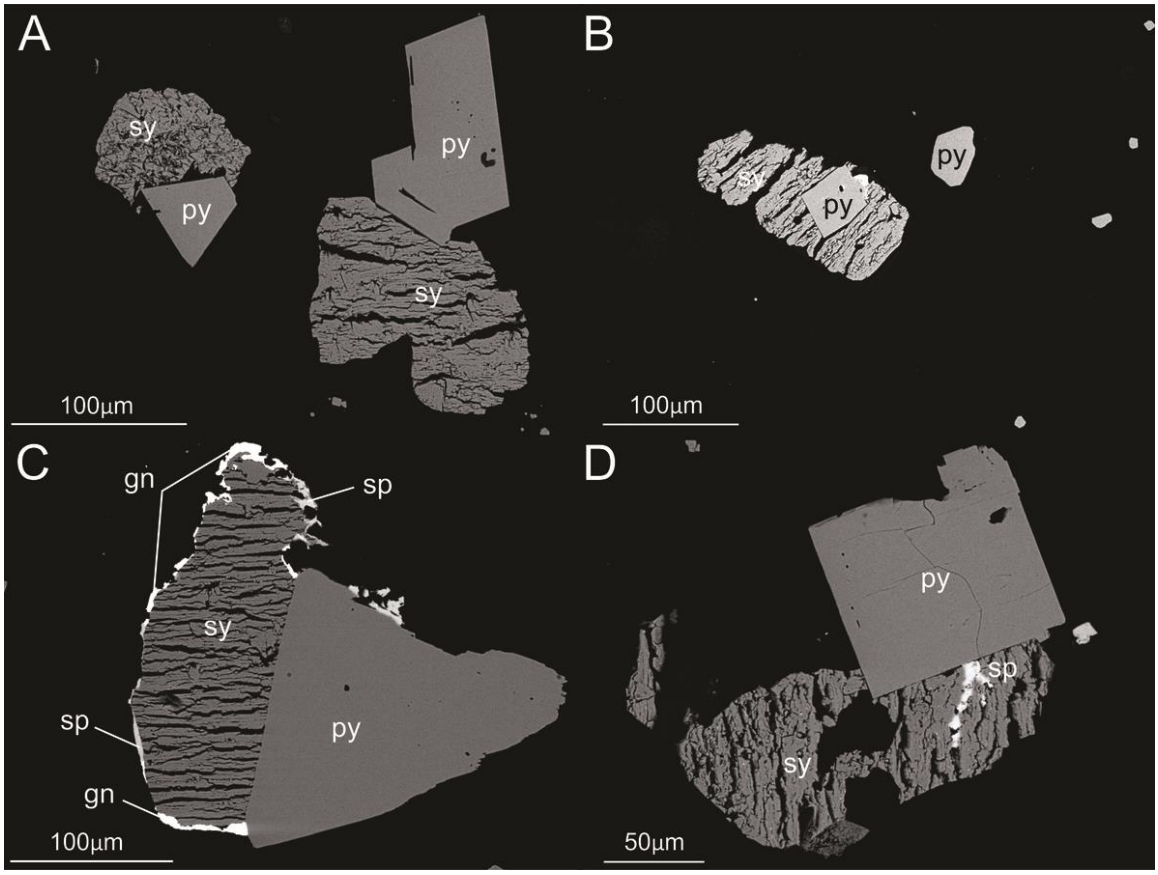

Figure 4.7: **SEM-BSE images of pyrite grains in mudstones.** A) Two fragmented and skeletal smythite grains with their adjoining cubic pyrite grains. B) A cubic pyrite grain enclosed within skeletal smythite. C) A fragmented and skeletal smythite grain and an adjoining pyrite, rimmed with sphalerite and galena. D) A smythite grain and an adjoining cubic pyrite with sphalerite forming from the boundary edge through the skeletal smythite.

Mineral abbreviations: gn=galena, py=pyrite and sp=sphalerite, sy=smythite

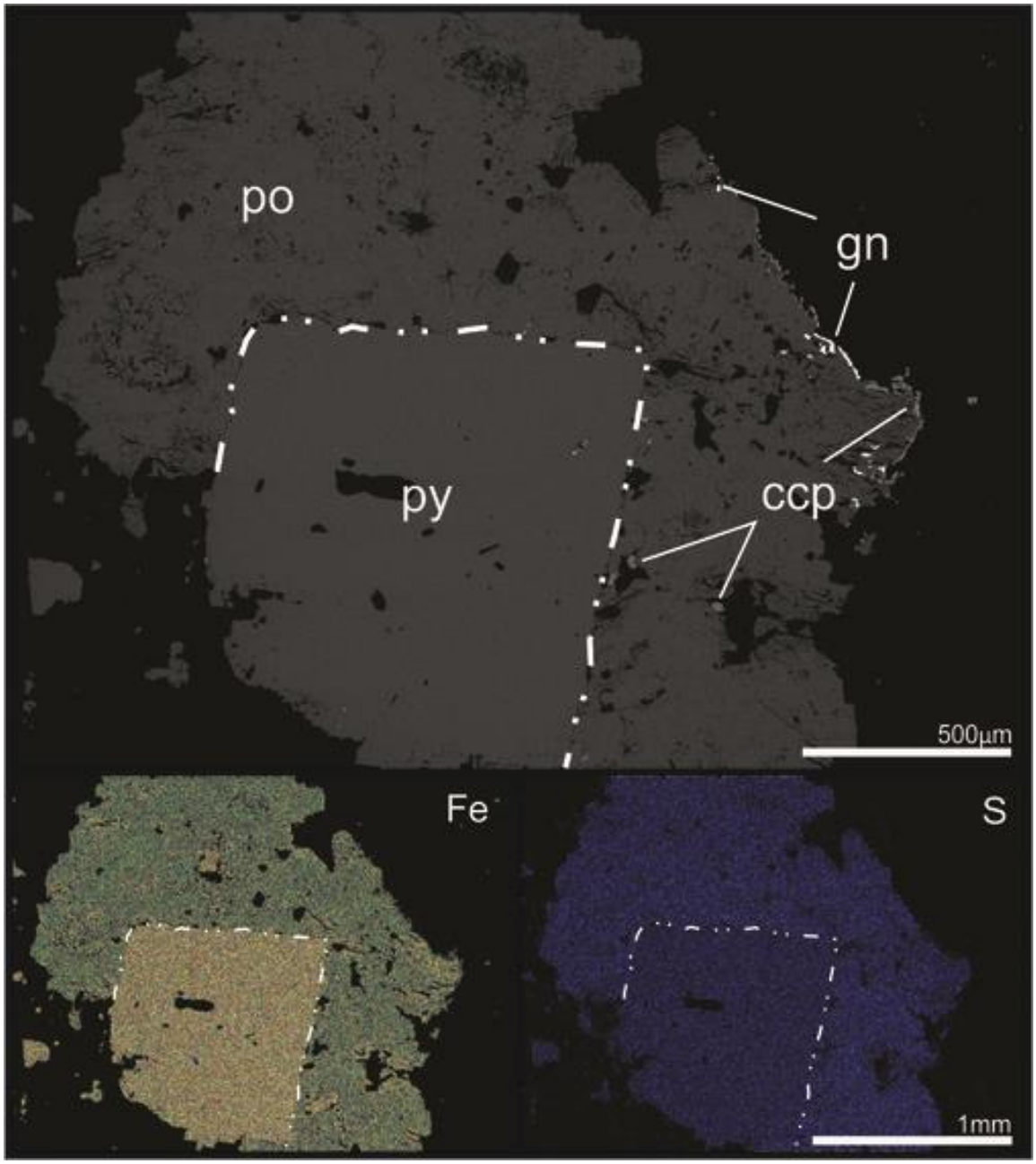

Figure 4.8: **SEM-BSE and EDS X-ray maps of a pyrite grain enclosed by pyrrhotite**. The added hatched white line illustrates grain boundary. A) SEM-BSE image of a large pyrite grain enclosed by pyrrhotite. Pyrrhotite is rimmed with galena and chalcopyrite. SEM-EDS X-ray maps B) highlighting an increase of S within the cubic pyrite grain and C) highlighting an increase of Fe within the fragmental (higher concentration=brighter).

Mineral abbreviations: ccp=chalcopyrite, gn= galena, py=pyrite, po= pyrrhotite, sp=sphalerite

Table 4.1: **SEM-EDS analyses of pyrrhotite, smythite and pyrite in textural association in mudstones,** samples 150.02 and 215.02.

Mineral	S wt%	Fewt%	As wt%	S atomic %	Fe atomic %	Fe atomic % / S atomic %	x
pyrrhotite	39.46	60.54		53.17	46.83	0.88	0.12
pyrrhotite	40.92	59.08		54.68	45.32	0.83	0.17
pyrrhotite	39.62	60.38		53.33	46.67	0.88	0.12
pyrrhotite	40.87	59.13		54.62	45.38	0.83	0.17
smythite	48.89	47.09	1.83	63.56	35.41		
smythite	49.82	46.29	2.02	64.34	34.53		
smythite	49.63	46.6	1.8	64.17	34.83		
smythite	49.22	50.78		62.8	37.2		
smythite	49.89	50.11		63.43	36.57		
smythite	49.58	50.42		63.14	36.86		
smythite	48.63	51.37		62.25	37.75		
smythite	48.39	51.61		62.02	37.98		
smythite	48.48	51.52		62.1	37.9		
smythite	48.22	51.78		61.86	38.14		
smythite	48.54	51.46		62.17	37.83		
smythite	48.93	51.07		62.53	37.47		
smythite	48.6	51.4		62.22	37.78		
smythite	48.45	51.55		62.08	37.92		
smythite	48.34	51.66		61.97	38.03		
smythite	48.23	51.77		61.87	38.13		
smythite	48.54	51.46		62.16	37.84		
smythite	48.46	51.54		62.09	37.91		
pyrite	53.53	46.47		66.73	33.27		
pyrite	53.29	46.71		66.52	33.48		
pyrite	53.75	46.25		66.93	33.07		
pyrite	53.37	46.63		66.59	33.41		
pyrite	53.48	46.52		66.69	33.31		
pyrite	53.17	46.83		66.42	33.58		
pyrite	53.22	46.78		66.46	33.54		
pyrite	53.06	46.94		66.32	33.68		
pyrite	53.31	46.69		66.54	33.46		
pyrite	53.28	46.72		66.52	33.48		
pyrite	53.05	46.95		66.31	33.69		
pyrite	53.38	46.62		66.6	33.4		
pyrite	53.76	46.24		66.94	33.06		
pyrite	53.43	46.57		66.65	33.35		

Note: 'x' is the parameter in $Fe_{1-x}S$, the general formula for pyrrhotite.

Each intergrowth most likely began as pyrite-pyrrhotite, but either upon cooling or an influx of S into the system, pyrrhotite converted to smythite. Equilibrium between pyrite and pyrrhotite only occurs within a specific fS_2 and temperature range (Toulmin and Barton, 1964). Thus, analysis of pyrrhotite in equilibrium with pyrite allows the temperature and fS_2 of the mineralizing fluid to be estimated using the calibration of Toulmin and Barton (1964). The analysis provided a maximum mineralizing temperature constraint of $400^{O}C$.

4.2 Bulk rock analyses

Analyses of drill hole STR-12-02 were taken at one meter intervals with a portable XRF to obtain major and trace element concentrations at different depths, allowing an examination of the relationship between mineralization and whole rock chemistry. The first mineralized anomaly (Zn-Cu-S) was observed at 113.3 m depth hosted within a type IA mineralized vein in basalt. At 150.2 m depth a (Zn-Pb-Cu-S) anomalywas seen within pyritic mudstone (Figure 4.6). Anomalies at 227.2 m, 228.4 m, 247.19 m, 252 m, 256.2 m and 259.07 m (Zn-Pb-S) correspond to type IA mineralized veins within the QFP (Figure 4.6). At depths between 302.26 to 308.1 m anomalies (Zn-Pb-S) were again observed in pyritic mudstone (Figure 4.6) and a (Cu-Fe-Pb-S) anomaly was observed at 415.30 m (Cu-Fe-Pb-S) as a type IA vein hosted in mafic volcanoclastic (Figure 4.6). All geochemical data is summarized in the appendix. It is clear that major mineralization anomalies are associated with pyritic mudstone units and type IA veins.

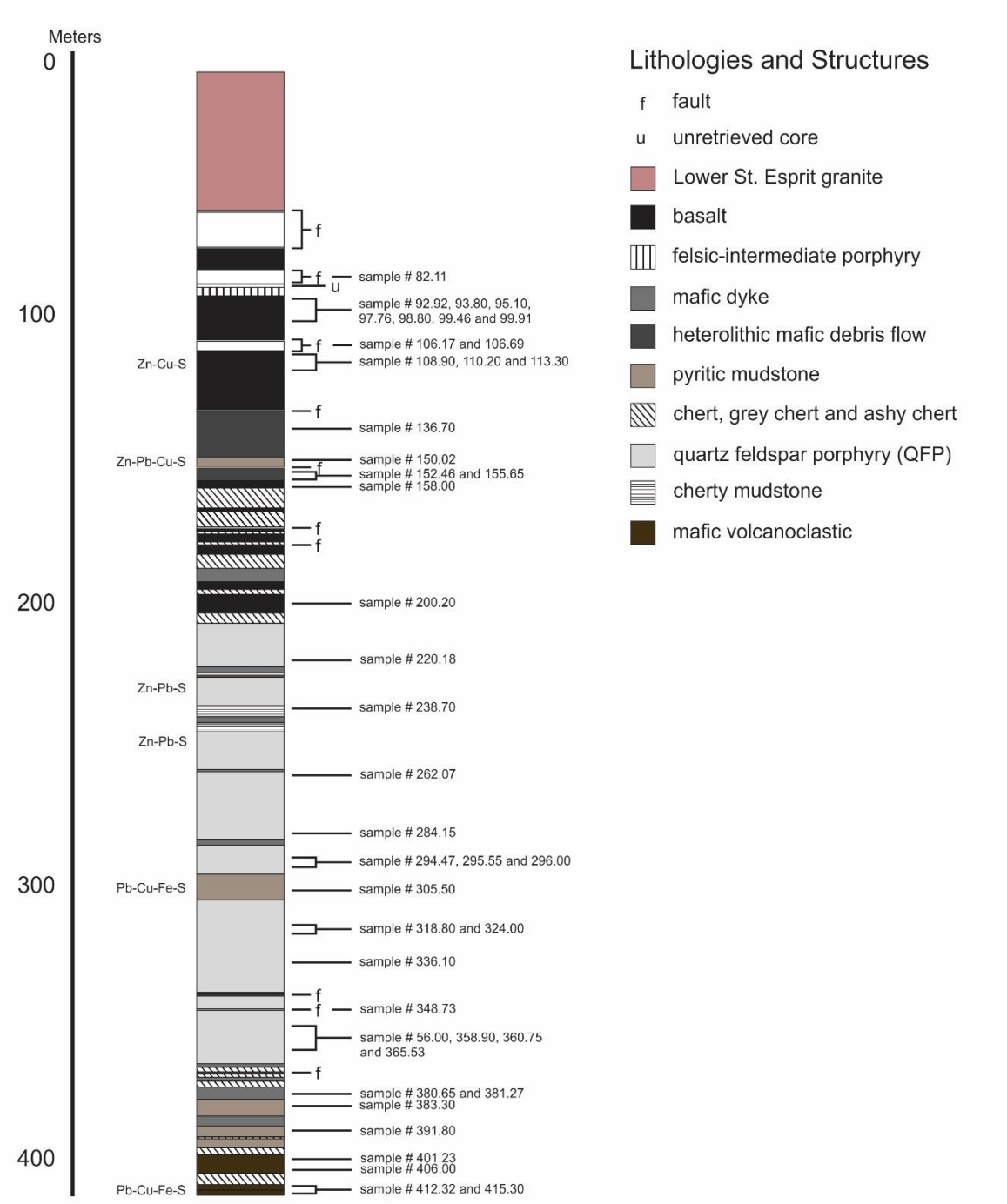

Figure 4.9: Extensive down-hole section of the drill hole STR-12-02. The section shows the host lithology relationships, sample locations and mineralization spikes. Detailed core log and XRF bulk rock analysis presented in Appendix.

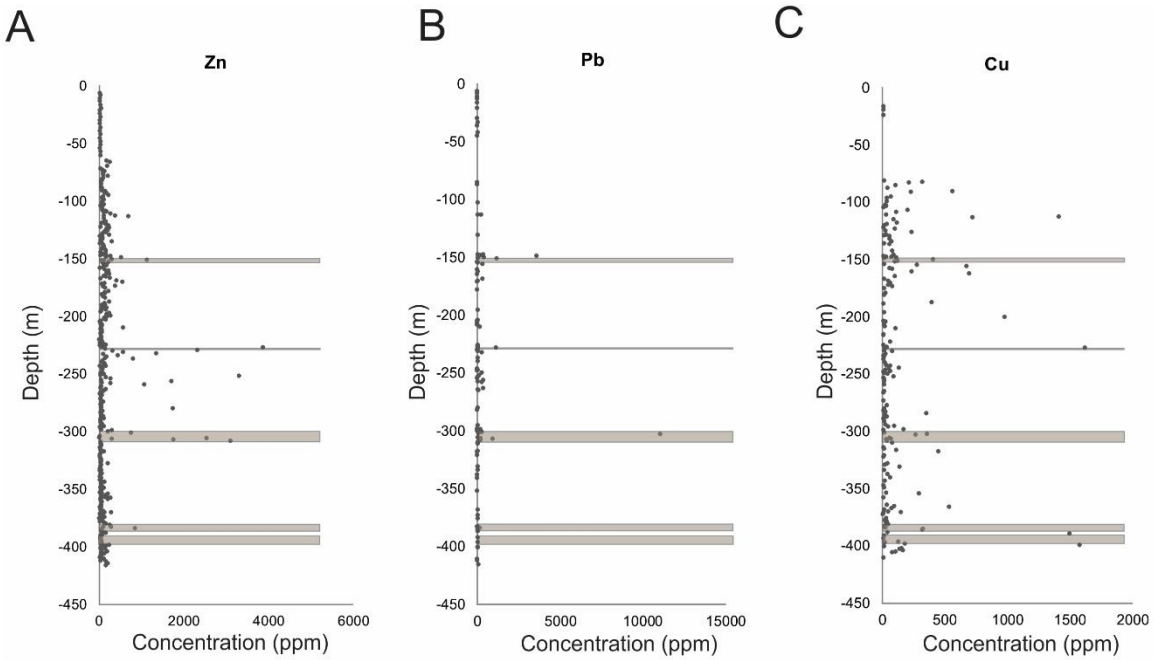
A
Zn
Depth (m)
Concentration (ppm)
B
Pb
Depth (m)
Concentration (ppm)
C
Cu
Depth (m)
Concentration (ppm)

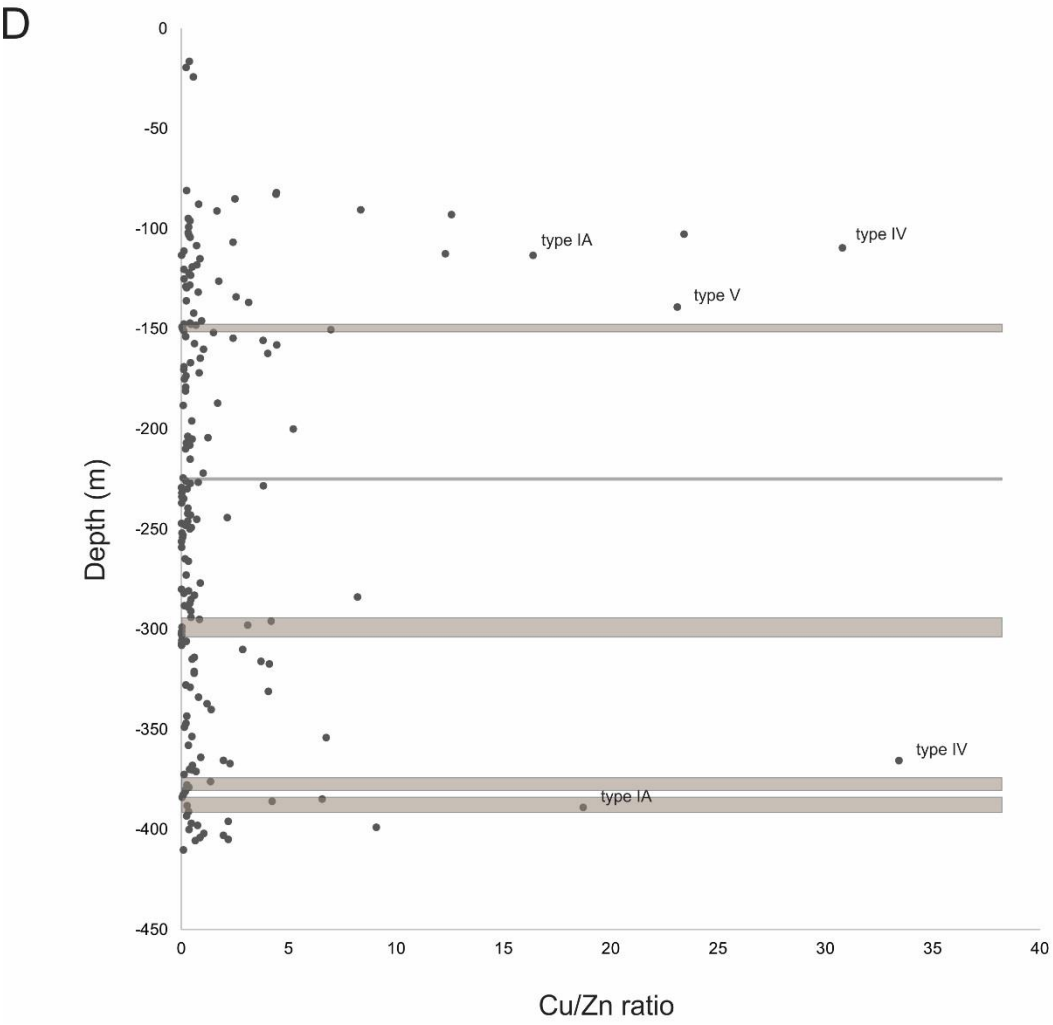
D
type IA
type IV
type V
type IV
type IA
Depth (m)
Cu/Zn ratio

Figure 4.10: previous page. **Bulk rock Zn-Pb-Cu assays and Cu/Zn ratio vs. depth.** Location of mudstone intervals are shown as brown boxes. A) Zn assays, note most enrichments are concentrated in areas of pyritic mudstone. B) Pb assays, note enrichments are concentrated entirely in areas of pyritic mudstone. C) Cu assays, note most enrichments are occurring outside of pyritic mudstone. D) Cu/Zn ratio, locations of high Cu/Zn are denoted with their corresponding vein style. Note high and low Cu/Zn values are occurring within a very close proximity to each other.

Zn, Pb, Cu and Cu/Zn ratio were examined with depth to determine whether they were varying between mineralized areas (Figure 4.10). Samples in areas with high Zn either relate to the host lithology pyritic mudstone or sphalerite bearing veins which commonly show potassic alteration styles (samples 97.76, 109.16, 262.07, 284.15, 294.47, 295.55, 318.80, 336.10 and 360.75)(Figure 4.10A and D). Whereas areas of high Pb follow mudstone distribution closely (Figure 4.10B), high Cu assays correspond to samples where veins IA, IV and V were present (Figure 4.10C and D). Where type IA veins show a potassic rind (within QFP and mudstone host units) the ratios show a great range in Zn and Cu values at a cm scale.

4.4.5 Fluid Inclusion Study

4.4.1 Fluid Inclusion Petrography

Samples chosen for petrographic study were those containing calcite-hosted fluid inclusion assemblages (FIA) in vein types V. Quartz-hosted FIAs ib other vein types (specifically type IA) were not workable because quartz/calcite A grains were cloudy and inclusions were far too small (<3μm) to obtain accurate measurements.

There was no evidence of growth zoning in the calcite crystals or oriented entrapment of the inclusions. However, inclusions do not occur along healed fractures so primary origin is suggested. Two types of calcite host inclusions (calcite A and calcite B). There is a large variation in inclusion size and the number of phases present at room temperature within single assemblages for both calcite types. Inclusions in calcite A contain an aqueous fluid and a vapor bubble; some inclusions contain a solid (halite) phase. Most inclusions are smaller than those within calcite B, with an average diameter of ~10μm;

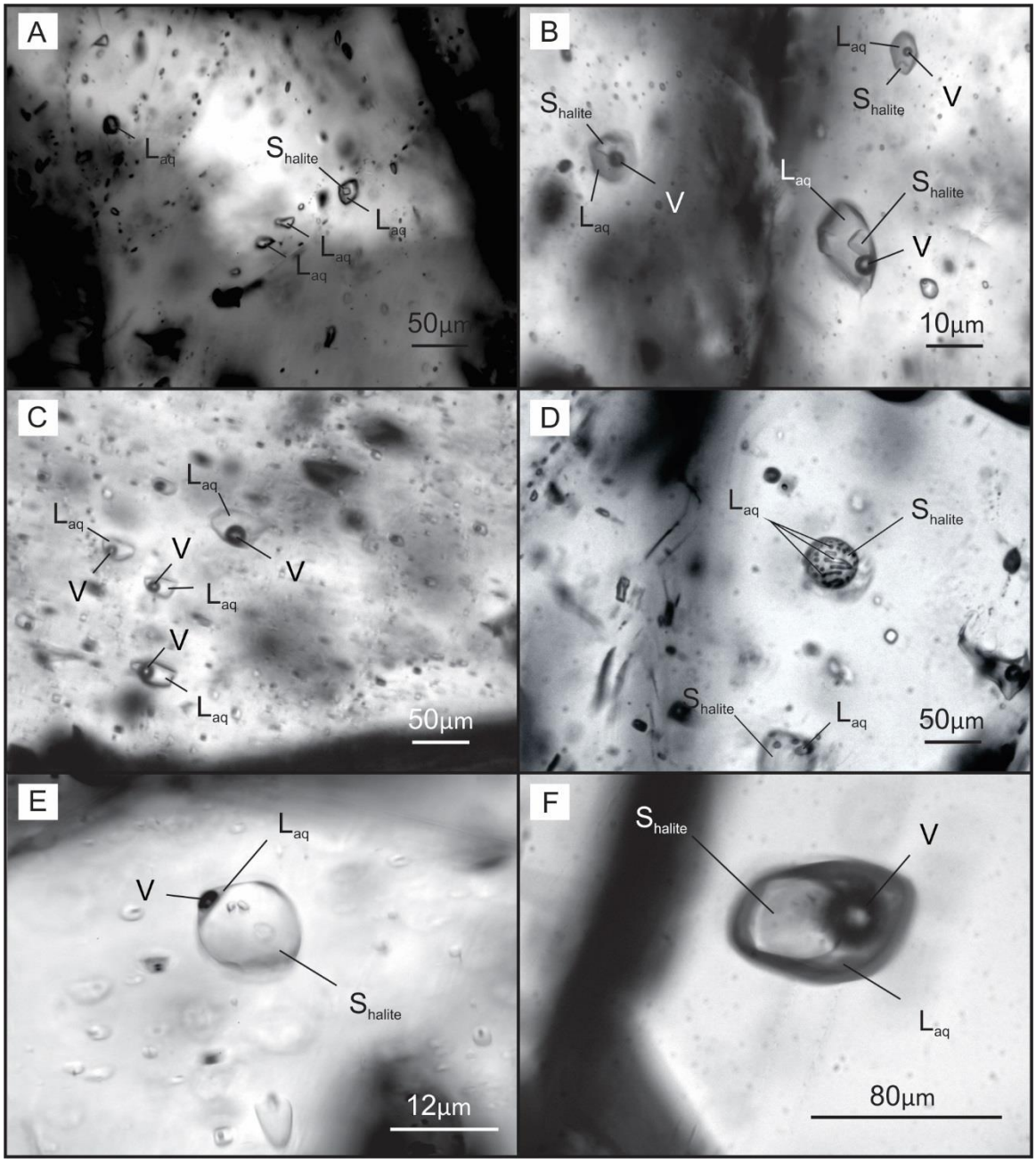

Figure 4.11: **Fluid inclusion petrography and example compositional types.** A) Photomicrograph of multiple one phase liquid (L_{aq}) inclusions and a single two phase L_{aq} + S_{halite} in calcite B. B) Photomicrograph of a fluid inclusion assemblage (FIA) featuring three phase vapor (V) + L_{aq} + S_{halite} inclusions in calcite B. C) Photomicrograph of two phase V + L_{aq} inclusions in calcite A. D) Photomicrograph of a two phase L_{aq} + S_{halite} inclusion where the inclusion is super salt saturated (almost 100% halite) with liquid films running along the inclusion surface in calcite B. E) Photomicrograph of a FIA, three phase V + L_{aq} + S_{halite} where the inclusion is super salt saturated (99% halite) with a very small pouch of liquid and vapor in calcite B. F) Photomicrograph of a large (80µm) three phase V + L_{aq} + S_{halite} – salt saturated inclusion in calcite B.

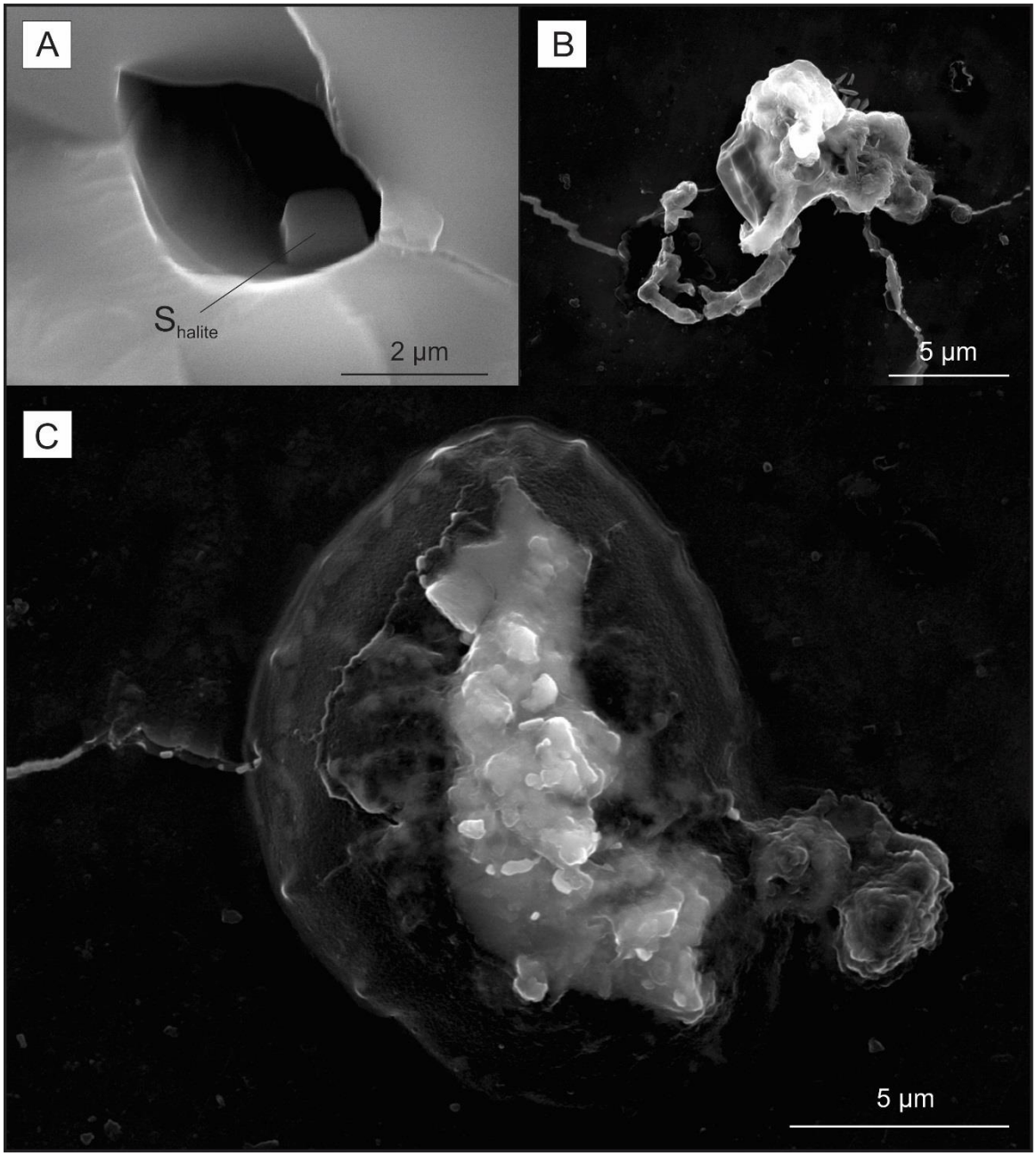

Figure 4.12: **SE High-resolution images of decrepitate salt mounds on calcite crystal surfaces.** A) Inclusion cavity with a defined S_{halite} crystal within. B) A Ca-rich salt mound on the sample surface. C) A large salt mound on calcite surface.

they are anhedral in shape and contain approximately 90% liquid. Calcite B was also host to phase-variant fluid inclusions. On average they have a diameter of 50μm, are anhedral in shape and contained ~75 - 95% liquid. Microscopic observations of fluid inclusions within both A and B calcite at room temperature (20^{o}C) revealed four phase variations: (i) one phase, L_{aq} (Figure 4.11A); (ii) two phase, L_{aq} + V (Figure 4.11C); (iii) two phase, L_{aq} + S_{halite} (Figure 4.11 A and D and (iv) three phase, L_{aq}+V+S_{halite} (Figure 4.11 B, E and F).

Inclusions containing a halite crystal at room temperature have varying salt crystal volume proportions. Figure 4.11 A and B show examples of L_{aq}+S_{halite} and L_{aq}+V+S_{halite} inclusions showing true daughter crystals. Figure 4.11 D, E and F show examples where the inclusion fluid was salt-saturated at the time of entrapment, now containing accidental halite crystals (ranging from 50-99 vol. % halite).

In order to detect the presence of other solutes in the inclusions calcite chips were heated to >500^{o}C in order to decrepitate the inclusions and create salt mounds on the sample surface. SE imaging was used to produce high-resolution image of the sample surface in order to locate salt mounds. Once located by SE imaging the composition of the salt mound was determined by SEM-EDS. Salt mounds had the following composition: Ca (52.1 wt. %), Cl (14.5 wt. %), Na (12.3 wt. %), Fe (8.1 wt. %), Al (4.2 wt. %), K (3.9 wt. %), Mg (2.1 wt. %), F (1.9 wt. %) and S (0.8 wt. %).

Aside from halite, identified by SEM-EDS, a rare scandium yttrium silicate $(Sc,Y)_2Si_2O_7$ (thortveitite) was identified within opened fluid inclusions (Figure 4.13). Due to the open-space filling habit of the thortveitite and its presence in not all inclusions, it was considered to be and accidentally trapped phase, coeval with surrounding fluid and acted as a nucleation point for inclusion formation.

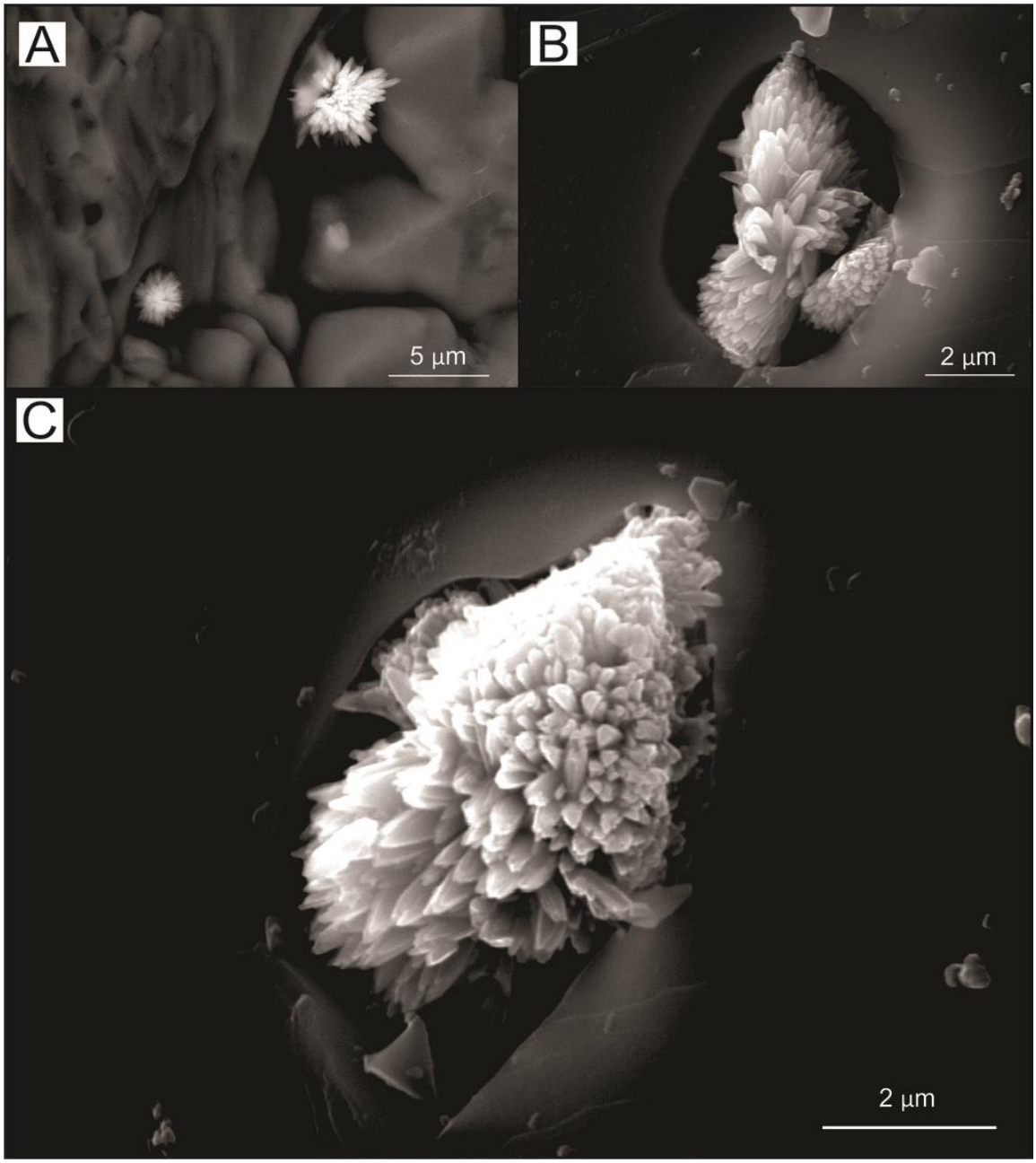

Figure 4.13: **SE high-resolution images of thortveitite within fluid inclusions.** A) SE high-resolution image of two thortveitite grains ranging in diameter from 2-5µm. Both are found within fluid inclusions. B) SE high-resolution image of a thortveitite grain (~5 µm) within a fluid inclusion C) SE high-resolution images of a thortveitite grain (~5 µm) within a fluid inclusion.

Thortveitite is a relatively rare scandium-bearing mineral associated with fluoride-rich fluids and is commonly magmatic in origin (Foord et al. 1993). Worldwide, thortveitite has been identified fewer than a dozen times (Potter and Mitchell, 2005, Dunn, 1995, Foord et al. 1993, Voloshin *et al.* 1991, Bianchi *et al.* 1988, Yamada *et al.* 1980, Amli 1977, Mathiesen 1970, Oftedal 1969, lto *et al.* 1968, Phan *et al.* 1967, Sakurai *et al.* 1962, Neumann 1961).Globally fluorite is commonly texturally associated with thortveitite but their relationship is poorly understood. Foord et al. (1993) believed that thortveitite occurrences are related to pegmatites, implying that fluid at Taylors Brook may have interacted with felsic rocks or had some contribution of (felsic) magmatic fluid added.

4.4.3 Microthermometry

Some FIAs in calcite showed ice formation at temperatures (T_F^{ice}) between -44.3 and -103.2ºC but the majority showed no visible bubble contraction or ice formation so they were cooled to a temperature of -180 ºC to promote freezing in the absence of visible evidence. The very low freezing temperatures suggest a high salinity fluid containing divalent cations. This is in agreement with the BSE decrepitate mound analysis that shows the presence of Ca^{2+}, Mg^{2+} and Fe^{2+}.

As the inclusions were heated there was a darkening of the inclusion associated with eutectic melting observed at temperatures between -65.7 to -26 ºC with an average of -49ºC (n=37). Between these temperatures most inclusions were three phase consisting of L_{aq} +V +$S_{hydrohalite}$. This eutectic range combined with hydrohalite dissolution temperatures (-52 to -12 ºC, n=35) restricts the persisting solid (above 0ºC) to a $CaCl_2$-

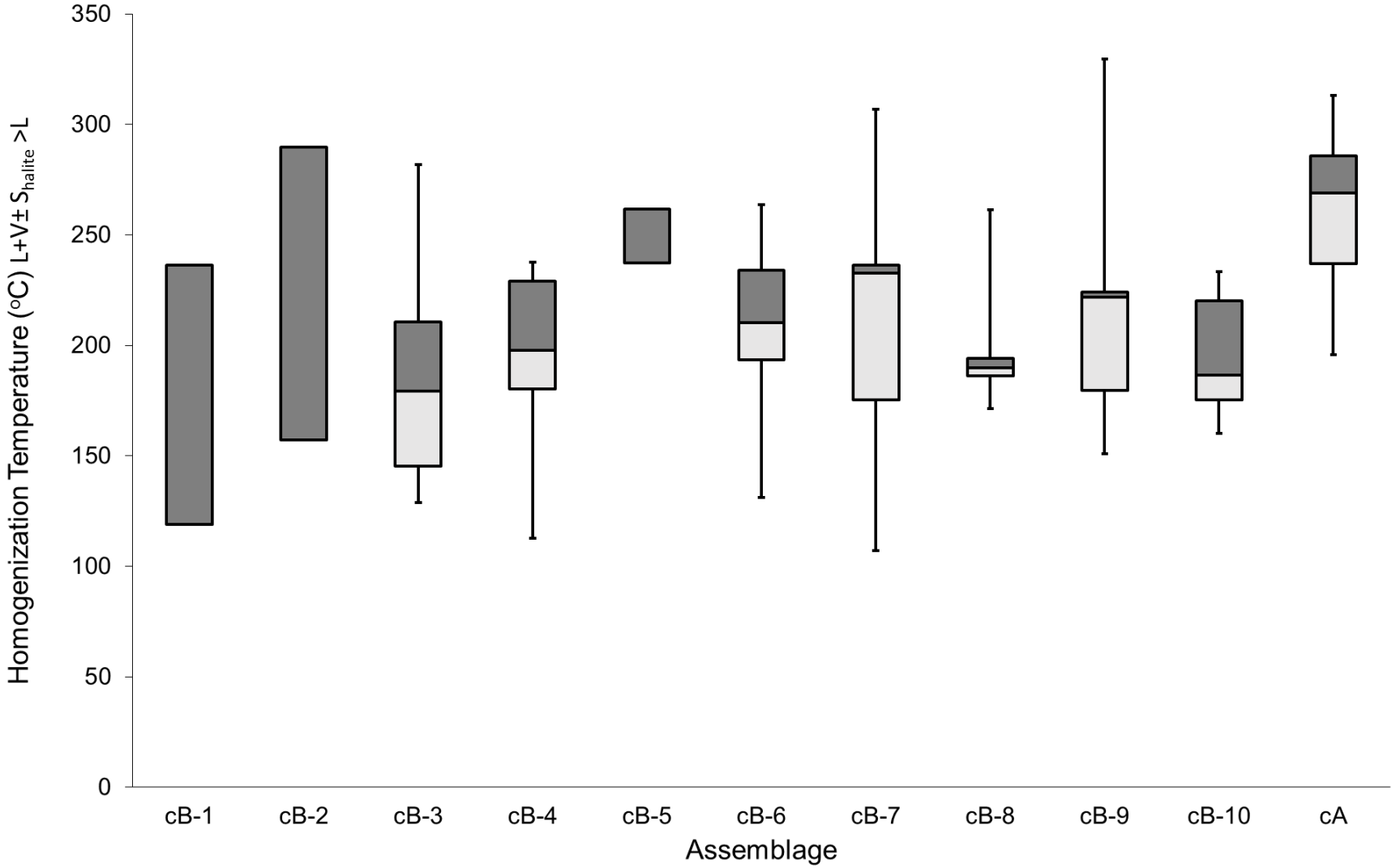
Homogenization Temperature (°C) L+V± S$_{halite}$ >L
350
300
250
200
150
100
50
0
cB-1
cB-2
cB-3
cB-4
cB-5
cB-6
cB-7
cB-8
cB-9
cB-10
cA
Assemblage

Figure 4.14: previous page. **Box and whisker plot of homogenization temperatures.** Homogenization temperatures of a vapor phase in calcite A (cA) and calcite B (cB) fluid inclusion assemblages. Upon homogenization, the two-phase (liquid and vapor) transitioned into a single-phase fluid. The upper limit of each box represents the upper quartile (Q3), or maximum, temperature of the FIA; whereas, the lower limit of each box represents the lower quartile (Q1), or minimum, temperature of the FIA. The whiskers represent maximum and minimum temperatures outliers and were not considered when describing the lower and upper T_h for each FIA.

hydrate. The inclusions contained a solid at temperatures ranging between 12 to 35ºC (n=38), leaving L_{aq}+V only.

Homogenization temperatures (T_h) were measured on inclusions in both calcite A and B; Calcite A had one measured FIA in which inclusions homogenized to liquid between 237 ºC (lower quartile, Q1) to 285 ºC (upper quartile, Q3) and an average of 266.4 ºC (n=19)(Figure 4.14). Calcite B FIAs homogenized to a liquid between 117 ºC (lower quartile, Q1) to 264 ºC (upper quartile, Q3) with an average of 198.5 ºC (n=85) (Figure 4.14). In three phase inclusions where halite crystals were present the halite dissolved at temperatures ranging 202.9 to >310 ºC (n=17). As the inclusions cooled there was no halite nucleation which an indication of metastability.

Final ice melting temperatures ($T_m$ice), antarcticite melting temperatures ($T_m$ant), and rarely, halite dissolution temperatures ($T_m$hl) (Table 4.2) were used to calculate bulk inclusion salinities (wt% total salt, NaCl and $CaCl_2$) using the model of Steele-MacInnis et al. (2011). In inclusions where only $CaCl_2$-hydrate melting was observed, $CaCl_2$ wt% equivalents were estimated graphically using the UNIQUAC model for the binary $CaCl_2$-H_2O systems (Sander *et al.*, 1986). The programs BULK and ISOC (Bakker, 2003) were used to model bulk fluid densities and isochores for fluids in the $CaCl_2$-NaCl-H_2O and $CaCl_2$-H_2O systems. Figure 4.15 shows the resulting isochore range with metamorphic facies to understand and enforce hydrothermal reactions and the pyrrhotite-pyrite boundary temperature constraint of 400ºC.

Table 4.2: **Microthermometric and calculated salinity data.**

Host	Hydrohalite melting (°C)	$CaCl_2$-hydrate melting (°C)	Vapor Homogenization (°C)	Halite Dissolution (°C)	$CaCl_2$ equivalent (wt%)	$CaCl_2$ (wt%)	NaCl (wt%)	$S_{wt\%}$	Density (g/cc)	Phases (20°C)
Cal B		31.7		205.0		43.5	10.0	53.5		L + V + H
Cal B		31.7	164.2	204.8		43.6	9.9	53.5	1.51	L + V + H
Cal B	-23.7	35.4	227.2			49.8	0.1	49.8	1.67	L + V
Cal B		12.2	203.9		40				1.38	L + V + H
Cal B	-37.6	85.9	233.0		59				2.69	L + V
Cal B		28.0	178.8		47				1.56	L + V
Cal B		28.4	164.9	209.8		42.2	10.8	53.0	1.47	L + V + H
Cal B		28.4	186.8	214.8		42.0	11.3	53.3	1.46	L + V + H
Cal B	-12.7	28.4	200.1		47				1.54	L + V
Cal B	-12.2	28.4	186.1		47				1.55	L + V
Cal B	-32.5	21.2	220.0			42.2	0.7	42.9	1.37	L + V
Cal B	-32.5	21.2	232.5			42.2	0.7	42.9	1.37	L + V
Cal B		31.1	235.2		50				1.65	L + V
Cal B		17.3	162.2		42				1.40	L + V
Cal B		17.9	165.5		42				1.40	L + V
Cal B		19.9	179.8		43				1.42	L + V
Cal B	-52.0	22.3	223.0			42.8	0.7	43.4	1.39	V + L
Cal B	-52.2	22.0	198.2			42.6	0.7	43.3	1.40	V + L
Cal B	-52.0	21.5	178.9			42.2	0.7	43.0	1.40	V + L
Cal B		22.9	104.9		44				1.50	V + L
Cal B		15.5	111.5		41				1.41	V + L
Cal B		21.6	235.7		43				1.39	V + L + H
Cal B		25.2	196.6		46				1.49	V+L
Cal B		18.2		274.6		32.5	20.0	52.5		V + L + H
Cal B		24.5	232.1		46				1.43	
Cal B		24.5	233.0		46				1.45	
Cal B		24.5	304.4		46				1.39	
Cal B		26.4	208.8		46				0.85	V + L + H
Cal A	-12.7	76.1	209.6		58				2.52	V + L + H
Cal A		28.4	295.5		47				1.49	V + L
Cal A		26.4	229.0		46				1.48	V + L
Cal B		25.9	221.5		46				1.47	V + L
Cal B		26.1	253.0		46				1.47	V + L
Averages	-23.8	31.3	210.9	210.8	46	42.3	6.0	48.3	1.51	

note: inclusions in column $CaCl_2$ equivalent (wt%) were estimated using UNIQUAC model for the binary $CaCl_2$-H_2O systems (Sander *et al.*, 1986). Inclusions with calculated $CaCl_2$ and NaCl wt% were derived from the model of Steele-MacInnis et al. (2011).

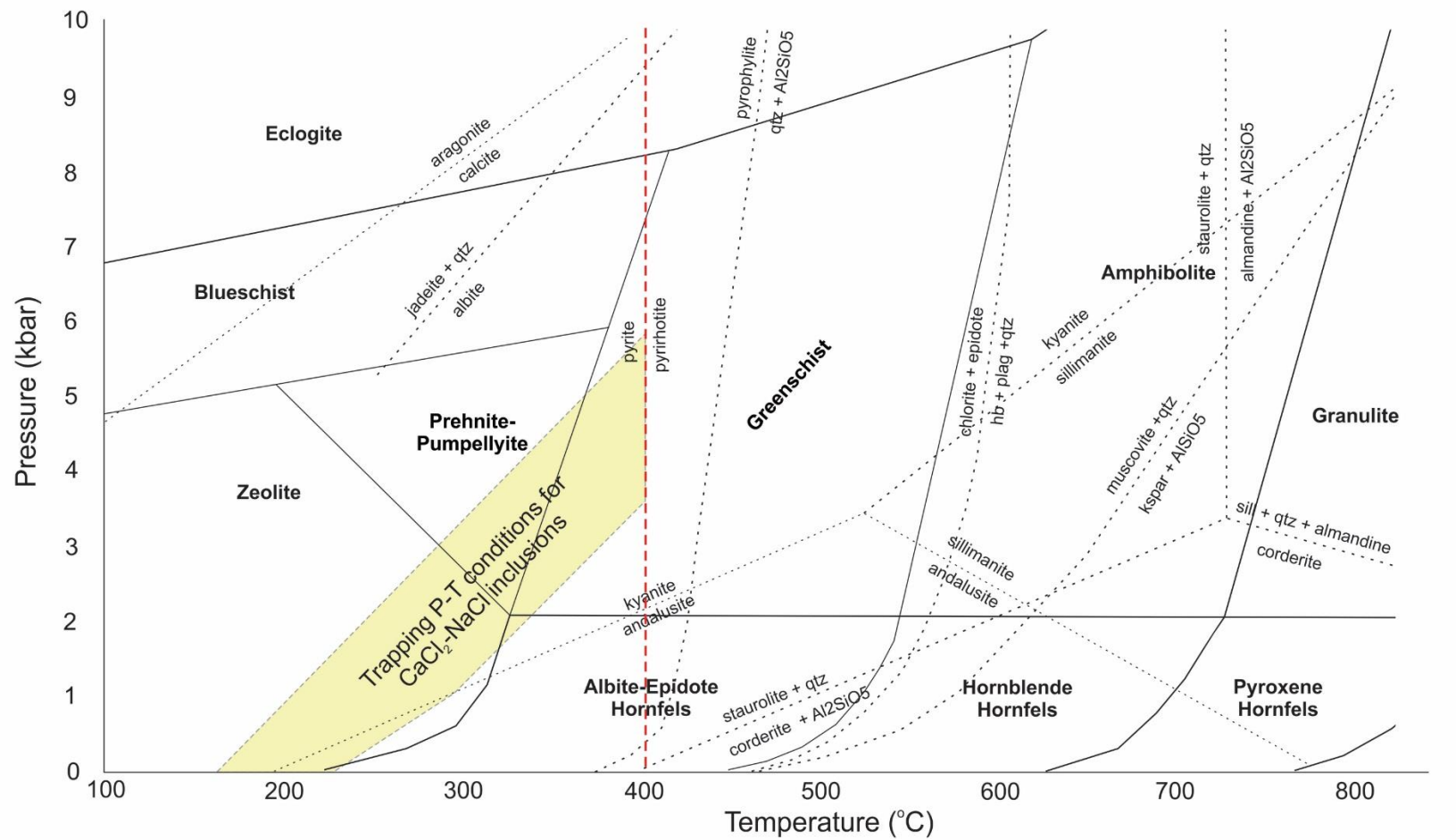

Figure 4.15: **Trapping pressure-temperature constraints for $CaCl_2$-NaCl-H_2O inclusion**s. The metamorphic facies are shown to help enforce hydrothermal alteration assemblages at temperatures and pressures seen within the mineralizing vein styles. Also plotted in red is the pyrite - pyrrhotite stability boundary, obtained by analysis of pyrrhotite in the pyritic mudstones and using T-fS_2 compositional relations from Toulmin and Barton 1964. This constrains the maximum temperature of mineralization to 400ºC and 5kbar.

5.0 Discussion

5.1 Mineralization and hydrothermal vein paragenesis

Based on the cross cutting relationships and bulk geochemistry data the hydrothermal system at Taylors Brook involved the circulation of a Zn-Cu-Pb-Ag-Te rich fluid leading to mineralized type IA veins. The alteration assemblages associated with this earliest mineralizing event are propylitic-potassic. Zoning in epidote in the veins is caused by variations in the Fe/Al ratio suggesting that fO_2 is fluctuating causing compositional zoning and replacement textures among hydrothermal minerals, as well as deposition of Zn-Pb-Cu sulphides. Also seen in the mineralized sulphidic mudstones is pyrrhotite altered to symthite, caused by fluctuating fS_2 or cooling, or both. Both the pyrrhotite-smythite replacement reaction and the epidote zoning is are important features because they suggest that a combination of cooling, fluctuating fO_2 and fS_2 were important steps in mineralization. These parameters rendered the metals insoluble causing their precipitation within vein type IA and in the mudstones. Textural observations conclude that spaherite, galena and chalcopyrite were precipitated late, after pyrrhotite altered to smythite.

The slightly later subset of barren type IB vein has an alteration assemblage of epidotization and silicification. The hydrothermal fluid must still be enriched with Mg-Al-Fe, a high Na content due to loss of K associated with the preceeding potassic alteration, and also added secondary silica.

Type II veins have associated alteration assemblages are serpentinization- propylitic. The hydrothermal alteration resulted in forsterite and orthopyroxene reacting to produce

serpentine and talc (Wolfgang *et al.* 2006) with the fluid enriched in Mg-Al-Fe. Type III veins have a propylitic alteration style associated with a fluid enriched in Mg-Al-Fe. Type IV veins have a potassic-carbonatization-zeolitic assemblage indicating a fluid rich in Al-Si-K-Na but deprived of Fe-Mg-Ca. The presence of analcime also indicates the fluid originated from fluids in equilibrium with silica-undersaturated rocks and is likely occurring at relatively low temperatures compared to earlier vein styles.

The fluid chemistry undergoes a notable change during Type V vein deposition. The presence of thortveitite $(Sc,Y)_2Si_2O_7$ indicates the fluid has some evolved felsic magmatic contribution. The fluid was enriched in Cu-Pb-Zn-Sc-Y-Ag-Te and had a bulk composition consistent with a Ca-Na-Cl hypersaline brine. The alteration assemblages associated with this late mineralizing event are silicification-carbonatization. Barren type VI record a late silicification distributed throughout the entire system.

5.2 Fluid origin in type V veins

In the interest of fluid origin and based on the results of the microthermometry and salinity studies, it was concluded that the trapped fluid in type V veins was an unusually high salinity and rich in divalent cations and anions (ie. Ca^{2+}, Mg^{2+}, S^{-2}) but particularly enriched in Ca. This distinct fluid composition can only be formed naturally under specific conditions and is very atypical of VMS fluids which are typically much lower in salinity, Na-dominant and commonly show evidence of boiling (Crowe, 1992 and Ohmoto, 1996).

There are four conceivable explanations for this Ca rich fluid. The first is boiling; if boiling of a Ca-rich fluid occurs the fluid can become supersaturated in salt as the liquid

(water) vaporizes. Eventually after some boiling, salt crystals would start to form in the system as the solution left from boiling becomes supersaturated in salt. In the case of the Taylors Brook showing this is most likely not the case because the fluid inclusions present do not show variable phase ratios consistent with boiling (Steele-MacInnis, 2012).

A second process that could lead to the formation of Ca-rich fluid is a cation exchange between Na and Ca; if a fluid initially carrying Na passes through the Ca-rich (Ca-plagioclase, Ca-pyroxene) volcanic country rocks can exchange between fluid and rock as temperature decreases. This would cause the fluid to become increasingly Ca-rich. (Hannachi, 2009) For example, if albitization (formation of Na-rich plagioclase) occurs, the Na^+ from a fluid is needed but as it goes into the structure of the feldspar, Ca^{2+} is released back into the fluid. Within the sample suite no albitization is observed suggesting this is not the case at the Taylors Brook showing.

A third explanation is evaporation of Ca rich paleoseawater; $CaCl_2$ basinal brines inherited their chemistry and salinity from evaporated paleoseawaters when Earth's oceans were Ca-rich and SO_4-poor ($CaCl_2$ seas) (Lowenstein *et al,. 2003)*. This coincided with periods of rapid seafloor spreading and high outfluxes of mid-ocean-ridge brines rich in $CaCl_2$. Later, elevated sea levels were associated with conditions that favored pore-space accumulation of marine $CaCl_2$ brines in marginal and interior continental basin sediments (Lowenstein *et al,. 2003)*. In evaporitic sequences the first saturation of a salt phase involves halite (NaCl) and as Na is removed from solution, the Ca concentration in the residual fluid increases. Eventually, the remaining fluid becomes Ca-rich and is otherwise known as a "bittern" brine. If this bittern brine gets trapped in sediments, or if it infiltrates basement rocks, fluid inclusions containing the Ca-rich brine can be trapped

(Spencer, 1987). However, a fluid this Ca-rich would be very late stage in the evaporitic sequence when residual fluid volumes are very low. The hydrothermal fluid needed for mineralizing and altering processes seen at the Taylors Brook showing greatly exceeds that generated in a late stage evaporitic sequence.

The fourth and most likely explanation is dissolution of an existing evaporitic sequence containing gypsum or carbonates by a hydrothermal fluid causing an increase in Ca fluid concentration. This is a probable explanation because bedrock surrounding Bras d'Or lake, immediately north of the Taylors Brook showing comprises the Carboniferous (330-338 Ma) upper (mudstone, sandstone, minor conglomerate, gypsum and shallow marine limestone, 100-700m), middle (halite, anhydrite, gypsum, mudstone, siltstone, sandstone and conglomerate, 300m) and lower (anhydrite, salt, gypsum, shale, marine dolostone and limestone, >150m) Windsor Group. However, this does not explain the high salinity of the fluid since dissolution of halides would contribute abundant Na and K to the evolving fluid but not Ca. Dissolution of a halide-gypsum-carbonate package could source both the observed salinity and Ca rich nature of the fluid.

5.3 Implication for mineral exploration

Exploration for this style of mineralization should focus in areas in proximity evaporates. Since these target areas help to explain the formation of the Ca-rich fluids that were responsible for metal transport.

It is also important to identify alteration styles associated with mineralization, notably potassic-propylitic-silicification-carbonatization assemblages. These alteration styles may

be identified directly during core logging. Thin section petrography is most appropriate because of the complexity of vein styles identified.

Once alteration styles/assemblages are confirmed, it is important to identify pathfinder elements associated with the hydrothermal system by XRF or SEM analysis; notably, K-Cu-Zn-Pb-Sc-Y-Ag-Te-S. The element most impacted by hydrothermal remobilization after pyritic mudstone mineralization is Cu (Figure 4.10).

5.4 Comparison to the Stirling deposit and other VMS systems

The Taylors Brook showing and Stirling deposit show similar host rock lithologies, alteration and mineralization styles. However, the most prominent alteration assemblage (quartz-talc-carbonate [QTC]) found at the Stirling deposit (O'Reily, 2008) is not present at the Taylors Brook showing. This alteration assemblage is particularly important due to its association with sulphide mineralization at the Stirling deposit. It is thought that the QTC rock is either an exhalative layer related to the same processes that gave rise to the massive sulphide lenses as hydrothermal plumes vented out onto the sea floor, or hydrothermal replacement of the host volcanics (*O'Reilly, 2008*). Perhaps, the Taylors Brook showing is a distal expression of these products.

The Duck Pond-Lemarchant deposits in Newfoundland are also comparable to the Taylors Brook showing. Both Duck pond and Lemarchant are situated in the northeast trending Tally Pond volcanic belt. Duck Pond is a Cu-Zn-Pb-Ag-Au VMS deposit hosted within felsic volcanic and volcaniclastic rocks and sedimentary rocks with mineralization occurring in numerous lenses (*Piercey et al., 2012*). Textural associations are interpreted

Table 5.1: A comparison of the Taylors Brook showing to other VMS systems

Deposit	Host Rocks	Key Alteration styles	Mineralization type
Taylors Brook occurrence Cu-Zn-Pb-S (Sc, Y, Ag, Te) (This study)	basalt/andesite flows, quartz feldspar porphyry, pyrite-pyrrhotite bearing mudstone, cherty mudstone, chert, andesitic lapilli tuff and ash.	propylitic-potassic	Zn (Pb) mudstones with overprinting vein hosted Cu (Zn)
Stirling deposit Zn-Pb-Cu-Fe(Ag,Au) (Kontak, 1997; O'Reily 2008)	monolithic felic breccia, pyritiferous-cherty zones, chert, basalt and basaltic andesite flows, felsic tuff, rhyolite porphyry, gabbro, and sedimentary rocks.	quartz-talc-carbonate (QTC)	multiple sulphide lenses (Zn-Cu-Pb)
Duck Pond deposit Cu-Zn-Pb (Ag,Au) (Piercey et al., 2012)	rhyolite flows and tuff breccias, pyrite-pyrrhotite bearing mudstone	sericite-silicification-chloritization	multiple sulphide lenses(Cu-Zn-Pb), grading inward to a Cu-rich center
Lemarchant deposit Cu-Zn-Pb (Ag,Au) (Squires et al., 1991, 2001)	felsic volcanic breccias, flows, lapillistone and lapilli tuffs, pyrite-pyrrhotite bearing mudstone	sericite-silicification-chloritization	semi-massive to massive sulphide (Cu-Zn-Pb) mineralization

to represent replacement-style mineralization (Squires et al., 1991, 2001). The Lemarchant deposit is a Cu-Pb-Zn-Ag-Au VMS deposit hosted within felsic volcanic breccias, flows, sedimentary rocks, lapillistone and lapilli tuffs with semi-massive to massive mineralization (*Fraser et al., 2012*). Both are classified bimodal felsic type VMS (formerly Kuroko-type). They are polymetallic in that they contain approximately equal enrichments in all three ore metals (Zn, Cu and Pb).

The Taylors Brook showing has features consistent with the bimodal felsic type VMS classification but its fluid characteristics from late mineralizing veins (type V) are inconsistent with VMS and are consistent with sediment hosted base metal deposits formed from Ca-rich basinal brines (eg. Mt. Isa, Australia: Heinrich *et al.*, 1995)

4.0 Conclusions

1. The hydrothermal system consists of 7 vein types and their relative order of formation is type IA, IB, II, III, IV, V and VI veins.

2. Alteration styles associated with mineralization events are potassic-propylitic-silicification-carbonatization.

3. Replacement textures and compositional zoning in epidote is caused by varying Fe/Al, corresponding to varying Fe^{3+}/Fe^{2+} ratios in associated fluids. This suggests that the fO_2 of the system was fluctuating, an important mechanism for metal precipitation.

4. The presence of thortveitite in type V veins indicates that the fluid at the Taylors Brook showing must have passed through felsic rocks or had some contribution of felsic magmatic fluid, and indicates that Sc and Y were mobile.

5. In the sulphidic mudstones, a replacement reaction from pyrrhotite to smythite occurred either by cooling or via an influx of S_2 into the system. Zn-Pb(Cu) sulphide precipitation in the mudstones occurred after smythite formation.

6. Equilibrium between pyrite and pyrrhotite only occurs within a specific fS_2 and temperature range. This constrains the maximum temperature of mineralization to 400^{o}C for the pyrrhotite composition at Taylors Brook.

7. Bulk rock analyses identified Cu-Zn(Pb) and Zn,Pb(Cu) anomalies to be associated with type IA veins and sulphidic mudstone, respectively. Bulk rock analyses also showed Cu/Zn ratios to be varying widely with depth and from vein type to vein type reflecting Cu remobilization.

8. Fluid inclusion petrography in type V veins identified four phase variations within calcite at room temperature (20^{o}C). Inclusions containing a halite crystal at room temperature have varying salt crystal volume proportions, with some clearly containing accidentally trapped salt crystals (ranging from 80-95 vol. % halite). This indicates that the fluid was salt saturated at the time of entrapment.

9. Microthermometry shows hydrohalite melting temperatures averaging -23.8^{o}C, antarcticite melting temperatures averaging 31.3^{o}C and halite dissolution temperatures averaging 210.90^{o}C. Homogenization or minimum trapping temperature averaged 210.90^{o}C, and was combined with fluid inclusion salinities and densities to create isochores. Isochoric data combined with pyrrhotite-pyrite equilibrium constrains a maximum pressure to 5 kbar and temperature to 400^{o}C.

11. The most likely source for ta high Ca-brine is either evaporation of a Ca-rich paleoseawater or dissolution of gypsum/carbonate/halide units, possibly the Windsor group. However, if this is true, then the mineralizing fluid must significantly post-date the associated host rocks, which is inconsistent with a VMS system.

12. The Taylors Brook showing has features consistent with the bimodal felsic type VMS classification but its fluid characteristics from late mineralizing veins (type V) are inconsistent with VMS and are consistent with sediment hosted base metal deposits formed from Ca-rich basinal brines (eg. Mt. Isa, Australia: Heinrich *et al.*, 1995)

5.0 References

Amli, R. 1977: Carbonatites, a possible source of scandium as indicated by Sc mineralization in the Fen peralkaline complex, Southern Norway; Economic Geology, v.72, p.855-869

Bach, W., Paulick, H., Garrido, C., Ildefonse, B., Meurer, W. and Humphris, S. 2006: Unraveling the sequence of serpentinization reactions: petrography, mineral chemistry, and petrophysics of serpentinites from MAR 15^{o}N (ODP Leg 209, Site 1274); Geophysical Research Letters, v.33, p.1-4

Bailes, A. and Galley, A. 1999: Evolution of the Paleoproterozoic Snow Lake arc assemblage and geodynamic setting for associated volcanic-hosted massive sulphide deposits, Flin Flon Belt, Manitoba, Canada; Canadian Journal of Earth Sciences, v.36, p.1789-1805

Bakker, R. 2003: Package FLUIDS 1. Computer programs for analysis of fluid inclusion data and for modelling bulk fluid properties; Chemical Geology, v. 194, p.3-23

Bianchi, R., Pilati, T., Diella, V., Gramaccioli, C.M. and Mannucci, G. 1988: A re-examination of thortveitite; American Mineral, v.73, p.601-607

Bonnet, A. L., and Corriveau, L. 2007: Alteration vectors to metamorphosed hydrothermal systems in gneissic terranes, in Goodfellow, W.D., ed., Mineral deposits of Canada—A synthesis of major deposit types, district metallogeny, the evolution of geological provinces, and exploration methods: Geological Association of Canada, Mineral Deposits Division, Special Publication No. 5, p. 1035–1049.

Canet, C., Franco, S., Prol-Ledesma, R., González-Partida, E., and Villanueva-Estrada, R. 2011: A model of boiling for fluid inclusion studies: Application to the Bolaños Ag–Au–Pb–Zn epithermal deposit, Western Mexico; Journal of Geochemical Exploration, v.10, i.2, p.118-125

Carr, P. and Cathles III, L. 2008: On the Size and Spacing of Volcanogenic Massive Sulfide Deposits within a District with Application to the Matagami District, Quebec; Society of Economic Geologists, v.103, n.7, p.1396-1409

Crowe, D., Nelson, S. Shanks, W and Valley, J. 1992: Geology and geochemistry of volcanogenic massive sulfide deposits and related igneous rocks, Prince William Sound, south-central Alaska; Economic Geology, vol.87, n.7, p.1722-1746

DNR Mineral Resources Branch, 2010: Geology Matters 2010: Growing the Economy; Nova Scotia Minerals Update, v.24, n.4

Dunn, P.J. 1995: Franklin and Sterling Hill New Jersey: the world's most magnificent mineral deposits; Mineralogical Magazine., v.60, i.3, p.537-538

Fraser, D. and Giroux, G. 2012: NI 43-101 Technical report and mineral resource estimate on the Lemarchant deposit, South Tally Pond VMS deposit, Central Newfounland, Canada; Paragon Minerals Corperation

Freeman, A., A.J.E, Bird, D. Friðleifsson G. 2009: Hydrothermal Minerals Record CO_2 Partial Pressures in the Reykjanes Geothermal System, Iceland; American Journal of Science, v.309, n.9, p.788-833

Hannachi, C., Hamrouni, B. Dhahbi, M. 2009: Ion exchange equilibrium between cation exchange membranes and aqueous solutions of K + /Na + , K + /Ca 2+ , and Na + /Ca 2+; Ionics, vol.15, n.4, p.445-451

Hannington, M.D., Santaguida, F., Kjarsgaard, I.M., and Cathles, L.M. 2003: Regional-scale hydrothermal alteration in the Central Blake River Group, western Abitibi subprovince, Canada: implications for VMS prospectivity; Mineralium Deposita, v.38, p.393-422

Heinrich, C., Bain, J., Mernaugh T., Wyborn, L., Andrew, A. S. and Waring C. L. 1995: Fluid and mass transfer during metabasalt alteration and copper mineralization at Mount Isa, Australia; Economic Geology, v.90, p.705–730.

Ishihara, S. 1974: Geology of Kuroko deposits; Tokyo; Society of Mining Geologists of Japan; Mining geology special issue, n.6, p.645-666

Ito, J. and Frondel, C. 1968: Syntheses of the scandium analogues of aegirine, spodumene, andradite, and melanotekite; American Mineralogy, v.53, p.1276-1280

King, H. 2005: Epidote; http://geology.com/minerals/epidote.shtml

Kontak, D.J. 1997: Preliminary Results of Geological and Geochemical Studies at the Stirling Deposit with Emphasis on Quartz-talc-carbonate (QTC) Rock Associated with Massive Sulphide Ore; NSDNR Report of Activities, p.49-70

Kontak, D.J. 1997: Observations on Field Relationships, Petrology and Metallogeny of Southeast Cape Breton Island; NSDNR Report of Activities, p.27-48

Koo, J. and Mossman, D. 1975: Evaluation of primary and secondary geological processes at the Flin Flon Cu-Zn deposit, Manitoba and Saskatchewan, Canada, using factor-vector analysis of ore geochemistry; Chemical Geology, v.16, p.1-14

Lee, K.Y. 1970: Some Rare earth mineral deposits in mainland China; U.S Geological Survey Bull., 1312N: p.N1-N34

Lowenstein, T.A., Hardie, L.A., Timofeeff, M.N, and Demicco, R.V. 2003: Secular variation in seawater chemisty and the origin of calcium chloride basinal brines; Geology, v.31, no. 10, p.857-860

Macdonald, A.S. and Barr, S.M. 1993: Geological setting and depositional environment of the Stirling Group of Southeastern Cape Breton Island, Nova Scotia; Atlantic Geology, v.29, p.137-147

Mathiesen, C.O. 1970: An occurrence of unusual minerals at Bidjovagge, northern Norway; Norges Geology Unders, v.266, p. 86-104.

Miller, C.K. 1979: The Geological setting and Environment of base metal deposition of the Mindamar Mine, Stirling, Richmond County, Nova Scotia; Unpublished M.Sc. thesis, Dalhousie University, Halifax, Nova Scotia, p.10-40

Neumann, H. 1961: The scandium content of some Norwegian minerals and the formation of thortveitite, a reconnaissance survey; Norwegian Geology Tidsskr, v.41, p.197-210

Ohmoto, H. 1996: Formation of volcanogenic massive sulfide deposits: The Kuroko perspective; Ore Geology Reviews, vol.10, n.3, p.135-177

O'Reily, G. 2008: Volcanogenic Massive Sulphides at the Stirling Zn-Pb-Cu Deposit; Mineral Inventory Files, Nova Scotia Minerals update, p.5

Oftedal, I. 1969: Minor elements in thortveitite; Narsk GeoIogy, v.49, p.77-79.

Petts, D., Longstaffe, F., Potter, J. Barr, S., and White, C. 2012 : Regional hydrothermal alteration and ^{18}O-depletion of the ca. 620 Ma Huntington Mountain pluton and related rocks, Cape Breton Island, Canada; Atlantic Geology, v.48

Phan, K.D., Fiossy, B. and Kerjean, M. 1967: le scandium dans les mineraux et les roches encaissantes de certaines pegmatites malagaches. Bureaux Recherche Géologie minéralogie, v.3, p.77-97.

Piercey, S. and Hinchey, J. 2012: Volcanogenic Massive Sulphide (VMS) deposits of Central Mobile Belt, Newfoundland; Field Trip Guidebook- B4, GAC-MAC, p.14-16

Potter, E.G. and Mitchell, R.H. 2005: Mineralogy of the Deadhorse Creek volcaniclastic breccia complex, northwestern Ontario, Canada; Contributions to Mineralogy and Petrology, v.150, 9.212-229

Reid, M.G. 2014: Petrography and Geochemistry of Drill Core from the Taylors Brook Property in the Stirling Belt, Southeastern Cape Breton Island, Nova Scotia; Unpublished B.Sc thesis, Acadia University, Wolfville, Nova Scotia. 73pgs.

Roscoe, W.E 1986: Report on the Stirling Property Cape Breton Island, N.S for Wilco Mining Company Limited by Roscoe Mining Service Inc.; Nova Scotia Department of Natural Resources Assessment Report, p.86-156

Sander, B., Rasmyssen, P. and Fredenslund, Aa. 1986: Calculation of Solid-Liquid Equilibria in Aqueous Solutions of Nitrate Salts Using an Extended UNIQUAC Equation; Chemical Engineering Science, v.41, p.1197-1202

Sakurai, K., Nagashima, K. and Kato, A. 1962: Thortveitite from Kobe Omiya Kyoto, Japan; Bulletin of Chemical Society of Japan v.35, p.1776-1779

Spencer, R. 1987: Origin of Ca-Cl brines in Devonian formations, western Canada sedimentary basin; Applied Geochemistry, v.2, i.4, p.373-384

Squires, G.C., Brace, T.D. and Hussey, A.M. 2001: Newfoundland's polymetallic Duck Pond deposit: Earliest Iapetan VMS mineralization formed within a sub-seafloor, carbonate-rich alteration system. In Geology and Mineral Deposits of the Northern Dunnage Zone, Newfoundland Appalachians. Field Trip Guide A2,: St. John's, NL, Geological Association of Canada/Mineralogical Association of Canada, p.167-187.

Squires, G.C., MacKenzie, A.C. and MacInnis, D. 1991: Geology and genesis of the Duck Pond volcanogenic massive sulfide deposit. In Metallogenic Framework of Base and Precious Metal Deposits, Central and Western Newfoundland. Geological Survey of Canada, Open File 2156, p.56-64.

Steele-MacInnis, M., Bodnar, R.J., & Naden, J. 2011: Numerical model to determine the composition of H2O-NaCl-CaCl2 fluid inclusions based on microthermometric and microanalytical data. Geochimica et Cosmochimica, Acta 75, p.21-40

Steele-MacInnis, M., Bodnar, R.J., & Lecumberri-Sanchez, P. 2012: A numerical model to estimate trapping conditions of fluid inclusions that homogenize by halite disappearance; Geochimica et Cosmochimica Acta, 1, vol.92, p.14-22

Toulmin, P., and Barton, P.B. 1964: A thermodyanmic study of pyrite and pyrrhotite. Geochimica et Cosmochimica Acta, 28, p.641-67l.

Voloshin, A.V., Gordienko, V.V. and Pakhomovskii, Y.A. 1991: Scandium mineralization and the first find of thortveitite, Sc2Si2O7, in granitic pegmatites of the Kola Peninsula; Dokl. Akad. Nauk SSSR, v.318, no. 4, p.972-976 (in Russ.)

Wang, X., Hou, Z., Song, Y. and Zhang, H. 2015: Geological, fluid inclusion and isotopic studies of the Baiyangping Pb–Zn–Cu–Ag polymetallic deposit, Lanping basin, Yunnan province, China; Journal of Asian Earth Sciences, v.111, p.853-871

Yamada, S., Okamoto, A., Takada, M., Fujwara, T. and Takemura, M. 1980: On the Thortveitite, fluocerire, pyroxferroite and other minerals from Isango mine, Oro, Nakagun Kyoto prefecture; Chigaku Kenkyu, v.31, p.205-222.

Appendix A

Relationship of host lithology, alteration style and vein mineralogy to vein type.

Appendix A: Relationship of host lithology, alteration style and vein mineralogy to vein type

#	Sample Number	Sample Start (m)	Sample End (m)	Thin Section type	Host Lithology	Vein type	Alteration type	Alteration Halo	Vein Textures	Inclusions
1	82.11	82.11	82.13	Doubly Polished		V	silicification/carbonatization			
2	92.92	92.92	92.92	Polished	Basalt	VI	silicification			
3	93.80	93.80	93.95	Doubly Polished	Basalt	III	potassic	-		
4	95.10	95.10	95.10	Doubly Polished	Brecciated Basalt	V	silicification-carbonatization			L + H/ L + V + H/V + L
5	97.76	97.76	97.95	Polished	Basalt	IV	potassic-carbonatization-zeolitic			
6	98.80	98.80	98.99	Polished	Basalt	VI	silicification			
7	99.46	99.46	99.62	Polished	Basalt	VI	silicification			
8	99.91	99.91	99.91	Doubly Polished	Basalt	IB	epidotization-silicification			
9	106.17	106.17	106.37	Doubly Polished	Brecciated Basalt	V	silicification-carbonatization			L + H/ L + V+ H/ V + L
11	108.90	108.90	109.16	Polished	Basalt	IV	potassic-carbonatization-zeolitic			
12	110.20A	110.20	110.39	Polished	Basalt	III	propylitic	-		
	110.20B	110.20	110.39	Doubly Polished	Basalt	IB	epidotization-silicification			
13	113.30	113.30	113.30	Doubly Polished	Basalt	IA	propylitic-potassic	Potassic rind		
14	136.70	136.70	136.80	Polished	Heterolothic mafic debris flow	III	propylitic	-		
15	150.02	150.02	150.02	Polished	Pyritic Mudstone		-			
16	152.46	152.46	152.57	Doubly Polished	Mafic Dyke	II	serpentinization-propylitic			
17	155.65A	155.65	155.85	Polished	Mafic Dyke	II	serpentinization-propylitic			
	155.65B	155.65	155.85	Doubly Polished	Mafic Dyke	II	serpentinization-propylitic			
18	158.00	158.00	158.10	Doubly Polished	Mafic Dyke	II	serpentinization-propylitic			
19	200.20	200.20	200.20	Doubly Polished		V	silicification-carbonatization			V + L
20	220.18	220.18	220.34	Doubly Polished	QFP	IA	propylitic-potassic	Potassic rind	Vuggy	
21	238.70	238.70	238.76	Polished	Pyritic Mudstone	-	-			
22	262.07	262.07	262.30	Polished	QFP	IB	epidotization-silicification			
23	284.15	284.15	284.30	Doubly Polished	QFP	IA	propylitic-potassic	Potassic rind		
24	294.47	294.47	294.75	Doubly Polished	QFP	IA	propylitic-potassic	Potassic rind		
25	295.55	295.55	295.79	Doubly Polished	QFP	IA	propylitic-potassic	Potassic rind	Vuggy	
26	296.00	296.00	296.37	Doubly Polished	QFP	III	propylitic			
27	305.50	305.50	305.68	Doubly Polished	Pyritic Mudstone	III	propylitic			
28	318.80	318.80	319.10	Doubly Polished	QFP	IA	propylitic-potassic		Vuggy	
29	324.00	324.00	324.43	Doubly Polished	QFP	IA	propylitic-potassic			
30	336.10	336.10	336.30	Doubly Polished	QFP	IA	propylitic-potassic			
31	348.73	348.73	348.73	Polished	Mafic Dyke	II	serpentinization-propylitic			
32	356.00	356.00	356.19	Doubly Polished	QFP	III	propylitic			
33	358.90	358.90	359.00	Doubly Polished	QFP	III	propylitic			
34	360.75	360.75	360.88	Polished	QFP	IA	propylitic-potassic	Potassic rind		
35	365.53	365.53	365.53	Doubly Polished	QFP	IB	epidotization-silicification			
36	380.65	380.65	380.80	Polished	Mafic Dyke	IV	potassic-carbonatization-zeolitic			
37	381.27	381.27	381.41	Polished	Mafic Dyke	IB	epidotization-silicification		Massive Intergrowth	
38	383.30	383.30	383.45	Doubly Polished	Pyritic Mudstone	III	propylitic			
39	391.80	391.80	391.93	Polished	Pyritic Mudstone	V	silicification-carbonatization			
40	401.23	401.23	401.37	Doubly Polished	Mafic Volcanoclastic	III	propylitic			
41	406.00	406.00	406.13	Doubly Polished	Mafic Volcanoclastic	IB	epidotization-silicification		Massive intergrowth	
42	412.32A	412.32	412.50	Polished	Mafic Volcanoclastic	III	propylitic			
	412.32B	412.32	412.50	Doubly Polished	Mafic Volcanoclastic	III	propylitic			
	412.32C	412.32	412.50	Doubly Polished	Mafic Volcanoclastic	III	propylitic			
43	415.30	415.30	415.30	Polished	Mafic Volcanoclastic	IA	propylitic-potassic			

Appendix B

Bulk geochemical data obtained via portable XRF.

Appendix B: Bulk geochemical data obtained via portable XRF.

Date	Depth (m)	Lithology	S (ppm)	Cl (ppm)	K (ppm)	Ca (ppm)	Ti (ppm)	Cr (ppm)	Mn (ppm)	Fe (ppm)	Ni (ppm)	Cu (ppm)	Zn (ppm)	As (ppm)	Rb (ppm)	Sr (ppm)	Y (ppm)	Zr (ppm)	Nb (ppm)	Ag (ppm)	Ba (ppm)	Pb (ppm)	Cu/Zn
7/7/2015	-6.57	granite			19560	10018	1733	25	284	10516	18		21.5		59.5	779		65	3.8	46	665	7.8	
7/7/2015	-8.00	granite			19025	11314	1938	38	369	14743	17		32	8.9	71.3	758		111	6.5	44	681	4.5	
7/7/2015	-11.10	granite			16540	11443	1043	21	158	6364			15.5		51.2	901	4.3	87	2.6	24	524	10.5	
7/7/2015	-13.11	granite			32764	8803	2157	70	288	13778	13		20.6	6.1	111.5	525	12.4	117	10	54	1291	6.8	
7/7/2015	-16.40	granite			21431	12464	2539	38	390	16819	20	10	27	10.5	75.8	580	5.4	61.9	5.3	41	833	8.3	0.37
7/7/2015	-19.45	granite			16019	9395	2547	110	471	17658	32	11	50	5.9	71.2	330	11.6	137	9.4	39	623		0.22
7/7/2015		granite		246	30226	6085	1371	19	221	7922	17		24.1	3.6	87.8	574	4.8	58.7	5.4	35	1052	8	
7/7/2015	-24.15	granite		258	27255	6457	1874	22	269	10492	11	10	17.8	6	88.6	356	4	90.1	5.5	48	972		0.56
7/7/2015	-27.00	granite		242	28546	4115	1539	37	313	16781	25		32	7.4	77.7	274	5.4	66.2	5	43	775		
7/7/2015	-29.95	granite		812	38273	3700	1352	31	219	8859	14		23.1	5.6	105	401		71.7	3.9	49	1061	7.7	
7/7/2015	-33.02	granite		261	44257	6312	1691	32	239	10920	16		23.5	11.6	104.4	610	5	73	5.1	52	1178	14.7	
7/7/2015	-36.00	granite		272	26266	6501	1768	25	290	12090	19		26.9	8.4	83	445	5.8	76.7	6.3	45	1114	5	
7/7/2015	-39.02	granite		491	24339	8929	1790	19	288	10660	20		22.2	6.5	69.4	368	5.7	90.1	5.1	33	690		
7/7/2015	-42.00	granite			38297	14959	1808	44	302	11629	14		40	11.7	121.6	1020		87	7.1	61	1317	17.1	
7/7/2015	-45.15	granite			64399	15598	1412	29	200	7000	15		13.1	5.4	142	377		36.2	5.1	49	1512	10.4	
7/7/2015	-48.00	granite		294	16554	7180	2702	26	313	13610	13		26.4	6.3	56.6	244		89	8.2	43	544		
7/7/2015	-51.12	granite			14632	7452	2475	21	384	15470	17		28.2	8.8	54	328	4.1	72.3	5.4	34	575		
7/7/2015	-53.92	granite			35111	13113	1514	60	201	6114			11.1	10.4	83.4	485		64.3	3.5	48	1312		
7/7/2015	-57.05	granite		1000	24737	8649	2742	37	425	17388	23		35	13.2	78.1	456	9.4	83.1	8.1	49	1157		
7/7/2015	-60.14	fault zone		549	378	261103	1686	47	979	69742			30	23.6	7.8	1645	20.8	17	7.6	94			
7/7/2015	-65.12	fault zone			11359	10011	7083	314	1194	64282	45		172	16.3	59.8	126	15.3	88.7	6.4	59	292		
7/7/2015	-66.00	fault zone		789	12529	34282	4443	350	2287	97428	33		259	22.1	27.9	91	5.9	21.8	2.7	77	297		
7/7/2015	-69.50	fault zone	4984	592	5875	117030	3890	307	1876	89227	63		194	22	15.4	553	13.9	25.3	4.4	81			
7/7/2015	-72.00	basalt		627	556	164955	6254		913	61888			37	33	12.7	2653	21.2	56	13.4	74			
7/7/2015	-73.16	basalt			4037	23843	3572	139	1477	66938	23		84	10.8	11	90	8	22.5	2.6	61	46		
7/7/2015	-74.00	basalt		408	4929	33001	3659	147	1502	64034	22		129	14.1	13.1	142	10.9	31.7	2.6	77	172		
7/7/2015	-75.00	basalt			6579	93214	3521	129	1347	54702	32		90	16.6	17.5	119	11.2	28.8	2.5	62	143		
7/7/2015	-76.10	basalt			16873	25289	2794	163	1461	54907	29		95	17.5	68.5	456	6.5	13.2		70	762		
7/7/2015	-77.00	basalt		369	8901	19995	4261	24	1148	52439			89	24.3	25	412	23.6	94	7.8	65	536		
7/7/2015	-78.02	basalt		401	4020	27522	2533	122	1913	61701	23		204	13	6.5	127	8.5	14.4		50	53		
7/7/2015	-79.98	basalt			24174	44028	2733	197	1854	64979	42		100	21.1	62.7	255	7.9	11.6		80	1040		
7/7/2015	-80.91	basalt	2068		6023	101131	1638	70	1370	52885	23	16	66	24.4	10.5	416	7.8	7.9	2.4	73	150		0.24
7/7/2015	-82.00	basalt		328	16650	81136	2710	143	1201	35377	42	319	72	11.2	46.1	267	14.3	19.9		61	747		4.4
7/7/2015	-82.80	basalt		384	479	64919	924	63	950	45251		212	48	9.6		127	12.7	6.5		59			4.4
7/7/2015	-85.05	Intermediate porphyry	1587	213	638	1592	2167		556	10949		105	42	6.3		92.2	12.9	90.8	2.3	31		10	2.5
7/7/2015	-86.87	Intermediate porphyry			646	196584	4213	52	698	58648				21	12.2	2002	13.4	72	11	89		8	
7/7/2015	-87.75	Intermediate porphyry	2911		11634	50613	5516	71	954	52281	31	41	51	19.6	50.5	657	18.8	78	7.7	67	352		0.80
7/7/2015	-88.23	basalt			7823	138719	1330	29	1181	38056	15		62	11.8	20.6	31.5	5.3	5.7		63			
7/7/2015	-89.10	basalt		401	9678	38393	2235	83	1530	47863	16		70	16.4	24	295	4.9	10.6	2.4	57	499		
7/7/2015	-90.57	basalt	**21010**	981	7466	47444	617	18	617	31679		560	67	35.5	17.6	341	10.2	37.6	7.3	54	220		8.4
7/7/2015	-91.10	basalt		728	8271	24094	2574	57	1632	71101		232	140	13.9	22.4	352	3.8	11.6		67	562		1.7
7/7/2015	-92.70	basalt		782	5023	58041	2435	42	2639	70373			133	16.2	13.1	426		11.1	2.7	79	234		
7/7/2015	-92.92	basalt	**117098**	851	2223	55892	1988	56	2729	215923		**2291**	182	36		237	8.7	10.9		121	54		12.6

Date	Depth (m)	Lithology	S (ppm)	Cl (ppm)	K (ppm)	Ca (ppm)	Ti (ppm)	Cr (ppm)	Mn (ppm)	Fe (ppm)	Ni (ppm)	Cu (ppm)	Zn (ppm)	As (ppm)	Rb (ppm)	Sr (ppm)	Y (ppm)	Zr (ppm)	Nb (ppm)	Ag (ppm)	Ba (ppm)	Pb (ppm)	Cu/Zn
7/7/2015	-94.88	basalt		492	5180	42495	2650	46	2057	61331		71	223	15	16.4	464	6.3	13.2		64	331		0.32
7/7/2015	-96.10	basalt		437	3522	44633	4739	304	1589	67732	41	39	97	18.4	10.1	259	25.2	78.5	5.1	66	84		0.40
7/7/2015	-96.86	basalt			5443	40131	579	11	785	23093			70	50.5	17.7	129	8	31.3	8	39	198		
7/7/2015	-99.10	basalt		415	3675	29767	2334	47	1688	76334	18	38	111	15.4	9.1	391	4.3	11.3	2.4	68	96		0.34
7/7/2015	-99.91	basalt		556	2828	68997	2481	70	1434	73731	31		88	19.4	4	431	5.6	13.8	2.7	69	57		
7/7/2015	-100.91	basalt		5293	5461	66941	1873	35	1158	52085	17		66	16.7	17.9	601	7.7	16		63	111		
7/7/2015	-102.02	basalt		1086	2808	49226	2297	54	1155	63387	20	27	84	11.9	5.4	378	6.1	12.1	2.5	67	67		0.32
7/7/2015	-102.74	basalt	**209351**	1133	2029	27424	900	37	1513	349283	111	**2787**	119	35		82	6.1			122	97	38	23.42
7/7/2015	-103.16	basalt			13156	72169	2190	50	1517	71713	18	33	95	17.3	31.5	201	6.5	12		68	392		0.35
7/7/2015	-104.24	basalt			24770	171377	709	21	527	23532		11	27	8.1	73.4	183	7.7	3.9		76	820		0.41
7/7/2015	-105.64	basalt		1410	12776	9398	4755	654	1083	53109	109		64	17.3	54.5	149	27.3	53.5	5.6	61	658		
7/7/2015	-106.69	basalt	**244973**	933	1407	12512	1137	32	1127	287603		205	85	94		31.7	8.5	5.9		116	155		2.41
7/7/2015	-107.80	basalt			3991	65615	2309	53	1484	41637	27		77	12.4	10.9	237	7	12		53	125		
7/7/2015	-108.40	basalt		577	2329	41853	2507	55	2474	57704	18	112	157	13.7	4.1	603	6.6	14.3		69	56		0.71
7/7/2015	-109.16	basalt		396	1158	11364	3121	67	1658	71200	30		174	12		136	6.5	19.2		54			
7/7/2015	-109.54	basalt	**142178**	1175	1357	12274	785	26	1172	230845		**3327**	108	29		133	5.4	6.5		113	90		30.81
7/7/2015	-111.10	basalt			7485	79530	2246	44	2492	63067		32	275	19	21.4	282	3.7	8.4		71	408		0.12
7/7/2015	-112.52	basalt	**66306**	739	25486	56534	2171	46	1875	90857		1415	115	29.5	64.9	622	5.5			110	1579		12.30
7/7/2015	-112.76	basalt		518	2602	48921	2680	60	3985	57177	16		382	16.6	5.6	263	3.7	12.9		64	329		
7/7/2015	-113.22	basalt	**59206**	1224	13534	54196	1913	71	2491	41273		725	**54448**	14	21.8	341	8.5	9.9		71	686	44	0.01
7/7/2015	-113.30	basalt	**660419**	2199	1557	79015	186	42	840	539460		**11421**	697			165	12			159		217	16.39
7/7/2015	-115.02	basalt	**20496**	387	1203	44023	2507	49	2808	69152		91	105	14.7		268	4.8	13.6		63	87		0.87
7/7/2015	-117.67	basalt			5497	180767	1034	15	1619	30857			133	11	8.2	73	8.2	7		68			
7/7/2015	-118.00	basalt	1154		765	6218	2603	64	795	32669	19	116	160	21.9		307	9	18.2		30			0.73
7/7/2015	-119.10	basalt		582	2579	59047	2464	51	1880	60581		36	71	11.2	4.1	320	4.1	13.3		71	99		0.51
7/7/2015	-120.30	basalt		552	1915	48594	2774	48	2065	77307	30	19	158	12.7	3.8	261	7.5	14.5		61	100		0.12
7/7/2015	-121.10	basalt		446	5122	16957	2980	66	2150	85890	18		214	13.9	12	403	5	15.4		64	466		
7/7/2015	-122.12	basalt		400	441	224793	876	17	1122	28231	16	12	34	16.1		216	4.7	4.4		77			0.35
7/7/2015	-123.22	basalt	6731		4381	52434	2521	41	2429	53873		102	235	14.9	12.6	306	8.1	17.3		76	158		0.43
7/7/2015	-124.15	basalt		489	7820	69126	2269	42	1969	56905	19		168	13.8	20.1	241	5.9	14.3		67	234		
7/7/2015	-125.09	basalt			26371	111346	2382	42	2182	53284	23	25	201	17.8	52.8	63.1	6.4	10.6		89	1081		0.12
7/7/2015	-126.20	basalt		497	5898	39441	2554	57	2706	75911		234	134	16.9	7.2	182	4.9	12.7		74	440		1.75
7/7/2015	-127.00	basalt		546	28927	28680	2982	50	1661	68044			155	20.5	74	181	6.4	9.1		81	1538		
7/7/2015	-128.10	basalt		390	9460	36171	3332	34	1611	61918		33	83	13.1	22.3	220	6.2	17.9		69	432		0.40
7/7/2015	-128.82	basalt		580	35853	62031	3345	37	1485	65773		16	77	23.5	85	410	21.6	20.8		101	1609		0.21
7/7/2015	-129.53	basalt		526	497	241974	799		2523	78828		57	229	20.2		88	28.3	7		103			0.25
7/7/2015	-130.60	heterolitic		939	674	207693	2583	78	1106	78229			14	30	3.8	1426	13.4	17	7.2	109		28	
7/7/2015	-131.68	heterolitic		503	5084	61670	3221	34	1945	56149		61	78	16	10.7	242	7.7	20.2		66	296		0.78
7/7/2015	-133.00	rhyolite		306	6888	55616	2560	22	1505	35024	15		88	15.6	14.9	214	5.8	18.5		61	407		
7/7/2015	-134.10	rhyolite			1711	29556	1457		490	15796		74	29	14.4	4.2	327	23.3	93.9	3.2	45	37		2.55
7/7/2015	-135.26	heterolitic			1383	199359	2034	24	1662	42751			306	21.2	5.8	857	24.1	24	2.9	83	97		
7/7/2015	-136.00	heterolitic		396	2549	65283	2635	30	1727	43264		15	65	9.4	2.6	326	6	19.6	3.3	59	122		0.23
7/7/2015	-136.82	rhyolite	2009	235	2247	15238	1234	8	530	14497		57	18.2	7	6.2	331	26.8	95.9	3	40	59		3.13
7/7/2015	-138.00	heterolitic		377	1217	36843	2120	27	1190	41624			97	11.2		93	3.1	14.5		57	50		
7/7/2015	-139.09	heterolitic	96451	893	12792	91561	1902	33	1976	132951		**2519**	109	35	39.4	1249	23	67	4.9	100	552		23.11
7/7/2015	-140.21	heterolitic			5689	76253	3185	56	1461	59449			85	16.1	8.5	166	12.8	19.4		67	205		
7/7/2015	-141.25	heterolitic		686	7648	35881	4001	35	1481	70045			67	11	17.1	173	7.7	23.7		70	379		
7/7/2015	-142.16	heterolitic	8422		11494	33927	2742	21	1456	62470		83	145	14.1	29.4	169	9.8	21.2		61	386		0.57
7/7/2015	-143.10	heterolitic		619	7870	33595	3360	43	1729	67927			158	16.2	19.4	247	12.1	27.2		64	322		
7/7/2015	-144.02	rhyolite		249	4595	7307	1522		395	14700			30	8.8	17.5	177	23.5	98.8	3.1	37	248		
7/7/2015	-145.00	heterolitic		374	6133	18836	3404	23	1843	65486			165	16.6	12.4	310	11.4	28.1		60	308		
7/7/2015	-146.00	heterolitic	28865	528	3346	58318	3289	19	2086	70952		93	99	32	5.2	194	15.4	32.1		73	80		0.94
7/7/2015	-147.10	rhyolite			4198	5055	1081		606	18519		12	30	9.7	9.8	156	13.5	93.8	3.5	38	171		0.40
7/7/2015	-147.50	pyritic	**51981**	1202	4847	8479	2269	40	987	109903	51		177	31	3.8	144	23.2	158	4.9	65	173	22	
7/7/2015	-147.60	pyritic	**58230**		15220	60721	1841	32	1033	77261		31	269	27	25	407	34	108	9.2	87	627	21	0.12
7/7/2015	-147.75	pyritic	**61311**	592	28212	34250	2268	37	1177	70899		75	167		72.8	297	30	118	12.1	93	1447	373	0.45
7/7/2015	-148.20	pyritic	**27061**	478	13506	24617	2260	39	1010	73547		111	164		32.8	232	19.1	105	9.9	84	1008	177	0.68
7/8/2015	-149.07	pyritic	**19674**	1534	4878	28504	4507	56	1317	65660	15	14	511	40	9.2	156	16	77.3	9	79	277	**3572**	0.03

Date	Depth (m)	Lithology	S (ppm)	Cl (ppm)	K (ppm)	Ca (ppm)	Ti (ppm)	Cr (ppm)	Mn (ppm)	Fe (ppm)	Ni (ppm)	Cu (ppm)	Zn (ppm)	As (ppm)	Rb (ppm)	Sr (ppm)	Y (ppm)	Zr (ppm)	Nb (ppm)	Ag (ppm)	Ba (ppm)	Pb (ppm)	Cu/Zn
7/8/2015	-150.02	pyritic	**17289**	804	2588	15725	3392	33	350	20683		409	**6906**		3.4	138	64	258	8.9	60	432	381	0.06
7/8/2015	-150.45	pyritic mudstone	**138299**	945	3364	32394	1172		1136	201141		**2103**	302	68		110	33	95	4.4	111	107	26	6.96
7/8/2015	-151	pyritic	**34282**	835	4065	17283	1977	22	681	57260		123	1132		8.1	150	34	123	10.4	69	105	**1170**	0.11
7/8/2015	-151.55	mafic debris	1223	1207	5348	1784	3288	55	1142	48932	25		115	17.7	13.7	32.6	9.1	18.7		38			
7/8/2015	-151.86	mafic debris	1525	487	12130	46831	3703		1567	55145		103	69	13.6	31.1	220	9.5	24.2		62	442		1.49
7/8/2015	-153.1	mafic debris		1237	8947	65599	4276	25	2058	58297	18		227	16.1	21.7	204	13.2	26.9		70	386		
7/8/2015	-153.86	mafic debris	2857		5000	7982	1601		267	7785		19	94	6.4	19.8	139	17.6	89.3	2.7	33	318	4	0.20
7/8/2015	-154.7	mafic debris		816	2635	30849	3966	24	795	53606	17	277	115	12.8	3.5	167	14.8	23.9	2.3	60	51	39	2.41
7/8/2015	-155.8	mafic debris	**62179**	607	1782	126361	2773	36	1864	91760		674	177			53.3	14	22.7		86		336	3.81
7/8/2015	-157.35	mafic debris		523	36842	34632	3383	61	1793	66678	14	60	98	14.6	83.7	186	5.4	14.8		72	1322		0.61
7/8/2015	-158	mafic debris	6700	2516		853585			329	5490	54	80	18			93	5.9			79			4.44
7/8/2015	-159	cherty ash			15174	942	2423		745	16516	18		127	12.4	53.1	11.2	38	148.5	10.1	37	329		
7/8/2015	-160.2	cherty ash	**28386**		22553	9437	3052	33	687	19627	11	236	228	9.4	77.3	168	47.3	198	12.2	62	1007	9.1	1.04
7/8/2015	-162.29	cherty ash	8846		16364	13592	2127	57	801	20366	35	696	173	19.1	63.3	150	56	198	12.9	48	637	34	4.02
7/8/2015	-163.1	cherty ash		266	3693	2655	1765	16	1137	24875	28		230	13.3	16.8	11.1	37.3	192	14.2	39			
7/8/2015	-164.7	cherty ash	**27068**		9128	7319	1869		448	22531	12	102	116	11.3	28.3	30.8	16.5	122.4	4.1	45	283	5.9	0.88
7/8/2015	-165.7	mafic dyke		739	3124	17772	7698	112	2340	62793	32		162	15.3	8.3	514	32	98	7.1	63	105		
7/8/2015	-166.5	mafic dyke		485	11204	33674	6350	170	1992	100090	78		257	19.5	15.5	190	20.2	87	6.5	75	507		
7/8/2015	-166.95	cherty ash	**10153**		1965	6171	1623	27	401	18704	15	17	40	8.9	3.2	115	41.1	175	11.9	44	93		0.43
7/8/2015	-168.9	cherty ash	2912		7877	8571	1865	16	810	13621	18	49	414		20.4	66	18	122.4	8.6	38	307	332	0.12
7/8/2015	-170.26	cherty ash	1686		3091	9394	1404	8	543	12030	15	63	550	8.6	6.7	100.3	17.1	123.6	8.2	34	187	18.1	0.11
7/8/2015	-171.17	cherty ash			9124	17276	2747	31	945	25132	21		128	10.6	20.2	213	32.2	172	11.6	43	522	5.2	
7/8/2015	-172	cherty ash	1183		38836	22432	2813	64	1485	16231		48	58	12.2	116.4	426	88	164	10	75	2058		0.83
7/8/2015	-173.5	basalt		450	28950	14990	5564	43	3612	76470		83	379	16.3	67.6	205	9.1	28.4		92	1250		0.22
7/8/2015	-174.2	cherty ash	1129	263	23597	12432	2095	33	1166	24167			95	7.8	72.7	196	21.7	81.4	2.6	67	1740		
7/8/2015	-175.14	basalt			1921	62015	4862	40	2330	50533		19	137	13.5		220	14.8	26.8		66	80		0.14
7/8/2015	-176.13	basalt			524	183454	2909	22	978	62414				19.4		650	11.6	18	3.6	93			
7/8/2015	-177.9	basalt			462	195834	2640		1060	70454				16		791	9.1	20	3.6	93		10	
7/8/2015	-178.36	cherty ash	1853	758	12332	9115	6316	54	1285	77045	19		218	17.3	26.5	175	13.5	32.9		68	773		
7/8/2015	-179.13	mafic dyke	5719		4731	34850	7664	30	2716	67787		25	126	15	15.4	586	27.7	115	9.5	66	232		0.20
7/8/2015	-179.74	mafic dyke	2543		10659	56774	10210	40	1892	89059			145	23.2	36.2	692	48	148	11.6	93	774		
7/8/2015	-180	mafic dyke		395	4630	50802	7277	34	2172	61485			131	17	15.8	659	33.4	115	10	76	501		
7/8/2015	-181.01	mafic dyke		421	4133	52404	6734	27	1768	52977		14	71	17	13.9	628	39.4	128	9	64	315		0.20
7/8/2015	-183	grey chert	**59469**		3496	5661	9946	61	1573	68642	36		93	29	9.4	19.7	31.8	247	23.8	82			
7/8/2015	-183.95	grey chert	1799		3891	2097	1926	15	817	23625	14		144	9.2	16.8	27	19	118.4	7.6	28			
7/8/2015	-187.1	mafic dyke	**16689**		3960	58227	2635	323	2396	58929	35	395	234	27.2	7.1	202	10.2	14.5		81	310		1.69
7/8/2015	-188.24	mafic dyke			1575	47755	2434	453	1682	65562	69	11	120	11.6		130	7.2	13.5		69	120		0.09
7/8/2015	-190	mafic dyke	2981	732	5895	8430	3792	575	835	65815	118		147	11.9	28.7	95	10.3	16.4		56	45		
7/8/2015	-190.46	mafic dyke		585	6221	14284	3453	397	806	52008	115		66	12.3	24.6	172	10.5	16.1		55	183		
7/8/2015	-191.6	mafic dyke		704	4477	6781	5674	481	1040	99371	150		107	10.1	19.5	48.1	10.7	24.5		58			
7/8/2015	-192.3	basalt			4265	78328	2483	472	2038	72739	71		173	10.6	6.5	182	7.9	15.4		77	323		
7/8/2015	-193.28	basalt			14885	142263	992	172	1230	35373	33		69	10.6	37.2	47.9	8.2	6.3		61	57		
7/8/2015	-194.34	basalt		658	25110	83992	2893	540	2303	72920	48		159	15	54	231	10.7	16.7		93	1282		
7/8/2015	-195.4	grey chert	938		4243	6584	1666	16	505	11957	15		56		9.8	79.8	26.1	157	10.7	33	183	11.3	
7/8/2015	-196	grey chert	1381	995	2608	14005	2119	27	513	13874	12	15	31	9.2	4.8	193	39.7	180	9.9	31	170		0.48
7/8/2015	-196.95	basalt			1565	38678	2454	509	2237	60678	57		234	12.8		121	5	14.8		64	58		
7/8/2015	-198	basalt		370	2530	60590	2021	395	2027	68821	64		174	11.8		20.8	6.8	12		61	45		
7/8/2015	-199.23	basalt		624	1976	85467	2538	481	3873	73593	53		265	16.2		215	6.9	14.1	2.5	63	69		
7/8/2015	-200	basalt	**19427**	354	10768	15166	3343	56	638	57393		980	188	30.3	31.8	265	15.4	21	2.6	69	634		5.21
7/8/2015	-201.1	basalt	2031	413	3825	46113	2010	382	1906	46183	26		120	11.9	12.7	326	10.2	12.4		55	289		
7/8/2015	-202.3	basalt		575	7657	50123	6134	154	1573	67881	76		119	14.1	18.2	458	32.6	83	4.6	81	394		
7/8/2015	-203	basalt		1243	2801	9651	7825	211	1068	79870	84		156	13.9	5.2	37	27.8	60.7		62	40		
7/8/2015	-203.75	cherty ash	**29337**		1677	9835	2357		516	24270	18	9	30	6.4	6.3	87.7	29.3	175	11.2	44	67		0.3
7/8/2015	-204.34	cherty ash	**49369**	316	880	10949	1901		332	30704	16	26	21	24.4		136	33.9	263	12.9	50	82	13	1.24
7/8/2015	-205.05	cherty ash	790		6075	6580	2196	22	529	12879		18	36	6.4	10.1	131	43.8	181	13.5	30	444	7.1	0.5
7/8/2015	-206.6	cherty ash	6954		1823	11628	2104	23	674	12787			38	7.2	4.5	122	44.6	199	12.5	35	220	7.8	
7/8/2015	-207	QFP	**17533**		29646	11271	2819	17	660	16242		16	69	5.1	59.1	144	16	81.7		56	1681	7.4	0.23

Date	Depth (m)	Lithology	S (ppm)	Cl (ppm)	K (ppm)	Ca (ppm)	Ti (ppm)	Cr (ppm)	Mn (ppm)	Fe (ppm)	Ni (ppm)	Cu (ppm)	Zn (ppm)	As (ppm)	Rb (ppm)	Sr (ppm)	Y (ppm)	Zr (ppm)	Nb (ppm)	Ag (ppm)	Ba (ppm)	Pb (ppm)	Cu/Zn
7/8/2015	-208.12	QFP	956		16156	17978	2761	19	1054	22117			58	8.9	41.6	339	25.5	69.4	2.9	56	592		
7/8/2015	-208.12	QFP	**10416**		8604	42336	2056	15	995	20077		20	51	6.2	26	236	21.7	71.9		50	549	6	0.39
7/8/2015	-210	QFP	2656		14147	14983	1181	31	602	10304		109	571		43.3	136	12.8	43.5		49	1222	160	0.19
7/8/2015	-210.33	QFP			5593	18927	1717	13	841	22170			50	3.9	17.6	195	23.9	70.2		39	464		
7/8/2015	-211.1	QFP	9885		30540	14387	2947	16	697	23223			38	7.2	47.4	203	21.5	87.6	3.7	57	1896		
7/8/2015	-212.22	QFP			3540	11357	1885		893	26554			64	6.7	10.4	378	15.3	85.8	3.5	36	376		
7/8/2015	-213.18	QFP	9260		17757	16850	2333		693	24873			47	7	42.2	241	19.6	78.6		48	713		
7/8/2015	-213.89	QFP			5000	13909	2537		775	25238			60	7.6	15.8	200	24.1	100.4		36	261		
7/8/2015	-215.07	QFP	**50006**		8941	49081	819	31	587	41232		11	27	12.9	19	328	29.3	43.3		69	312		0.41
7/8/2015	-216.12	QFP	**33179**	354	15300	42878	1050	18	464	24562		9		12.9	30	275	34.3	24		78	1656		
7/8/2015	-217	QFP	6716		33182	15431	2425		859	28960			55	9.3	66.1	148	25.1	70.2	3.1	57	1049		
7/8/2015	-217.95	QFP			9420	14672	2065	10	575	19556			55	5.8	27.2	198	22	87.6	4	51	415		
7/8/2015	-219.07	QFP			6918	17027	1567	13	608	19889			51	6.3	23.4	293	23	89.9		42	256		
7/8/2015	-220.16	QFP			20081	41749	1251	30	1620	12803			6.6	5.2	70.7	224	65	34.9		56	903		
7/8/2015	-221	QFP			5943	7496	1796		662	20254			72	6.3	19.5	314	14.5	81.2		35	328		
7/8/2015	-222.04	QFP	**11947**	319	4686	17470	2451		974	21286	11	63	62	6.8	19.4	206	16.2	90	3.3	39	283		1.02
7/8/2015	-223.07	mafic dyke	4883		3195	37312	1129		396	11918			16.7	4.8	7	60.8	20.9	66.6	2.5	42	74		
7/8/2015	-224	mafic dyke			3918	85457	8368	60	3408	67201	27		111	15.6	5.5	321	30.1	94	10.1	80	255		
7/8/2015	-224.5	mafic dyke	6071	666	8034	77685	8516	96	3276	71467	24	12	152	14.7	17.5	400	29.7	106	10.2	79	276		0.08
7/8/2015	-225.3	QFP	2301	225	6923	10398	2003	36	531	12281			22.1	4.4	19.9	348	16	59.4	2.5	28	365		
7/8/2015	-226	mafic dyke	**14446**	363	5004	25306	3538	34	926	30784		17	82	7.9	12.8	309	34.4	68.3	2.5	52	217	18.7	0.21
7/8/2015	-226.6	QFP	**83993**	683	7319	30263	2537	87	1163	65990		36	46	12	14.3	235	24.9	64.2		85	361	42	0.78
7/8/2015	-227.2	QFP	**247079**	1148	15751	28687	3099		2166	242572		1622	**3860**	21	66	60	43	91		103	318	40	0.42
7/8/2015	-228.02	QFP	**19068**	288	14153	12984	2748		913	15261			148		40.6	91.9	19.2	72.9	3.2	55	389	29.4	
7/8/2015	-228.4	QFP	**638804**	2257	12589	30022	676		946	553368		**40961**	**10718**		30	77	46			140	115	**1122**	3.82
7/8/2015	-229.32	QFP	**19199**		34539	27125	2472	23	923	16617		19	**2316**	11.8	88.4	193	25.8	83.9		80	2228	30	0.01
7/8/2015	-229.92	QFP	**31920**		19707	34089	3652	19	1996	43188		83	310	10.1	54.2	223	29.4	89.4	3.3	50	643	11	0.27
7/8/2015	-230.9	QFP	3428		7067	12397	1243	11	759	11115			563		22.7	153	13.7	75.4	2.9	39	359	18.7	
7/8/2015	-232	QFP	4370		11027	18003	2108	11	761	13886		27	1349		27.6	169	22.1	84.4		43	479	272	0.02
7/8/2015	-233	QFP	**22402**	283	8820	18775	2668	11	1269	22392			96	5.3	28.3	123	25.3	75.7	3.6	47	452		
7/8/2015	-233.89	QFP	**11287**	989	9953	44057	1791		700	12909		9	435	5.7	25.7	27.1	19.5	61.5		58	393		0.02
7/8/2015	-234.8	QFP	**36519**		21740	12225	3366	22	1488	34583		19	173	18.7	60.2	73.4	18.6	68.3	2.7	59	1723		0.11
7/8/2015	-236.06	QFP	2173		10554	16799	2243	10	1051	12144			141		29.8	136	14	66.8		33	401		
7/8/2015	-237	QFP	2954		7193	21182	2599	17	1121	14863	11	12	794		20.8	208	18.7	86.4	2.9	35	628	50	0.02
7/8/2015	-238.49	pyritic		507	27128	75385	5032	162	1999	49492	32		82	12.3	64.6	528	19.7	38		86	1507		
7/8/2015	-239.56	pyritic	5517		8129	5949	1999	14	430	11684	21	21	68		35.1	102	22.2	134	8.8	21	406	29.6	0.31
7/8/2015	-241	mafic dyke		612	15663	76859	3600	991	2149	73527	288		131	15.8	38.8	108	13.8	31.5		61	299		
7/8/2015	-242.25	mafic dyke	1705	536	4048	68734	5504	144	2822	60679	68	32	107	15	7.9	511	20.8	67	4.6	73	200		0.30
7/8/2015	-243	mafic dyke	**29463**		2924	56692	5708	96	2589	97283	38	66	156	18.1	5.5	368	27.3	78	4.5	62	121		0.42
7/8/2015	-243.2	pyritic	899		5780	28785	976	22	566	9744	9		18.1		7.5	238	37.3	90.7	6.9	37	135		
7/8/2015	-244.3	pyritic	**231558**	945	1256	7923	2221	42	918	124079		135	63	13		168	40.9	101	6.5	61	77		2.14
7/8/2015	-245.14	pyritic	4393		1231	6096	1496	11	701	13685	22	54	75	4.4		104.7	16.3	103.5	6.7	38	113		0.72
7/8/2015	-246.02	pyritic	**13954**		2306	7566	3709	34	758	18154	21	25	84	3.9	4.4	97.7	37.4	172	14.1	34	200	5.5	0.30
7/8/2015	-247.19	QFP	**20781**	812	24724	20971	9877	202	1680	44775		63	**16963**	25	48.3	630	63	89	4.8	117	2715	16	0.00
7/8/2015	-248.1	QFP	7357		13789	8665	2051	13	735	11058		11	60		40.4	105	15	74.8	3.4	43	1553	7.9	0.18
7/8/2015	-249.27	QFP	9487		25631	5421	2175	19	915	15117		19	41	4.6	66.6	96.6	11.7	73.2		50	1629		0.46
7/8/2015	-250	QFP	**20033**		31599	7110	1347	16	459	11376	9	44	112		80.7	74.5	9.8	55.1	3.3	56	1450	277	0.39
7/8/2015	-250.9	QFP	3368		20414	14985	2476	12	1050	16358			40	4.3	55	121	20.3	79.4		51	1339		
7/8/2015	-252	QFP	**11772**		19739	25785	6492	45	1669	39838		92	**3304**		50.2	157	27.3	81.9	4.3	59	514	117	0.03
7/8/2015	-253	QFP	3686		24982	19630	3553		1403	27524		12	161	6.3	54.8	123	22.6	72.9	2.5	60	855	12.1	0.07
7/8/2015	-254.16	QFP	**14405**		10591	18822	2279	12	1019	24069		16	270	4	30.3	244	21.9	86.1		49	450	5.7	0.06
7/8/2015	-255	QFP	5156		11903	14767	1630		691	13646			53	3.5	32.5	181	13.9	64.7		33	608		
7/8/2015	-256.2	QFP	9780		17102	4671	566	14	578	7043		15	1705		63.1	75.6	14.3	29.7		35	629	367	0.01
7/8/2015	-257.3	QFP	6716		13109	18929	2176	17	842	19488	10		71		45.6	175	18.1	84.8	3	37	577	22.4	
7/8/2015	-258.18	QFP	**32108**	342	12583	22419	5006		1294	32830			261		28.4	114	28.3	79.3	2.8	65	591	274	
7/8/2015	-259.07	QFP	1209		12556	15468	2308	22	976	21960		18	1072	6.8	28.1	191	17.4	70.3		47	553		0.02
7/8/2015	-260.1	QFP		6839	663	183471	771		732	5222				3.4		24.8	16	24		58	252		
7/8/2015	-260.63	mafic dyke	6540	446	21974	46238	2885		1180	34022			49	12									

Date	Depth (m)	Lithology	S (ppm)	Cl (ppm)	K (ppm)	Ca (ppm)	Ti (ppm)	Cr (ppm)	Mn (ppm)	Fe (ppm)	Ni (ppm)	Cu (ppm)	Zn (ppm)	As (ppm)	Rb (ppm)	Sr (ppm)	Y (ppm)	Zr (ppm)	Nb (ppm)	Ag (ppm)	Ba (ppm)	Pb (ppm)	Cu/Zn
7/8/2015	-260.63	mafic dyke	6540	446	21974	46238	2885		1180	34022			49	12	47.8	305	17.8	47.8	3.2	67	527		
7/8/2015	-261.2	mafic dyke		468	8904	54572	3154		1698	40603			55	11.6	32.1	709	18	59	3.3	64	240		
7/8/2015	-262.07	QFP	5440	279	6774	21886	1528	12	672	14170			28	7.8	20.1	213	17.3	77.4	2.8	56	589		
7/8/2015	-263.1	QFP	**26369**	390	4676	13539	1478	30	539	19653			152		13.3	98.8	15.6	48.6		40	372	372	
7/8/2015	-264.25	QFP	**34751**	576	8930	44720	3565		1556	47242			110	13.2	19.5	220	24.8	61.9	3.2	53	380	28	
7/8/2015	-264.9	QFP	4047	617	5500	67597	2190		1540	18273		16	92		11.9	196	19.7	63.9	2.7	56	197	53	0.17
7/8/2015	-266.06	QFP			7515	23399	2202		1131	26938		13	40	4.5	18.6	207	19.7	67.4		53	445		0.33
7/8/2015	-267.1	QFP	4859	254	13671	14076	1525	18	715	18515			20.8	6.1	41.4	193	20.1	78.5	2.7	45	582		
7/8/2015	-268.2	QFP	**66969**	700	15767	21447	1904		1528	65525			60	13.7	37	172	21.3	67.5	2.8	85	722		
7/9/2015	-268.95	QFP	2920		4925	23983	1243		737	16023			43	4	13.2	186	17.1	80.7		37	227		
7/9/2015	-270.3	QFP	9242		4295	84838	446	10	662	15765				8.9	8.3	400	35.7	24.1		51	109		
7/9/2015	-271.07	QFP	**10535**		7340	23709	1635		811	21522			39	3.8	21.3	135	19.2	73.5		44	249		
7/9/2015	-272	QFP		351	7902	18925	1603		790	18312			33	5.7	20.6	156	15.5	63.7	2.5	58	362		
7/9/2015	-273	QFP	5705	268	7701	19634	2225	14	762	20758		11	50	6.7	19.3	170	14.3	60.9	2.7	46	406		0.22
7/9/2015	-274	QFP			19850	29523	2087		2133	33752			94	7.3	61.2	287	25.5	68.9		62	1013		
7/9/2015	-275.1	QFP		298	14500	17759	2192		791	24263			55	7.9	50.4	300	19.8	87.1	3.4	46	294		
7/9/2015	-276.17	QFP			13666	22034	1474		632	19869			40	6.3	40.7	204	14.4	63.1	2.6	46	488		
7/9/2015	-277	QFP	1534		17431	31702	2196		876	26803		38	43	7.3	54.8	155	22	75.1		48	386		0.88
7/9/2015	-278.13	QFP		313	11877	39702	2301		1020	18662			42	6.8	23.8	205	24.6	87.8	3.2	41	394		
7/9/2015	-279.24	QFP	1445		8222	31309	1101		702	18339			46	4.5	24.4	159	17.7	73.5		51	288		
7/9/2015	-280.07	QFP	**25891**	363	11625	20233	4320	15	1062	33120		16	1737	13.3	33.7	228	29	109	4.2	46	515	16.5	0.01
7/9/2015	-280.93	QFP	5705	253	9542	18626	1455		732	15514	10	16	48	4.4	29.1	152	15.5	62.2		47	518		0.33
7/9/2015	-282.1	QFP		282	10196	23523	2329		1073	23185	15	9	78	6	27.8	176	19.1	80.9	2.9	39	434	6.1	0.12
7/9/2015	-283.1	QFP			6878	18717	1438		674	18703		25	41	6.9	23.9	190	14.2	71.1	2.5	40	268		0.61
7/9/2015	-283.94	QFP	**73365**	512	8555	23295	1981	17	733	53875		353	43	15.5	28.3	256	18.9	86	3.8	53	411		8.21
7/9/2015	-285.18	QFP	2039	359	7153	20020	2375		701	17178		22	49	4.7	23.7	184	20.8	83.2	3.2	39	346		0.45
7/9/2015	-286	QFP	1904		4872	11844	1299	18	634	15215			46	3.8	14.9	148	12.3	58.2		44	242		
7/9/2015	-287.05	mafic dyke		535	9190	56136	3889	62	1345	55752		37	94	14.1	32.2	565	9.8	27.6	5.1	66	281		0.39
7/9/2015	-288.3	mafic dyke		632	8710	75846	4594	62	1391	53624	17	15	107	14.7	22.1	565	18.1	38.4	2.8	52	176		0.14
7/9/2015	-289	QFP		318	10751	14665	1440		649	12969		11	34		24.5	227	15.9	79.4	3.5	34	602		0.32
7/9/2015	-290.05	QFP	1194		7665	11328	2112		523	11530	12		27.6	4	25.2	142	17.6	64.2	2.4	48	337		
7/9/2015	-291	QFP	6895		9550	8712	1355		508	15151		18	41	3.5	24.6	99.3	14	72		35	360		0.44
7/9/2015	-292	QFP	2405	296	5239	12703	1233		585	15683			33	4.1	17.8	137	11.6	64.3		38	304		
7/9/2015	-293.1	QFP	9712	259	9822	20493	1756	13	793	20538			62	6.2	31.9	260	23.5	78.1		35	544		
7/9/2015	-294.1	QFP	2537	415	8633	26089	2454		989	19186		28	62	5.7	21.6	193	22.6	84.4		41	380		0.45
7/9/2015	-295.12	QFP	9660	307	4258	17823	1749		697	18864		99	117	6.1	7	151	13.6	60.9		47	485	37	0.85
7/9/2015	-296	QFP	2723		9749	104306	1727	16	1368	32950		46	11	9.5	24.6	348	26.1	47.2		73	841		4.18
7/9/2015	-297.27	QFP		317	3239	11295	1286		832	20775			38	6.7	9.2	234	15.6	75.7	2.4	42	251		
7/9/2015	-298	QFP			3216	20541	1386		849	17862		170	55		7.9	229	16.6	73.6	2.5	42	118	6.7	3.09
7/9/2015	-299	QFP	10376	309	7383	15280	1632		630	13348		9	295		28.1	106	19.2	75.8		36	415	183	0.03
7/9/2015	-300	pyritic	7116		319	4593	707	10	184	7825			210	4.2		51.3	19.8	118.1	7.2	23		9.7	
7/9/2015	-301	pyritic	8700		759	5769	1293	14	588	16979	19	19	757			63.4	27.7	105.6	9.1	41	37	260	0.03
7/9/2015	-302.26	pyritic	**217961**	3545	11318	31810	9422	356	4371	252468		359	**148029**			140	117	143		145	405	79	0.00
7/9/2015	-303	pyritic	**51285**	1842	12630	56134	4346	107	3784	112337	135	267	**12960**		15.7	198		75	12.9	116	631	**11020**	0.02
7/9/2015	-304	pyritic			533	8194	1379	13	591	7734			13.9			84.7	27.5	110.9	5	26			
7/9/2015	-305	pyritic		787	452	3676	1758	17	557	9044			5			69	22	139.7	6	27			
7/9/2015	-305.6	pyritic	**15300**	903	4195	34704	5008	193	3063	80035	43	59	**2542**	29		109	29.9	58.7	2.9	75	192	21	0.02
7/9/2015	-306.1	pyritic	**28707**	673	7040	18909	6645	216	2137	86297	41	70	304		12.5	129	44	96	8.1	67	537	206	0.23
7/9/2015	-307	pyritic	**26803**	713	13956	21200	4875	83	1742	58667	41	31	1760		35.5	150	65	185	12.5	91	1086	909	0.02
7/9/2015	-308.1	pyritic	**43162**	658	8149	23851	4870	44	1648	60316	74	40	**3098**	45	21.5	155	39	177	12.2	83	414	183	0.01
7/9/2015	-308.9	QFP		349	11841	16792	1918	14	604	13617			37	4.3	28.4	169	17.1	66.1	2.9	51	843		
7/9/2015	-310.15	QFP	3408		21528	9208	1576	19	429	11352		80	28		38.1	174	14.3	73.8		48	1187	32.5	2.86
7/9/2015	-311	QFP	9437	383	9177	12610	2289	28	829	23236			44		25.3	182	15.9	70.8		50	321	46	
7/9/2015	-312	QFP		401	22394	22761	2486	98	1239	27222			55	9.5	66	230	22.7	77.1	2.5	60	872		
7/9/2015	-313	QFP	**13124**		17539	10916	2203	13	796	21261			29	6.5	54.1	123	17.8	76.3	3.2	46	732		
7/9/2015	-314.05	QFP	**18206**		16040	8291	2556	23	845	22601		11	18.2	7.3	50.6	104	20.8	88.3	2.3	58	830		0.60
7/9/2015	-315	QFP	2199		7110	13693	1980	9	721	12054		14	28		33.2	152	20	86.1		35	267		0.50
7/9/2015	-316.07	QFP	2685	369	17520	3048	1775	20	819	16503		115	31	4.1	58.7	28.2	15.4	76.8		57	1088		3.71

Date	Depth (m)	Lithology	S (ppm)	Cl (ppm)	K (ppm)	Ca (ppm)	Ti (ppm)	Cr (ppm)	Mn (ppm)	Fe (ppm)	Ni (ppm)	Cu (ppm)	Zn (ppm)	As (ppm)	Rb (ppm)	Sr (ppm)	Y (ppm)	Zr (ppm)	Nb (ppm)	Ag (ppm)	Ba (ppm)	Pb (ppm)	Cu/Zn
7/9/2015	-317.35	QFP	**208466**	1243	10206	15286	1833		2158	150101		451	110	29	29.2	171	52	40.4		109	270	13	4.10
7/9/2015	-318	QFP	**14525**	292	9997	22468	2196		984	17139			49	5.4	35.6	136	28.3	60.7		48	371	8.3	
7/9/2015	-319	QFP	2116	585	12866	17007	1829	16	961	17250			41	4.2	31.5	156	24.3	74.4		48	700		
7/9/2015	-320.14	QFP	990	288	6807	6522	2078		690	12738			17.9	3.7	21	129	8.3	63.8	2	40	442		
7/9/2015	-321.13	QFP	**50024**	536	25067	17567	2276	20	1184	41030		15	25	9.4	54.9	158	20.9	73.6		58	677	6.1	0.60
7/9/2015	-322	QFP	5282		5375	22750	1269	9	637	11517		13	21.7		15.3	148	16.3	66.4	2.4	36	280		0.60
7/9/2015	-323	QFP			6118	21552	1472		727	14683			33	4.3	20.1	137	16.8	81.4	2.5	52	341		
7/9/2015	-324	QFP	6162		8234	20717	1345		753	14989			51	5.8	27.3	120	13.9	60.6		40	293		
7/9/2015	-325	QFP	2133	315	7435	18626	1750		810	16368			37	4.1	24.5	153	20.3	71.9		32	466		
7/9/2015	-326	QFP	**59447**	679	9550	14286	3073		1173	66786			55	14.6	24.5	149	25.8	71.7	4.5	77	656		
7/9/2015	-327	QFP	**13598**		15393	11647	2085		701	16790			29	5.5	47.2	421	20.4	80.2		47	742		
7/9/2015	-327.85	QFP		306	18492	11416	1113	14	604	8643		43	204		56.9	133	6.2	46.8		35	1167		0.21
7/9/2015	-329	QFP	**108382**	954	11775	21760	2999	19	1311	78136		23	56	14.3	27.8	191	21.2	94	4.1	95	641		0.41
7/9/2015	-330	QFP	4072	275	7709	12901	1673	14	796	18799			26	3.8	18.1	198	17.7	73.2		46	577		
7/9/2015	-331.1	QFP	3017	324	6993	17519	1508	20	841	18742		138	34	6.9	17.7	214	15.1	72	3.4	46	430	14.7	4.06
7/9/2015	-332	QFP	**32232**	571	16283	25264	3480	15	1149	31996			25	7.6	41.7	166	29.3	61.2		47	606		
7/9/2015	-333.15	QFP	**54324**		13028	31525	4501	25	1338	51525			54	10.3	32.8	158	25.3	62.2	2.9	61	509		
7/9/2015	-334	QFP	**10527**	464	10683	41062	1152		665	9941		15	18.7	12.6	29	69.5	14	30		37	873	48	0.80
7/9/2015	-335	QFP			13992	13665	2468		917	20578			29	6.9	45.6	221	23.9	67	2.6	49	706		
7/9/2015	-336	QFP			13153	20327	3822	44	1184	30329			60	7.5	37.4	153	22.6	75.3	2.6	51	444		
7/9/2015	-337.22	QFP	**22441**		24589	13274	3145	16	614	28623		42	35	7.1	74.8	138	21.7	78.4	3.7	51	942		1.20
7/9/2015	-338.05	QFP		381	23647	13620	2581	21	633	18110			41	5.4	53.1	148	15.7	75.7		52	1405	4.8	
7/9/2015	-339.1	QFP	5799	483	16579	86393	2326	32	1205	35695			13	9.9	47.2	351	27.9	58.3	4.3	80	681		
7/9/2015	-340.1	QFP		297	8677	21942	2074	18	786	22378		64	46	7.7	25.6	214	19	80.1	3.4	49	347		1.39
7/9/2015	-341.1	QFP	**14146**		20880	25010	2509	13	616	17405			29	7.5	50.3	104	16.6	70.5	2.3	52	1012	6.2	
7/9/2015	-341.89	QFP	1632		13340	116571	1096		1301	35108			20	11.8	37.9	599	30.8	50	4.1	75	453		
7/9/2015	-343	QFP	3982		9074	24341	1601		684	20368			42	4.4	29.4	294	17.4	69.5	2.3	54	434		
7/9/2015	-343.4	mafic dyke	1899		5309	75692	5789	279	1715	52545	82	21	82	12.5	14.4	345	21.9	79	3.8	71	159		0.26
7/9/2015	-343.7	mafic dyke	3260		9849	65143	6671	341	1254	68722	126		128	11	24.8	338	25.2	65.8		74	230		
7/9/2015	-344.1	QFP			3196	958	1913		860	35837	16		71	6.5	17.7	17.1	10.4	72.9	3.3	33			
7/9/2015	-345	QFP	**62564**		16962	14019	2522	16	702	37204			48	8.6	51.9	151	15.7	69.2	2.5	63	704		
7/9/2015	-346.2	QFP	**98586**	702	12698	19572	2268		1215	65843			52	14	32.9	157	25.6	51.5		78	450		
7/9/2015	-347	QFP	3305		5870	21027	1063		661	15309		13	61		22.3	159	19.4	62.6		50	272		0.21
7/9/2015	-348.1	QFP	1150	254	9103	16556	1862	16	672	14042			36		32.4	177	15.1	81.6	2.8	47	411		
7/9/2015	-348.6	mafic dyke	3279		20353	12149	1613	12	539	17947			34	5.1	60.6	158	18.2	66.5		52	931		
7/9/2015	-348.95	mafic dyke			9211	81764	6110	177	2054	69928	83	15	104	14.3	21.8	390	23.1	64	5.5	73	360		0.14
7/9/2015	-350	QFP	4083		16122	31367	2194		1318	31867			60	9.3	53.7	273	28.4	35.6		57	401		
7/9/2015	-351.1	QFP	2440		10153	16078	1648	14	873	19320			43	4.4	33.8	431	23.4	68.8	2.9	51	630		
7/9/2015	-352	QFP	**12286**	316	15048	13234	2530	27	836	20617			55	4.3	45.4	109	17.7	78.4		45	656	5.8	
7/9/2015	-353.1	QFP	4101	249	5539	9474	892		483	10831			23.4	4.2	14	229	11.7	56.6		28	351		
7/9/2015	-353.63	QFP	4850		6817	18426	2002	11	669	21291		34	69	4.9	21.5	174	19.5	71.5		52	357		0.49
7/9/2015	-353.76	mafic dyke		490	3902	76096	5213	432	3894	67289	121		205	12.2	3.7	134	24.7	56.6		67	125		
7/9/2015	-354.2	QFP	3169		5112	12125	2810		960	21569		297	44	6.2	12.8	359	21.9	71.1	2.7	39	178		6.75
7/9/2015	-354.9	mafic dyke			29132	61426	5259	400	3479	60978	153		157	12.8	65.2	108	20.9	46.8	2.8	81	1343		
7/9/2015	-355.1	QFP	1742	300	5350	23139	1779	11	578	15941			43	3.9	15.5	167	21.3	75.2	2.9	48	328		
7/9/2015	-356.2	QFP		280	7421	6431	1506		561	17460			50	3.9	15.8	111	19.4	65.6		40	243		
7/9/2015	-356.68	mafic dyke			6881	24642	8597	97	1021	68417	39		120	13.7	13.7	148	22.3	81.2	4.4	63	381		
7/9/2015	-357	mafic dyke		590	5970	60547	8208	94	3209	72068	37		184	13.7	11.5	230	29.7	70.1	3.8	78	307		
7/9/2015	-357.4	mafic dyke	1722		8706	38219	8374	95	1939	74659	56		263	12.2	21.7	202	28.1	73.7	4.5	66	322		
7/9/2015	-358	QFP	1262	408	14619	13761	1922		671	23516		13	40	6.7	47.4	285	13.7	71.9	2.6	58	725		0.33
7/9/2015	-358.71	mafic dyke	6872	755	7059	15559	7015	450	2964	89590	56		209	15.7	11.9	322	37	66.1	2.9	88	349		
7/9/2015	-359.1	QFP		318	6145	6500	1170		559	16379			31	5.2	12.5	203	17	59.2		36	176		
7/9/2015	-360	QFP		266	5777	12279	1278		566	17427			43	5	23	243	17	64.9		45	319		
7/9/2015	-361	QFP	2260		11290	18058	2645	13	782	17487			57	3.9	38.2	100.8	20.8	75.7		42	431		
7/9/2015	-362.05	QFP	4172	528	1843	155994	587	28	1564	46167				12.6	4.5	490	29	20.8		78	203		
7/9/2015	-363.25	QFP	6611		11027	35374	2065	15	1384	38027			54	9.7	26.5	208	25.1	59.8		53	318		
7/9/2015	-364	QFP	8738		10636	24399	1845	14	677	19147		39	43	7.1	28.1	145	23.9	71.4	2.8	53	567		0.91
7/9/2015	-364.95	QFP	2389		10355	12568	939		401	9977			30		24.6	107	11.4	49.7		32	451		

Date	Depth (m)	Lithology	S (ppm)	Cl (ppm)	K (ppm)	Ca (ppm)	Ti (ppm)	Cr (ppm)	Mn (ppm)	Fe (ppm)	Ni (ppm)	Cu (ppm)	Zn (ppm)	As (ppm)	Rb (ppm)	Sr (ppm)	Y (ppm)	Zr (ppm)	Nb (ppm)	Ag (ppm)	Ba (ppm)	Pb (ppm)	Cu/Zn
7/9/2015	-356.2	QFP		280	7421	6431	1506		561	17460			50	3.9	15.8	111	19.4	65.6		40	243		
7/9/2015	-356.68	mafic dyke			6881	24642	8597	97	1021	68417	39		120	13.7	13.7	148	22.3	81.2	4.4	63	381		
7/9/2015	-357	mafic dyke		590	5970	60547	8208	94	3209	72068	37		184	13.7	11.5	230	29.7	70.1	3.8	78	307		
7/9/2015	-357.4	mafic dyke	1722		8706	38219	8374	95	1939	74659	56		263	12.2	21.7	202	28.1	73.7	4.5	66	322		
7/9/2015	-358	QFP	1262	408	14619	13761	1922		671	23516		13	40	6.7	47.4	285	13.7	71.9	2.6	58	725		0.33
7/9/2015	-358.71	mafic dyke	6872	755	7059	15559	7015	450	2964	89590	56		209	15.7	11.9	322	37	66.1	2.9	88	349		
7/9/2015	-359.1	QFP		318	6145	6500	1170		559	16379			31	5.2	12.5	203	17	59.2		36	176		
7/9/2015	-360	QFP		266	5777	12279	1278		566	17427			43	5	23	243	17	64.9		45	319		
7/9/2015	-361	QFP	2260		11290	18058	2645	13	782	17487			57	3.9	38.2	100.8	20.8	75.7		42	431		
7/9/2015	-362.05	QFP	4172	528	1843	155994	587	28	1564	46167				12.6	4.5	490	29	20.8		78	203		
7/9/2015	-363.25	QFP	6611		11027	35374	2065	15	1384	38027			54	9.7	26.5	208	25.1	59.8		53	318		
7/9/2015	-364	QFP	8738		10636	24399	1845	14	677	19147		39	43	7.1	28.1	145	23.9	71.4	2.8	53	567		0.91
7/9/2015	-364.95	QFP	2389		10355	12568	939		401	9977			30		24.6	107	11.4	49.7		32	451		
7/9/2015	-365.53	QFP	**53664**	311	3689	25605	548		983	30694		98	50	8.8	8.6	91	25.2	33.3		43	194		1.96
7/9/2015	-365.65	QFP	**199095**	812	864	93735	131		662	107491		535	16	30		48.1	13.1			92			33.44
7/9/2015	-367.15	QFP	2321		2831	31668	1587		891	10983		77	34	3.5	3.9	248	15.8	74.5	2.3	32	228		2.26
7/9/2015	-368	QFP	5769	339	3899	19566	2564	13	653	15706		15	29		6.3	207	23.3	90.4		38	128	47	0.52
7/9/2015	-368.95	QFP	**11998**	472	10070	44875	7860	49	2392	74384			91	16.2	21	293	69	224	10.3	73	368		
7/9/2015	-370	mafic dyke	2969	488	19912	52365	6972	88	1927	57138	25	51	133	14.7	43.8	221	25.6	62.7	3	85	881		0.38
7/9/2015	-370.36	chert	5901	543	6301	5953	2919	106	1649	57818	24	152	291	9.7	15.8	118	8.4	15.9		57	366		0.52
7/9/2015	-371.1	chert			708	39377	618		582	14874	19	10	14.5	5.5		231	28	45.8	2.9	45			0.69
7/9/2015	-372.56	chert	894	373	3617	823	627	12	556	11338		8	62		10.3	22.1	12.1	59.2		27	318		0.13
7/9/2015	-372.88	chert	**15941**		2470	6305	1365		408	14667			27	6.1	9.8	69.5	26.7	120	5	41	93	18	
7/9/2015	-374	mafic dyke		647	5237	82757	5093	165	2033	52303	76		124	9.8	12.2	352	19.6	70	6.1	72	373		
7/9/2015	-374.53	mafic dyke		819	13027	40526	5562	146	1033	58005	65		75	11.7	32.7	263	21.4	67.4	4.3	78	1177		
7/9/2015	-375.1	chert	786	212	2576	2498	845		197	5756			9.5		12.2	39.4	12.5	85.9	4.5	21	308		
7/9/2015	-376.1	chert	**76471**	468	8609	12193	1714	40	296	64308	50	34	25	22	11.4	150	33.9	83	4.9	76	392	23	1.36
7/9/2015	-377.8	chert	**15207**	682	687	8283	3198	22	607	39420	56	20	76	11.3		74.5	48.5	178	10.5	64			0.26
7/9/2015	-378	mafic dyke	**28301**	541	3474	179090	2842		1210	84773			17	27	12.2	1649	10	20	6.9	97			
7/9/2015	-379	mafic dyke	3166	919	5675	72069	9443	32	2957	107193		40	115	19.3	12.5	728	24.2	44	4.7	88	446		0.35
7/9/2015	-380	mafic dyke	4101	797	7553	42009	9403		2438	102588		32	161	14.1	17	379	31.3	58		80	531		0.20
7/9/2015	-381	mafic dyke		4015	12251	45432	4013	166	2495	73619	40	47	254	11.9	27.3	194	14	28.4		74	1234		0.19
7/9/2015	-382.7	chert	8313	398	1761	10767	2318	17	763	24401	34	24	278	11.5	3	82.7	34	130	8.7	43	146	43	0.09
7/9/2015	-382.9	chert	**165184**	1138	4467	19313	3073	64	1261	121947			97	20	9.1	145	31.6	79		86	526	10	
7/9/2015	-384	chert	5807	399	2314	5738	1431	19	479	15781	33	29	841		2.6	53.8	26.8	91.9	5.3	34	48	172	0.03
7/9/2015	-384.9	chert	**83790**	590	33189	3405	2925	24	692	56551	54	328	50	14.6	96.9	32.2	28.6	151	10	60	1109	16	6.56
7/9/2015	-386	chert	**18453**	2934	10528	29264	2591	37	1049	35454	44	321	76	10	33.4	159	53	121	7.2	57	342	44	4.22
7/9/2015	-386.9	chert	4363	290	2468	6941	1617		482	11421	13		66	5.2	8.1	67.3	21	89.5		26	159	18.5	
7/9/2015	-388.15	mafic dyke	**69131**	877	1570	43485	4389	140	2484	123330		44	162	19		244	29	55	5.4	83	74		0.27
7/9/2015	-389	mafic dyke	**101801**	1204	3795	64932	1654	41	1328	175944		1498	80	26	4.4	258	13.5	30.3		85	374		18.73
7/9/2015	-390.15	mafic dyke		566	15358	141307	2876	38	952	45687	24		41	16.8	46.7	546	12	35.7	5.2	76			
7/9/2015	-391.15	cherty pyritic	7873		32470	39702	3793	69	589	37296	70	18	54	10.8	78.2	381	52	133	5.5	90	2312		0.33
7/9/2015	-391.95	cherty pyritic	**67823**	743	3420	1484	2717		626	83993	28		32	21	5.8	11.8	20.2	99	5.2	63		43	
7/9/2015	-393.3	cherty pyritic	**20434**	719	1931	975	2052		645	36117	31	10	41	8.9	6.6	18.2	18	104.9	6.5	54			0.24
7/9/2015	-394.2	cherty pyritic			799	8941	1496	18	569	8685	21		46			55	30.2	93.9	6.9	23			
7/9/2015	-396	cherty pyritic	**217397**	1009	7632	9804	1186	37	873	109599		129	59	33	20.6	109	53	82		62	319	45	2.19
7/9/2015	-397	cherty pyritic		961	757	163862	2669		1311	67947		23	50	14.8		524	10.8	25.7		86			0.46
7/9/2015	-398	cherty pyritic	**10152**	511	1709	20723	3595	27	2117	44041		181	240	9.6		133	13.9	47.5	2.5	46	68		0.75
7/9/2015	-398.95	cherty ash	**88235**	720	3639	26742	3073	42	1928	72854		**1581**	174	13.7	6.8	314	18.2	51.7	3.4	71	155		9.09
7/9/2015	-399.0	cherty ash		351	7844	14274	3468	28	1449	24081	24		112	6.7	23.8	87.1	43.9	173	12.8	47	480		
7/9/2015	-400.1	cherty ash	**97392**	810	5691	15343	2026	37	550	57347		17	47	15	7.5	103	37.2	127	8.4	78	368	28	0.36
7/9/2015	-401	cherty ash	8190		1207	8962	2172	14	490	16886	35		41	5		111	45.6	180	13.5	40	66	13.8	
7/9/2015	-402	mafic		749	2521	46637	557		2520	77684		156	149	16.3	5.5	396	10.4	9.9		63	331		1.05
7/9/2015	-402.95	mafic		500	10026	73149	2765	54	1481	76921	20	141	72	11.4	24	257	6.1	15		79	285		1.96
7/9/2015	-404.07	mafic	**11914**	959	30444	43932	2519	80	2314	99301		164	189	17.2	73.3	203	8	11.6		106	1538		0.87
7/9/2015	-405	mafic		1158	26041	27505	3009	64	749	69339	14	107	49	14	62.3	252	4.7	12.9		86	2213		2.18
7/9/2015	-405.6	mafic		609	6466	41357	2701	41	1642	74801	19	81	125	8.5	11.6	222	7.1	16.7		63	403		0.65
7/9/2015	-407	mafic		613	1039	148445	3465	30	1543	68115	19		70	16.5		799	13.9	39	4.7	71			
7/9/2015	-408.1	mafic		679	593	191133	1665	24	1389	71123			37	18		998	10.2	20	4.2	74			
7/9/2015	-409.36	cherty ash	**12324**	299	4575	7442	594		207	7790	14		24.8		13.4	34.4	11.1	54.5	3.3	23	95		
7/9/2015	-410.25	cherty ash	1701	427	2081	9463	6552	32	857	32361	31	10	105	8	4.5	96.3	63.2	304	14.8	43	101		0.10
7/9/2015	-411.1	cherty ash	1576		13155	1867	821	7	143	3331					30.1	55.4	17.7	69	3.8	31	393	4.8	
7/9/2015	-412	cherty ash		237	1530	6789	834	13	211	6323	10		30.2		3.1	57.5	14.7	93.6	4.6	25	85	4.6	
7/9/2015	-412.7	mafic		547	1595	96846	2721	140	2084	64662	25		152	11.5		285	12	22		76			
7/9/2015	-414.1	mafic		449	10072	35492	2960	124	1799	68752	53		207	13	22	114	10.1	20.2		68	249		
7/9/2015	-415.3	mafic flow	**372264**	1399	1593	86445	876		605	404467	263	**2070**		170		1100	28		4.9	151		62	
7/9/2015	-416	mafic flow		835	6093	104280	2565	112	1924	53882	41		162	12.6	11.1	307	9.8	15		63	219		

Appendix C

Summary of microthermometric data.

Mineral	ID	Eutectic (°C)	Hydrohalite melting (°C)	CaCl2-hydrate melting (°C)	Vapor Homogenization (°C)	Halite Dissolution (°C)	CaCl2 equivelent	CaCl2 (wt%)	NaCl (wt%)	S_{wt}	Density (g/cc)	Phases
Cal B	106.17			3.1	118.9							L + V
Cal B	106.17				236.3	176.1						L + V + H
Cal B	106.17			31.7		205.0		43.5	10.0	53.5		L + V + H
Cal B	106.17			31.7	164.2	204.8		43.6	9.9	53.5	1.51	L + V + H
Cal B	106.17											
Cal B	106.17	-47.4	-16.6		88.6	greater than 304						L + V + H
Cal B	106.17	0.3	-1.9		223.8							L + V
Cal B	106.17	-50.2			157.2							L + V
Cal B	106.17	-37.5	-22.6		289.8							L + V
Cal B	106.17	-37.5	-20.7									L + V
Cal B	106.17				186.3	greater than 240						L +V + H
Cal B	106.17		-8.2		172.5							L + V
Cal B	106.17		-7.8		111.1							L + V
Cal B	106.17		-8.2		119.6							L + V
Cal B	106.17				142.8							L + V
Cal B	106.17				152.7							L + V
Cal B	106.17				206.4							L + V
Cal B	106.17		-23.7	35.4	227.2			49.8	0.1	49.8	1.67	L + V
Cal B	106.17		-24.0		224.1							L + V
Cal B	106.17	-38.6	-23.4		212.2	greater than 280						L +V + H
Cal B	106.17		-23.4		181.0							L + V
Cal B	106.17	-63.2			240.2							L + V
Cal B	106.17				261.4							L + V
Cal B	106.17			12.2	203.9		40				1.38	L + V + H
Cal B	106.17				190.9							L + V
Cal B	106.17				194.6							L + V
Cal B	106.17	-40.3	-18.1		171.3							L + V
Cal B	106.17	-65.7	-30.7		197.9							L + V
Cal B	106.17	-65.8	-21.9		296.2							L + V
Cal B	106.17				175.2	200.5						L + V + H
Cal B	106.17	-65.7	-30.1		209.6							L + V
Cal B	106.17				176.9							L + V
Cal B	106.17				179.2							L + V
Cal B	106.17	-52.7	-21.1		205.5							L + V
Cal B	106.17				181.8							L + V
Cal B	106.17				172.4							L + V
Cal B	106.17	-60.2	-15.2		231.3							L + V
Cal B	106.17				226.5							L + V + H
Cal B	106.17	-51.8	-37.6	85.9	233.0		59				2.69	L + V
Cal B	106.17				261.6							L + V
Cal B	106.17				252.7							L + V
Cal B	106.17				237.4							L + V
Cal B	106.17			28.0	178.8		47				1.56	L + V
Cal B	106.17			28.4	164.9	209.8		42.2	10.8	53.0	1.47	L + V + H
Cal B	106.17		-12.7	28.4	186.8	214.8		42.0	11.3	53.3	1.46	L + V + H
Cal B	106.17	-46.0	-12.7	28.4	200.1		47				1.54	L + V
Cal B	106.17		-12.2	28.4	186.1		47				1.55	L + V
Cal B	106.17	-81.6	-32.5	21.2	220.0			42.2	0.7	42.9	1.37	L + V
Cal B	106.17		-32.5	21.2	232.5			42.2	0.7	42.9	1.37	L + V
Cal B	106.17	-52.4		31.1	235.2		50				1.65	L + V
Cal B	106.17	-52.4		17.3	162.2		42				1.40	L + V
Cal B	106.17	-52.4		17.9	165.5		42				1.40	L + V
Cal B	106.17	-53.2		19.9	179.8		43				1.42	L + V
Cal B	106.17				220.1							L + V
Cal B	106.17				164.0							V + L
Cal B	106.17				199.8							V + L
Cal B	106.17				220.7							V + L
Cal B	106.17				267.5							V + L

Cal B	106.17	-57.1	-34.4		296.2							V + L
Cal B	106.17	-64.0	-52.0	22.3	223.0			42.8	0.7	43.4	1.39	V + L
Cal B	106.17	-64.0	-52.2	22.0	198.2			42.6	0.7	43.3	1.40	V + L
Cal B	106.17	-64.0	-52.0	21.5	178.9			42.2	0.7	43.0	1.40	V + L
Cal B	106.17											
Cal B	106.17	-51.4		22.9	104.9		44				1.50	V + L
Cal B	106.17			15.5	111.5		41				1.41	V + L
Cal B	106.17	-72.1	-38.2		238.0							V + L
Cal B	106.17			21.6	235.7		44				1.39	V + L + H
Cal B	106.17			25.2	196.6		46				1.49	V+L
Cal B	106.17			18.2		274.6		32.5	20.0	52.5		V + L + H
Cal B	106.17			24.5	232.1		45				1.43	
Cal B	106.17			24.5	233.0		45				1.45	
Cal B	106.17			24.5	304.4		45				1.39	
Cal B	95.10				186.9							V + L
Cal B	95.10				188.2	212.7						V + L + H
Cal B	95.10				184.4							V + L
Cal B	95.10				191.2							V + L
Cal B	95.10				119.0							V + L
Cal B	95.10											L + H
Cal B	95.10	-25.6	-14.7		201.4							V + L
Cal B	95.10				191.6							V + L
Cal B	95.10											L + H
Cal B	95.10											L + H
Cal B	95.10	-32.5		26.4	208.8		46				0.85	V + L + H
Cal B	95.10			31.5								V + L + H
Cal A	95.10					212.0						L + H
Cal A	95.10					197.3						L + H
Cal A	95.10		-12.7	76.1	209.6		58				2.52	V + L + H
Cal A	95.10				218.8							V + L
Cal A	95.10				227.7							V + L
Cal A	95.10				255.7							V + L
Cal A	95.10	-34.0		183.1	266.7							V + L
Cal A	95.10	-34.0			271.5							V + L
Cal A	95.10	-34.0			286.3							V + L
Cal A	95.10	-34.0			276.3							V + L
Cal A	95.10	-34.0			233.3							V + L
Cal A	95.10				283.9							V + L
Cal A	95.10	-41.8	-22.1		248.3							V + L
Cal A	95.10	-41.5		28.4	295.5		47				1.49	V + L
Cal A	95.10		-13.0		314.0							V + L
Cal A	95.10			26.4								V + L
Cal A	95.10			26.4	229.0		46				1.48	V + L
Cal A	95.10	-54.5	-30.6		269.8							V + L
Cal A	95.10	-54.5	-28.6		314.2							V + L
Cal A	95.10				327.0							V + L
Cal A	95.10				267.8							V + L
Cal B	200.20				74.4							V + L
Cal B	200.20				221.9							V + L
Cal B	200.20				165.7							V + L
Cal B	200.20			25.9	221.5		46				1.47	V + L
Cal B	200.20			26.1	253.0		46				1.47	V + L
Cal B	200.20			26.1								V + L
Cal B	200.20				225.0							V + L
Averages		-48.8	-23.8	31.3	210.9	210.8	46	42.3	6.0	48.3	1.51	